Graphical limit state analysis

Application to statically indeterminate
trusses, beams and masonry arches

Graphical limit state analysis

Application to statically indeterminate
trusses, beams and masonry arches

Thesis submitted in partial fulfillment of the requirements
for the degree of *Docteur en sciences de l'ingénieur* by

Jean-François Rondeaux

April 2019

Composition of the jury:

Prof. Dr Eng. Arch. Denis Zastavni, Supervisor
Université catholique de Louvain

Prof. Dr Arch. Jean-Louis Vanden Eynde
Université catholique de Louvain

Prof. Dr Eng. Santiago Huerta
Universidad politécnica de Madrid

Prof. Dr Eng. Arch. Corentin Fivet
École Polytechnique Fédérale de Lausanne

Prof. Dr Eng. Joseph Schwartz
Eidgenössische Technische Hochschule Zürich

Prof. Dr Arch. David Vanderburgh, Chairman
Université catholique de Louvain

Acknowledgments

First of all, I would like to thank my supervisor, Professor Denis Zastavni, for his patient support during these six years. I particularly appreciated the large autonomy I received for choosing my topic and for deciding the directions to give to my researches, and I am grateful for the valuable advice he gave me throughout all the research and writing process.

This thesis has been reviewed by my committee, namely the Professors Jean-Louis Vanden Eynde, Santiago Huerta, Corentin Fivet and Joseph Schwartz. I would like to thank them for the constructive comments they provided me. They largely improved the quality of this text, and gave me helpful advice during my research. I also thank Professor David Vanderburgh for accepting to chair the jury, and Professor Jean-Louis Vanden Eynde for beeing its secretary.

To prepare this dissertation, I received the financial support of the UC-Louvain, as a teaching assistant at the Faculty of Architecture, Architectural Engineering, Urban planning (LOCI). I would like to thank this venerable institution for having believed in me as a teacher and a researcher. I am particularly thankful for the intense collaboration I developed with my students and colleagues of Brussels and Louvain-la-Neuve, especially with Yvette Pelsser, Brigitte De Groof, François Nizet and Pierre Latteur who shared with me their profound knowledge and experience in teaching structural analysis.

Amongst the aforementioned colleagues, I must thank warmly Brigitte de Terwangne and Stéphanie Lozes from the Faculty staff, for their efficient and helpful assistance during the last steps of this thesis preparation. I am also grateful to Laurence Bertrand and Émilie Brichart from the Science and Technology Sector for their kind attitude towards me.

I would also like to thank heartily the members of my research lab *Structures & Technologies*, as well as all the researchers of the *Vinci* and *Lemaire* buildings, for their friendly company. I must particularly thank

Aurélie Deschuyteneer and Jean-Philippe Jasienski for sharing passionately our discoveries and for helping me to improve the quality of this text.

I also received the precious help of colleagues and friends – Cécile Vandernoot, Amélie Collard, Johan Maricq, François Nizet, Pierluigi D'Acunto – who unearthed most of the linguistic, syntactic, logical and aestethic misprints in this manuscript.

Last but not least, I would like to thank deeply my whole family, with a particular intent to my little brother Thomas for his *legendary* expertise in English, as well as to my parents who always encouraged me through all my projects.

Summary

Area of research. Structural analysis

Keywords. Theory of Plasticity · Limit state analysis · Static equilibrium · Strut-and-tie modelling · Graphic statics

Abstract. The art of structural design is related to various fields – amongst which intellectual, functional, aesthetic or ecological – for each of which specific methods and tools are required.

Plastic design using strut-and-tie models is one of those tools. The simplicity of its theoretical prerequisites, the freedom it offers to the designer and the clarity of its results make it particularly interesting for early stage structural design.

This technique, based on the Theory of Plasticity, consists in modelling the structural behaviour through a network of pin-jointed straight bars, whether in compression or in tension. This network has to abide by the equilibrium conditions between the bars and the applied loads. Its strength is obtained by an appropriate *dimensioning* of the bars cross sections. This equilibrium can be examined and manipulated thanks to the reciprocal diagrams of graphic statics: the form diagram $\mathbf{F}$ describes the strut-and-tie network's geometry while the force diagram $\mathbf{F}^*$ represents its vectorial static equilibrium.

The improvement of the structural performances in terms of strength, stiffness, robustness or in response to formal or constructive requirements may force the designer to make the network's geometry more complex. This often results in statically indeterminate form diagrams for which numerous static equilibrium states can be determined. During the design phase, the lower-bound theorem of plasticity allows the designer to avoid

any overestimation of the load bearing capacity of the structure hence helping in the selection of one of these possible equilibrium states. This theorem can also be used to perform a limit state analysis of the structure, allowing the identification of the equilibrium states for which the load bearing capacity of the structure is attained.

The premise of the thesis is that the limit state analysis is a better support for the design process when it shares the same methods and tools, especially its graphical environment. Our ambition is to review the conditions allowing the implementation of this limit state analysis only using the reciprocal diagrams of graphic statics.

It begins by analyzing the principles for constructing a geometrically indeterminate reciprocal force diagram when considering a form diagram corresponding to a statically indeterminate structure. The proposed methodology for this construction consists in considering the force diagram as a group of series of independent force diagrams. One of them represents a stress state in static equilibrium with the external forces; the others correspond to self-stress states. Each of these states can be described using the relative position of one of the vertices of its own force diagram within the assembled one, so that the force diagram's geometry becomes parametric.

Manipulating these points allows the modification of the stress distribution without modifying the form diagram's geometry. As such, it becomes possible to identify specific positions for these particular points to obtain force diagrams corresponding to statically admissible limit states. Taking advantage of the lower-bound theorem of plasticity, the comparison of these limit states allows for the identification of the collapse one and of the ultimate load bearing capacity of the structure. The methodology is directly applicable to the analysis at collapse of pin-jointed trusses for which the geometrical and mechanical characteristics are known.

The methodology is also applicable to the analysis of statically indeterminate beams subjected to bending thanks to funicular polygons. Then, the position of the pole of these polygons within a geometrical domain is the essential geometric parameter. Each of the vertices of the polygonal boundary of this domain is the position of the pole corresponding to one of the statically admissible limit states. Among these, it is easy to recognize the one corresponding to collapse.

Using similar constructions for compression funicular polygons only, the methodology is extended to the study of the load bearing capacity of masonry arches.

The analysis of these admissible domains for the parametric points of the force diagram, as well as the possibility of manipulating the stress states through the position of specific points allows a better understanding of the behaviour of statically indeterminate structures at limit state and may be helpful when designing them.

Résumé

Domaine de recherche. *Analyse structurale.*

Mots-clefs. *Théorie de la plasticité · Analyse aux états limites · Équilibre statique · Modèles de bielles-et-tirants · Statique graphique.*

Abrégé. *La conception des structures est un art aux visées multiples – intellectuelle, fonctionnelle, esthétique, écologique – dont la pratique requiert l'usage de méthodes et outils spécifiques.*

Parmi ceux-ci, la conception plastique à l'aide de modèles de bielles-et-tirants tient une place particulière par l'extrême concision de ses fondements théoriques, la grande liberté qu'elle accorde au concepteur et la lisibilité des résultats qui en découlent. Prenant appui sur la Théorie de la plasticité, elle propose de modéliser le comportement des structures par un réseau composé d'éléments rectilignes comprimés ou tendus en équilibre avec les charges appliquées et dont la résistance est assurée par un dimensionnement approprié. Cet équilibre peut être vérifié et manipulé à l'aide des diagrammes réciproques de la statique graphique. Le diagramme de situation $\mathbf{F}$ *décrit la géométrie du réseau de bielles-et-tirants tandis que le diagramme des forces* $\mathbf{F}^*$ *en représente vectoriellement l'équilibre statique.*

Or, la complexification de ce réseau en vue d'en améliorer les performances structurales en termes de résistance, rigidité ou robustesse, mais également de rencontrer des impératifs formels ou constructifs, résulte fréquemment en des diagrammes de situation statiquement indéterminés, c'est-à-dire dont l'équilibre statique ne peut être déterminé de manière univoque. En phase de conception, le théorème statique de la plasticité autorise le concepteur à opérer un choix parmi ces équilibres possibles en garantissant que l'état d'équilibre considéré ne surestimera pas la capacité portante de la structure. En termes d'analyse, ce même théorème sert

également de fondement théorique aux méthodes visant l'identification, parmi tous ces états d'équilibre, des cas limites pour lesquels la capacité portante du système structural est assurée.

Partant de l'hypothèse que cette analyse aux états limites permet d'autant mieux d'informer le processus de conception qu'elle en partage les méthodes et outils, et en particulier l'environnement graphique, la thèse a pour ambition d'explorer les conditions de sa mise en œuvre au moyen exclusif des diagrammes réciproques de la statique graphique.

Considérant que le diagramme de situation correspondant à une structure statiquement indéterminée a pour réciproque un diagramme des forces géométriquement indéterminé, les principes qui en régissent la construction sont analysés. La méthodologie proposée pour ce faire consiste à considérer le diagramme des forces comme l'assemblage d'une série de diagrammes correspondant à des états d'équilibre statique indépendants : l'un d'eux équilibre les charges appliquées, les autres sont des états d'autocontrainte.

Chacun de ces états étant décrit par la position de l'un des sommets de son diagramme des forces propre relativement aux autres diagrammes, il en résulte un diagramme assemblé paramétrisé géométriquement par la position relative de ces points spécifiques, qui en permettent la manipulation sans modifier la géométrie du diagramme de situation. Il est alors possible d'identifier les positions de ces points qui correspondent à des états limites au sens du théorème statique de la plasticité. La comparaison de ces états permet d'en extraire celui qui mène à la ruine et d'en déduire la capacité portante de la structure.

Cette méthodologie est appliquée de manière directe pour l'évaluation de la charge ultime applicable à des treillis articulés dont les caractéristiques géométriques et mécaniques sont connues.

Elle est dans un second temps adaptée aux poutres fléchies par l'usage de polygones funiculaires dont la position du pôle au sein d'un domaine géométrique constitue le paramètre essentiel. Chacun des sommets de la limite polygonale de ce domaine détermine la position d'un pôle correspondant à l'un des états limites statiquement admissibles desquels il est aisé d'extraire celui qui mène à la ruine.

Sur base des principes similaires limités à des polygones exclusivement comprimés, cette méthodologie est étendue à l'étude de la capacité portante des arcs en maçonnerie.

L'analyse des domaines statiquement admissibles de ces points spécifiques du diagramme des forces, tout comme la possibilité de manipulation des états de contrainte résultant de sa paramétrisation, ouvrent le voie à une compréhension plus approfondie du comportement limite des structures statiquement indéterminées et en éclairent la conception.

Contents

Introduction **19**

1 Plastic design and limit state analysis **25**
1.1 Structural design and analysis 25
1.2 Theory of Plasticity 27
1.3 Fundamental theorems of Plasticity 30
1.4 Limit state analysis 33
1.4.1 Kinematic *versus* geometric views of statics 33
1.4.2 Kinematic approaches and upper-bound theorem . 36
1.4.3 Static approaches and lower-bound theorem 40
1.4.4 Complete limit state analysis 41
1.5 Plastic design 43

2 Strut-and-tie modelling using graphic statics **49**
2.1 Strut-and-tie networks for structural analysis and design . 49
2.2 Classical graphic statics 52
2.2.1 From parallelogram of forces to form and force diagrams 52
2.2.2 Graphical analysis through reciprocal diagrams . . 54
2.2.3 Elasticity and static indeterminacy 57
2.3 Graphical tools for interactive structural design 62

3 Reciprocal diagrams and static indeterminacy **67**
3.1 Static indeterminacy in structural design 67
3.2 Static indeterminacy as a combination of independent stress states 71
3.3 Geometrical freedom of force diagrams 75
3.4 Limit state analysis using reciprocal diagrams 80
3.5 Designing with indeterminate force diagrams 87

4 Pin-jointed trusses **93**
4.1 Working hypotheses 93
4.2 Complete graphical limit state analysis 94
4.3 Optimization procedure on the force diagram 103
4.4 Case studies: internally and externally statically indeterminate trusses 107
4.5 Perspectives 115

5 Beams **121**
5.1 Bending and funicular polygons 121
5.2 Statically admissible limit states of funiculars polygons . . 127
5.3 Admissible geometrical domains 135
5.4 Case studies: statically indeterminate beams 154

6 Masonry arches **165**
6.1 Kinematic and static methods for structural assessment of masonry arches: a short overview 165
6.2 Conciliating lower bound theorem and thrust line theory: the equilibrium approach 174
6.3 Admissible geometrical domains 176
6.4 Graphical safety of masonry arches 185
6.4.1 Stability under self-weight 187
6.4.2 Stability related to the abutments 193
6.5 Current work and perspectives 194

Conclusion **199**

List of Figures **203**

References **223**

Introduction

"There is nothing more practical than a good theory."

James C. Maxwell

Context. For a structural engineer, no theory can be more satisfactory than the one of Plasticity. Besides the absolute conciseness of its fundamental principles, it has the great advantage to give the designer a large freedom in the shaping of structures. Indeed, provided that the structural material presents a sufficiently ductile rheological behaviour, Theory of Plasticity is applicable to any kind of structures: metallic trusses, reinforced concrete frames or walls, masonry vaulted systems, etc. Moreover, it provides safe methodologies for structural design since the lower-bound theorem ensures that any chosen distribution of stresses within the structure that nowhere exceeds the material specific strength is a solution to the design problem that cannot overestimate the load bearing capacity of the structure.

For all these reasons, the *UCLouvain* research lab *Structures & technologies*, led by Prof. Denis Zastavni, has been developing an increasing interest for methods based on this theorem, in terms of research as well as for teaching activities. One of them consists in modeling design stress fields by strut-and-tie networks, which geometry can be managed together with the internal forces distribution thanks to graphic statics. Indeed, the use of reciprocal form and force diagrams provides a visual, intelligible and potentially interactive environment which supports actively the decision-making process.

Objectives. The essential idea of the thesis is to explore the links between the complete Theory of Plasticity and graphic statics. Indeed, plastic design is only one possible application of this theory; the other one being its use for limit state analysis, *i.e.* the analysis of the conditions of collapse of ductile structures. Since structural design and analysis are the two sides of the same coin, it is assumed that the latter can better support the first if it shares a common design environment. Therefore, the thesis is devoted to the implementation of limit state analysis on statically indeterminate structure using reciprocal diagrams.

Organization of the content. This dissertation is divided into six chapters. The first two ones give a synthetic overview of the theoretical and methodological founding principles of the thesis; the third chapter then focuses on static indeterminacy within reciprocal diagrams, while the last three chapters are devoted to the application of graphical limit state analysis of three different types of structures.

In **Chapter 1**, the theories for structural engineering are explored (Section 1.1), with a particular focus on the Theory of Plasticity. Its fundamental hypotheses are outlined (Section 1.2) and the classical results of limit state analysis are established formally (Section 1.3). Then, the static and kinematic approaches for limit state analysis are discussed (Section 1.4). Finally, the application of the Theory of Plasticity to plastic design is outlined (Section 1.5).

Chapter 2 begins with a brief overview of the specificity linked to the use of strut-and-tie networks for modelling various structural behaviours (Section 2.1), followed by a historical review of the classical theories and tools for graphical analysis (Section 2.2) with a specific focus on the question of elastic deflection lines in statically indeterminate structures. The chapter ends with an overview of the graphical tools available for structural design (Section 2.3).

Chapter 3 is the core of the thesis, since it is exclusively devoted to the question the consequences of static indeterminacy onto the reciprocal diagrams' geometric characteristics. The concept of static indeterminacy is first defined then discussed (Section 3.1) and its interpretation in terms of combination of independent stress states is proposed (Section 3.2). The understanding of the reciprocal relationships between the states of self-stress and the mechanisms in both form and force diagram are an essential prerequisite for their understanding (Section 3.3). Consequently, the implications of those relations in terms of limit state analysis of strut-and-tie networks are outlined (Section 3.4) and several perspectives for plastic design are suggested (Section 3.5).

The last three chapters are devoted to the application of graphical limit state analysis of three different types of structures: pin-jointed trusses (Chapter 4), beams subjected to bending (Chapter 5), and masonry arches (Chapter 6).

Pin-jointed trusses are first chosen to apply the graphical methodology proposed. The first section of **Chapter 4** recalls the fundamental assumptions adopted for this type of structures (Section 4.1). Afterwards, the methodology for performing a complete graphical limit analysis is presented (Section 4.2) and a six-steps optimization procedure is proposed to obtain the limit load corresponding to the limit state analysis (Section

4.3). This procedure is then applied to several case studies (Section 4.4). This section ends with some perspectives towards an extended use of parametric force diagrams for analysis as well as for design purposes. (Section 4.5).

In **Chapter 5**, we apply the same kind of graphical procedure to beams subject to bending. We begin by establishing formally the link between funicular polygon and bending moments (Section 5.1). These concepts are then applied to the limit state of funicular polygons (Section 5.2). Then the concept of geometrical admissible domain for the poles of the funicular polygons is introduced (Section 5.3). Its construction for statically determinate and indeterminate beams is detailed and applied subsequently to several case studies (Section 5.4).

Finally, the case of masonry arches is addressed in **Chapter 6**. After a brief overview of the main theories for masonry arches (Section 6.1), and a specific focus on the thrust line theory (Section 6.2), admissible geometrical domains are constructed for masonry arches (Section 6.3) using the concepts developed for beams in the previous section. Some graphical indicators of the structural safety of these specific structures are then proposed and discussed (Section 6.4).

The final conclusions recall the main results obtained and suggest some future work that would allow the approach to be integrated within graphical plastic design procedures, as well as necessary developments in the field of structural safety estimation.

Chapter 1

Plastic design and limit state analysis

In this chapter, the Theory of Plasticity is presented. It consists in a mechanical theory for which specific rheological assumptions are made on the ductile behaviour of the structural material.

The first section highlights the field in which this theory is used for structural design and analysis. The formal hypotheses and the consecutive fundamental theorems are then synthetically exposed. Finally, the available methods for applying this theory to the limit state analysis or design of structures are exposed.

1.1 Structural design and analysis

The role of structural engineering. The structural engineer's main task consists in ensuring three primary requirements: stability, strength and stiffness (Heyman, 2008). The first of these fundamental requirements is fulfilled as soon as the reaction forces and the internal stresses distribution are in equilibrium with the applied loads. The second requirement consists in ensuring that these internal stresses nowhere exceed the structural material's carrying capacity. The last one is related to the behaviour of the structure in service state and consists in ensuring its good response in terms of deformations under the various working load cases.

Recently, additional requirements concerning the robustness of the structural design has been integrated in design codes. Robustness is defined as the ability of a structure to withstand events like fire, explosions, impact or the consequences of human error, without being damaged to an extent disproportionate to the original cause (EN90, 1990). Various approaches exist for achieving this objective that are linked with the understanding of this definition. For instance, when considering robustness as a form of insensitivity to local failure, it emphasises the capacity of force redistribution in a structure (Deschuyteneer et al., 2015).

Beside these requirements, other considerations related to architectural space and significance, construction processes, sustainability, maintenance, cost, etc. hugely affect the design process and usually involve many other protagonists of the building sphere (Addis, 1994; Fivet, 2013).

Theories for structural engineering. Structural engineers may adopt different design or analysis strategies to ensure that these requirements are fulfilled, taking into account the available data, theories, methods and tools. Fivet (2013) identifies three types of theories available for structural analysis and design:

– Rheological models describing the properties of structural materials: yield strength, stress-strain relationships, time-depending behaviour, etc.

– Mechanical theories concerning the behaviour of structures. The most significant ones date back from the nineteenth century (Heyman, 1998; Charlton, 2002) and aim to understand the relationship between forces in equilibrium and the related displacements.

– Theories concerning modeling tools for predicting or analyzing the response of the structures in terms of equilibrium, strength and stiffness.

Ultimate limit states theory. The Theory of Plasticity is a particularly interesting mechanical theory based on very specific rheological assumptions about the behaviour of the structural material. It provides a theoretical framework for the ultimate limit state (ULS) analysis and design of structures as defined by the eurocodes (EN90, 1990). Taking advantage of this theory, particularly of its lower-bound theorem (see section 1.3), engineers have developed methodologies for structural design that allow them to chose - with several restrictions - distributions of stresses for ensuring the stability and strength criteria. The following sections highlight the hypotheses and the consecutive fundamental theorems of this theory, as well as the methods developed for applying it to the limit state analysis or design of structures.

1.2 Theory of Plasticity

When equilibrium considerations only are not sufficient to define the stress distribution within structures because of their static indeterminacy, engineers may search for other constraints to describe it unequivocally. Considering linear proportionality between stresses and strains is one of them, that has been popularised by the elastic beam theory of Henri Navier (1826).

> *For many generations, engineers have based the analysis and design of structures on a linear theory of elasticity with satisfactory results.* (Hodge, 1959)

However, during the second quarter of the twentieth century, scientists from the theory of structures and applied mechanics disciplines exposed the linear elastic stress-strain relationship expressed by Hooke's law to the criticism of reality (Kurrer, 2008).

For engineers, elastic design methods have indeed its disadvantages. The first one is that elastic analysis of all but the simplest structures is far from easy to achieve (Hodge, 1959). The necessary simplifying assumptions often create a gap between the rigorous elasticity theory and its engineering applications. One of these assumptions is that the structure would be free of stress before the loads are applied, which is rather uncommon. Indeed, the initial stress state acting within the structure before loading may influence the elastic solution, so that elastic analysis is frequently unrealistic. Furthermore, although most of the classic structural materials follow a linear elastic behaviour under the working conditions, some (steel, aluminum, reinforced concrete...) present a ductile behaviour characterised by strains much larger that those encountered within the elastic limit. This means that stresses calculated using elastic stress-strain compatibility may be incorrect, particularly when looking into the ultimate load capacity of statically indeterminate structures. For structures presenting this property, local stresses exceeding the elastic capacity may be due to support settlements, thermal and shrinkage effects, fabrication and construction imperfections, localised self-stresses, etc. (Massonnet and Save, 1961).

This discrepancy between elastic solution and actual bearing capacity has been evidenced by experiments on some specific steel structures in the very early twentieth century by Kazinczy (Heyman, 1998), followed by Maier-Leibnitz (Kurrer, 2008). The theoretical development of an ultimate load theory initiated by Kist in 1917 has been developed by Gvozdev in Russia and then independently established by Drücker, Greenberg, and Prager in 1951 (Kamenjarzh, 1996). The latter, together with Baker and then Heyman, introduced and mainstreamed the ultimate load method in the UK and the USA for steel frames; see for instance Baker et al. (1956) or Hodge (1959). The fundamental theorems of limit analysis already established by Gvozdev in 1936 are presented in the next section. More recently, the theory has been extended to reinforced concrete structures (Muttoni et al., 1996; Massonnet and Save, 1961) and even to masonry structures by Heyman (1995).

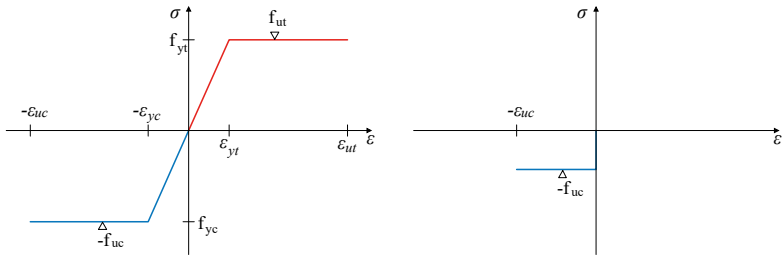

Figure 1 *Material behaviour law following the Theory of Plasticity. Left: idealised stress-strain curve for an isotropic elastic-plastic material. Right: idealised stress-strain curve for a rigid-plastic material without tensile strength.*

This so-called *Theory of Plasticity* offers thus at least a partial answer to the objections made against elasticity: it takes into account the ductility and its consequent stresses re-distributions, and provides mathematically simpler methods. The essence of this theory is to consider any structure as an *intelligent structure* (Hodge, 1959), *i.e.* a structure able to reorganise its internal stresses distribution following the loading conditions. One may even consider them as *benevolent structures* since they will adopt such a distribution of stresses in equilibrium in order to avoid collapse as long as it is possible.

The method is not fundamentally suited to address the question of deformations - although this is possible (Hodge, 1959). On the contrary it is essentially devoted to determine the strength of a structure, providing its constitutive material is sufficiently ductile (elastic-plastic or rigid-plastic materials), and that no local nor global instability can occur.

1.3 Fundamental theorems of Plasticity

Collapse load factor. The ultimate goal of the Theory of Plasticity is thus to provide methods for the design or the analysis of a structure, *i.e.* for anticipating or evaluating correctly its overall strength. This can be measured by the ratio λ_u of the maximum safe load that may be applied on the structure, to the actually applied one. By extension, given a loaded structure, the ultimate goal of limit analysis is to evaluate this collapse load factor λ_u. It is defined as the maximum multiplier applicable to the magnitude of all forces that constitute the external load case applied to the structure $\{\mathbf{q}\}$, in order to obtain the set of forces $\{\mathbf{q}\}_u$ that make the structure collapsing. This proportionality is expressed by Equation 1:

$$\lambda_u \cdot \{\mathbf{q}\} = \{\mathbf{q}\}_u \tag{1}$$

Definitions. Three well-established fundamental theorems allow to determine the maximum multiplier λ of the applied loads $\{\mathbf{q}\}$ that a structure made of elastic-plastic or rigid-plastic material can support. We use the following concepts to express these theorems:

Load factor λ**,** any multiplier applied to the external loads $\{\mathbf{q}\}$;

Collapse load factor λ_u**,** the maximum multiplier that may be applied to the external loads $\{\mathbf{q}\}$;

Statically admissible stress state S**,** a distribution of stresses over the entire structure satisfying the following two conditions:

- The stresses are in internal and external equilibrium with the external loads $\lambda \cdot \{\mathbf{q}\}$;
- The stresses nowhere exceed the yield stresses in magnitude;

Static load factor λ_s**,** a load factor for which it exists at least one statically admissible field in equilibrium with the loads $\lambda_s \cdot \{\mathbf{q}\}$;

Kinematically admissible mechanism K**,** a mechanism described by a field of virtual displacements permitting an infinitesimal motion of all or parts of the mechanism, without violating the boundary and support conditions;

Kinematic load factor λ_k**,** a load factor for which it exists at least one kinematically admissible mechanism produced by $\lambda_k \cdot \{\mathbf{q}\}$.

The three fundamental theorems of the Theory of Plasticity may then be expressed in terms of possible values for the load factor λ as follows (Heyman, 2008):

Upper-bound theorem. Any kinematic load factor λ_k calculated from a kinematically compatible mechanism is greater than or equal to the collapse load factor λ_u.

$$\lambda_{k,i} \geq \lambda_u \qquad \forall i \tag{2}$$

Lower-bound theorem. Any static load factor λ_s calculated from a statically admissible stress field is lower than or equal to the collapse load factor λ_u:

$$\lambda_{s,j} \leq \lambda_u \qquad \forall j \tag{3}$$

Uniqueness theorem. The collapse load factor λ_u is unique.

These three theorems can be synthetically expressed by Equation 4:

$$\lambda_{s,j} \leq \lambda_u \leq \lambda_{k,i} \qquad \forall i, j \tag{4}$$

where $\lambda_{k,i}$ is the load factor corresponding to the ith kinematically compatible mechanism and $\lambda_{s,j}$ the load factor corresponding to the jth statically compatible stress field.

A complete proof of these theorems can be found in numerous books; see for instance Hodge (1959).

Limit state analysis *versus* plastic design. The plastic theorems have been extensively used to analyse the behaviour of ductile structures at collapse, *i.e.* to perform structural limit state analysis. Depending on the approach followed (kinematic or static), this analysis makes use of either the upper-bound theorem or the lower-bound theorem to determine the collapse load factor.

Besides the development of limit state analysis, design-oriented methodologies have been elaborated to take advantages of the lower-bound theorem of plasticity. These safe and flexible methods for structural design are commonly referred in the following as "plastic design".

The theoretical foundation of both limit state analysis and plastic design are examined on the next two sections of this chapter.

1.4 Limit state analysis

Applying the Theory of Plasticity to the limit state analysis of given structures implies choosing a modelling strategy in accordance with the hypotheses leading each of the fundamental theorems. Approaches for limit state analysis of structures may be divided in two categories, kinematic and static, based on either the upper-bound or the lower-bound theorem. Their differences are outlined in the following sections.

1.4.1 Kinematic *versus* geometric views of statics

Numerous approaches have been developed through history for modelling the behaviour of structures. These structural theories can be gathered within two groups, depending on the fundamental point of view adopted for developing them, what Karl-Eugen Kurrer (2008) calls *the kinematic or geometric view of statics*.

Kinematic view of statics. The kinematic view consists in considering a structure as a mechanism without movement. The approaches related to this view mainly refer to the first law of thermodynamics (conservation of energy). Consequently, a structure in an unstable equilibrium is considered as a conservative system. In such a system, the work done by the external forces must be equal to the one done by the internal stresses (Eq. 5).

$$W_{ext} = W_{int} \tag{5}$$

The fundamental Principle of Virtual Works (PVW) states that this relationship is valid for any kinematically admissible virtual field of displacements $\delta\mathbf{u}$ and its related strains $\delta\boldsymbol{\epsilon}$. Equation 5 can be then be developed as follows:

$$\delta W_{ext} = \int_{\Omega} \mathbf{q} \cdot \delta\mathbf{u} \, \mathrm{d}\omega = \delta W_{int} = \int_{\Omega} \boldsymbol{\sigma} : \delta\boldsymbol{\epsilon} \, \mathrm{d}\omega \tag{6}$$

With:

– Ω a conservative mechanical system,

– $\mathrm{d}\omega$ any infinitesimal part of this system,

– $\mathbf{q}$ the external forces vector applied on $\mathrm{d}\omega$,

– $\delta\mathbf{u}$ the virtual displacement vector of $\mathrm{d}\omega$,

– $\boldsymbol{\sigma}$ the tensor of the internal stresses,

– $\delta\boldsymbol{\epsilon}$ the tensor of the virtual strains.

During the 19th century, this principle has generated important results in the field of elastic systems theory, known as the energetic theorems of Menabrea Menabrea (1875), Betti, Maxwell (1864b), Castigliano (1873), etc.

In **Figure 2** this principle is applied to calculate the value of the bending moment in the middle span of the simply supported beam AB. Thanks to a kinematically admissible field of displacements, for which the rotational deformations are concentrated within this section, the virtual works can be written as follows:

$$W_{ext} = q \cdot \frac{\theta L}{2} = W_{int} = M \cdot 2\theta \leftrightarrow M = \frac{qL}{4} \tag{7}$$

In particular, the virtual field of displacements may be chosen to correspond to a kinematically admissible mechanism (Timoshenko and Young, 1945). In such a way that the upper-bound theorem of limit analysis may be applied to classical structures like pin-jointed trusses and beams, as well as to structures showing a more complex behaviour like masonry arches. The latters' structural analysis is far from being obvious because of the discontinuous, heterogeneous, inelastic properties of the structural material. Taking the arch as a kinematic assembly of rigid blocks in equilibrium is one of the possible ways to deal with it.

Geometric view of statics. During the same period, celled by Kurrer (2008) *discipline-formation period of theory of structures*, another type of approaches was developed. Those methods make statics dependent of geometry, focusing on the equilibrium conditions of resulting forces acting on elements while considering real rather than potential static conditions. These approaches are based on the *Principle of forces equilibrium* or, graphically, the *Principle of the parallelogram* (Timoshenko and Young, 1945). Benvenuto (1985) analysed this principle in depth while analysing

its historical development. Based on the geometric view of statics, a structure is seen as a materialised system of forces. Their equilibrium can be defined analytically by equating the components of the resulting vectors and its moment to zero. Graphically, the equilibrium can be defined by the closure of the polygon of forces applied to any point of the structure. In **Figure 2**, the bending moment acting in the central cross section of the simply supported beam is deduced from geometrical equilibrium considerations expressed graphically on each node:

$$M = \mu \cdot H = \frac{L \cdot tan(\theta)}{2} \cdot \frac{q}{2 \cdot tan(\theta)} \leftrightarrow M = \frac{qL}{4} \tag{8}$$

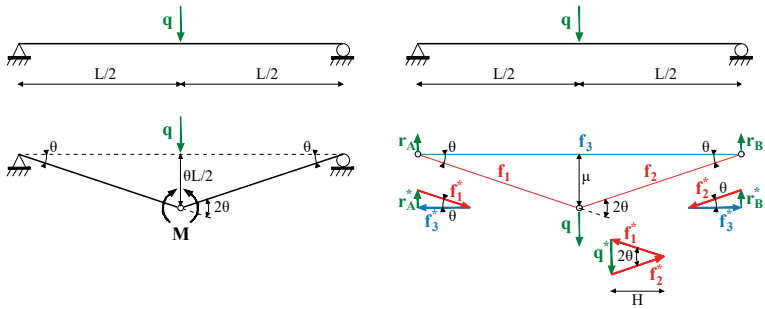

Figure 2 *Kinematic (left) versus geometric (right) views of statics.*

Kinematic *versus* static approaches for structural analysis. Both types of approaches are valid; choosing one or the other depends on the structural typology, on the assumed behaviour for the structural material, on the objective to reach in terms of design or analysis, and of the tools available to achieve it. In particular, if the structural material presents sufficient ductile properties for the Theory of Plasticity to be applied, and if the structure's geometry presents some static indeterminacy allowing the internal redistribution of stresses, limit state analysis can be achieved using either kinematic or a static approaches. The first ones refer to the upper-bound theorem and to the kinematic view of statics, while the second ones take advantage of the lower-bound theorem of plasticity within a geometric view of statics. The relationship between Kurrer (2008)'s views of statics, Timoshenko and Young (1945)'s fundamental

theorems for structural analysis, and static and kinematic approaches in the context of the Theory of Plasticity are drafted in **Figure 3**.

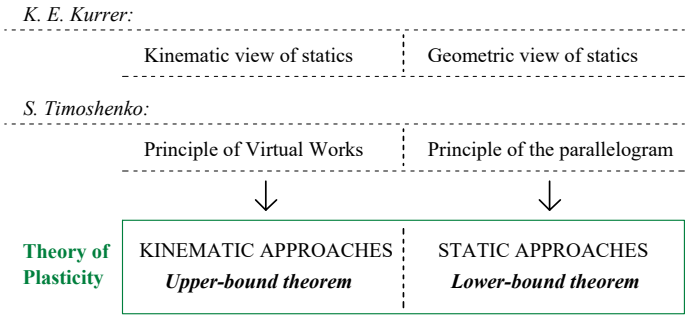

Figure 3 *Kinematic vs geometric views of statics in relation to the theorems of plasticity.*

1.4.2 Kinematic approaches and upper-bound theorem

The kinematic approaches for limit state analysis are founded on the upper-bound theorem of plasticity (Eq. 2). They aim at finding the exact value for λ_k, *i.e.* the minimum value of all the possible kinematic load factors, by identifying the collapse mechanism and determining its related load factor. Since the plastic behaviour of the material at collapse implies that the superposition principle of structural actions cannot be applied, all the possible kinematically compatible mechanisms and their corresponding load factors $\lambda_{k,i}$ should be taken into account in order to obtain the actual collapse load factor:

$$\lambda_u = min_i\{\lambda_{k,i}\} \tag{9}$$

It is common to use energetic considerations on rigid-body-like mechanisms K (Marti, 2013). The Principle of Virtual Works (PVW) appears particularly useful to achieve this kinematic limit analysis due to the fact that the work originated from the external forces and the one resulting from the internal stresses are equal (Thompson and Haywood, 1986), as expressed by Equation 6. Indeed, when choosing a kinematically admissible mechanism as virtual field of displacements, the work of the internal

stresses acting within the structure is assumed to be equal to the one produced by yielding, since the working strains can be neglected with respect to the ones corresponding to yielding. Equation 6 can then be adapted to any kind of structures provided hypotheses of the Theory of Plasticity are respected, in particular to the ones discussed in chapters 4, 5 and 6 of this dissertation: pin-jointed trusses, beams and masonry arches.

Pin-jointed trusses. In case of pin-jointed trusses, only normal forces can act within the bars. Therefore the yield condition can be written as follows:

$$\mathrm{f_b} \leq \mathrm{f_{u,b}} \tag{10}$$

$\mathrm{f_b}$ being the magnitude of the normal force acting in bar b and $\mathrm{f_{u,b}}$ the magnitude of the ultimate plastic normal force that can be supported by bar b without local instability.

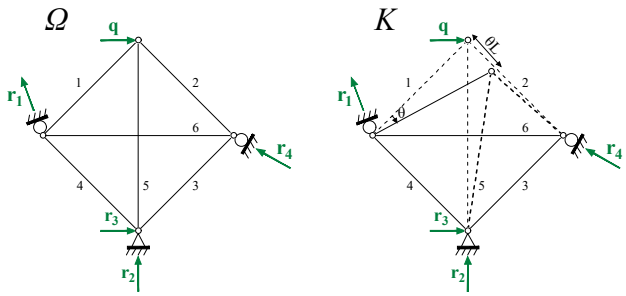

Figure 4 *Kinematic limit state analysis of a statically indeterminate pin-jointed truss.*

When applying a limit analysis, we consider that elastic strains may be neglected with respect to plastic ones (Hodge, 1959). This way, the internal work produced by deformations can be calculated taking into account the yielded bars only, *i.e.* the bars β subject to normal forces which magnitude is equal to the full plastic normal force $\mathrm{f_u}$. Equation 6 becomes:

$$\delta W_{ext} = \sum_n \mathbf{q_n} \cdot \delta \mathbf{u_n} = \delta W_{int} = \sum_\beta \mathrm{f_{u,\beta}} \cdot \delta l_\beta \tag{11}$$

With $\mathbf{q_n}$ the force acting on node n, $\delta\mathbf{u_n}$ the displacement vector of node n, $\mathrm{f_{u,\beta}}$ the ultimate normal force acting in yielded bar β, and δl_β its variation in length.

Figure 4 shows a kinematic limit state analysis using the PVW on a simple pin-jointed truss Ω using mechanism K:

$$W_{ext}^{K} = \mathrm{q} \cdot \theta L \frac{\sqrt{2}}{2} = W_{int}^{K} = \mathrm{f_{u,2}} \cdot \theta L + \mathrm{f_{u,5}} \cdot \theta L \frac{\sqrt{2}}{2} \tag{12}$$

Beams. In case of a plane structure Ω subject to bending, the internal work is due to the bending stresses reduced for any cross section ω to a shear force V_ω and a bending moment M_ω with γ_ω and θ_ω respectively representing the shear and rotational deformations of section ω. Being $\{\mathbf{u}\}$ a set of external displacements that constitute a kinematically admissible field, and being $\{\mathrm{V}_\omega, \mathrm{M}_\omega\}$ a set of internal stresses in internal and external equilibrium with a set of applied loads $\{\mathbf{q}\}$, the virtual works equation (Eq. 6) can be written as:

$$\delta W_{ext} = \int_\Omega \mathbf{q} \cdot \delta\mathbf{u} \, \mathrm{d}\omega = \delta W_{int} = \int_\Omega \mathrm{V}_\omega \cdot \gamma_\omega + \int_\Omega \mathrm{M}_\omega \cdot \theta_\omega \tag{13}$$

A fundamental assumption when applying plastic analysis to bending structures is that shear forces, axial forces and torsional couples have no effect upon the carrying capacities of beams and frames. This assumption is in accordance with experiment and mathematically justified (see for instance Hodge (1959)). It tremendously simplifies the analysis because the resistance of a section is exclusively defined by its full plastic moment M_u. In the sections where the moment equals this value, most of the fibers are at the yield stress and extend indefinitely. In those sections, a plastic hinge κ is formed. A plastic hinge is defined as a cross section that does not allow any angular discontinuity as long as the bending moment M remains less than M_u in magnitude, and that is able to turn freely in the direction of an applied moment which magnitude is equal to M_u (Massonnet and Save, 1961).

In case of a kinematic limit analysis the field of internal deformations $\{\gamma_\omega, \theta_\omega\}$ and external deflections $\{\mathbf{u}\}$ is chosen to correspond to a kinematically admissible mechanism K in which the internal work is produced exclusively within the plastic hinges κ by the full plastic moment

$M_{u,\kappa}$ onto the corresponding rotational discontinuities θ_κ.

Equation 13 then becomes:

$$W_{ext}^K = \int_K \mathbf{q} \cdot \mathbf{u} = W_{int}^K = \sum_\kappa \mathrm{M_{u,\kappa}} \cdot \theta_\kappa \tag{14}$$

Figure 5 shows a kinematic limit state analysis of a statically indeterminate beam Ω:

$$W_{ext}^K = \mathrm{q_1} \cdot \theta_A L_1 + \mathrm{q_2} \cdot \theta_B L_3 = W_{int}^K = M_{u,A} \cdot \theta_A + M_{u,2} \cdot (\theta_A + \theta_B) \tag{15}$$

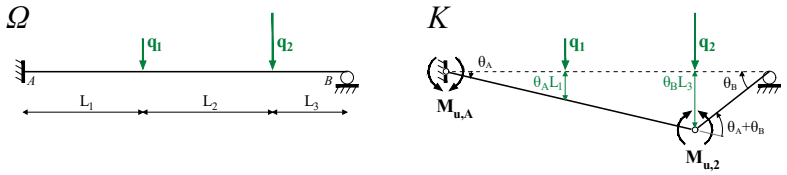

Figure 5 *Kinematic limit state analysis of a statically indeterminate beam.*

Masonry arches. Considering the potential kinematic equilibrium conditions of the various kinematically admissible collapse mechanisms of masonry arches **(Fig. 6)**, a limit state analysis can be applied using the PVW. Foce and Aita (2005) and Smars (2002) propose a deep discussion of the hypotheses necessary to study this kind of structures.

Kinematic methods are very efficient when it comes to find the value of the load factor $\lambda_{k,i}$ associated with every kinematically compatible mechanism K_i. Yet, the potential high amount of possible mechanisms and their kinematical complexity remain an evident drawback. Furthermore, the given solutions for these load factors are unsafe in the sense that Equation 2 states they all are upper-bound values for the actual collapse load factor λ_u. This means that being able to know only an incomplete subset of all the possible mechanisms may lead to overestimating the bearing capacity of the structure.

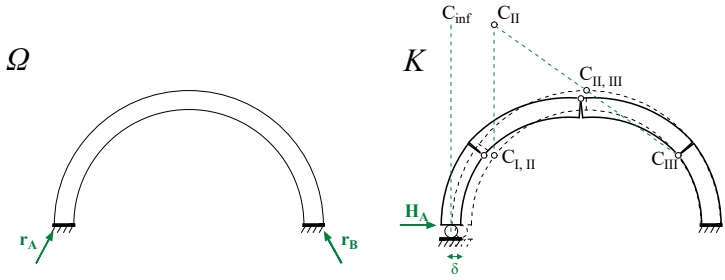

Figure 6 *One possible collapse mechanism for a masonry arch.*

1.4.3 Static approaches and lower-bound theorem

Static approaches for limit state analysis have been developed on the basis of the lower-bound theorem of plasticity. They take into account the successive plasticizing of elements when increasing the load factor until the structure is turned into a collapse mechanism. Every possible load factor $\lambda_{s,i}$ obtained using a static approach that respects the boundary and yield conditions should be calculated (Rjanitsyn, 1959), so that:

$$\lambda_u = max_j\{\lambda_{s,i}\} \tag{16}$$

A classical method consists in studying the internal forces distribution by means of superimposition of free and reactant diagrams in equilibrium on statically determinate sub-structures (see for instance Massonnet and Save (1961); Horne (1979); Heyman (2008)). The final force distribution must satisfy the equilibrium and yield conditions. If this distribution is such that the full plastic resistance is reached in a sufficient amount of parts of the structure to form a mechanism, then, the value of the load factor is the value of the collapse one. Contrarily to the kinematic approaches, these approaches can be regarded as safe. Indeed, were some of the statically admissible distributions of forces to be omitted, this incomplete analysis would only lead to an underestimation of the effective collapse load factor λ_u.

In **Figure 7**, we illustrate this approach in the case of a masonry arch: the geometrical conditions for its static equilibrium are verified by tracing a thrust line (*i.e.* a path for the resulting compressive force acting inside

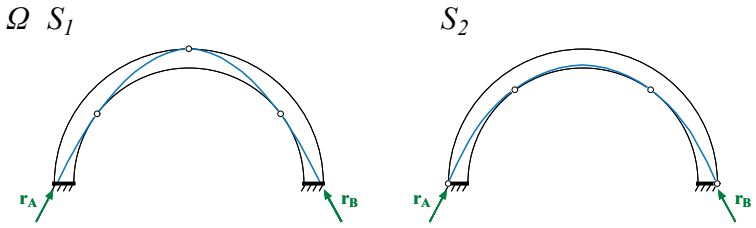

Figure 7 *Geometric view of statics: two admissible stress states (thrust lines) S_1 and S_2 within a semi-circular masonry arch.*

the arch) that lies entirely within the masonry envelope. This *equilibrium approach* (Huerta, 2001), called the thrust line theory for masonry arches, was developed almost two centuries ago for the design and assessment of masonry arches and is developed in the last chapter of this dissertation.

One specific static approach that uses reciprocal diagrams of Graphic Statics is proposed in the next chapters of this dissertation.

1.4.4 Complete limit state analysis

Combining both upper-bound and lower-bound theorems of limit analysis with the uniqueness theorem results into a complete limit state analysis of the structure: if a given system of applied loads in equilibrium with the internal stresses corresponds to a kinematically admissible mechanism on the one side, and to a statically admissible stress state on the other side, the value of the load factor associated with this system of loads should be exactly equal to the collapse one λ_u. Therefore, if the same load factor is obtained by both a kinematic limit state analysis on admissible mechanisms and a static limit state analysis on admissible stress states, it ensures that this load factor is the one that needs to be applied on the loads to provoke the collapse of the structure.

Table 1 gives a synthesis of this statement. It is illustrated in **Figure 8** by an example inspired by Schwartz (2016): the limit analysis of the statically indeterminate beam is made by means of three possible limit cases in equilibrium. In the first case (A), the mechanism K_A is kinematically admissible but corresponds to a stress state S_A (*i.e.* a bending moment diagram) in which the yield condition is violated ($M_2 \geq M_u$). On the con-

Condition:	Type of limit analysis: Static	Complete	Kinematic
Equilibrium	ok	ok	ok
Yield condition	ok	ok	-
Mechanism	-	ok	ok
Theorem:	Lower-bound		Upper-bound
Load factor:	$\lambda_{s,j} \leq$	λ_u	$\leq \lambda_{k,i}$

Table 1 *Lower-bound and upper-bound theorems of limit analysis.*

trary, the statically admissible stress state S_B respects the yield condition in every section ($M \leq M_u$) but the corresponding mechanism K_B is not kinematically admissible since it does not respect the support conditions. The collapse limit state is identified as case C where both mechanism K_C and stress state S_C are admissible. They consequently give the same value for the collapse load factor:

$$\lambda_{k,u} = \lambda_{s,u} = \frac{2M_u}{5qL} \tag{17}$$

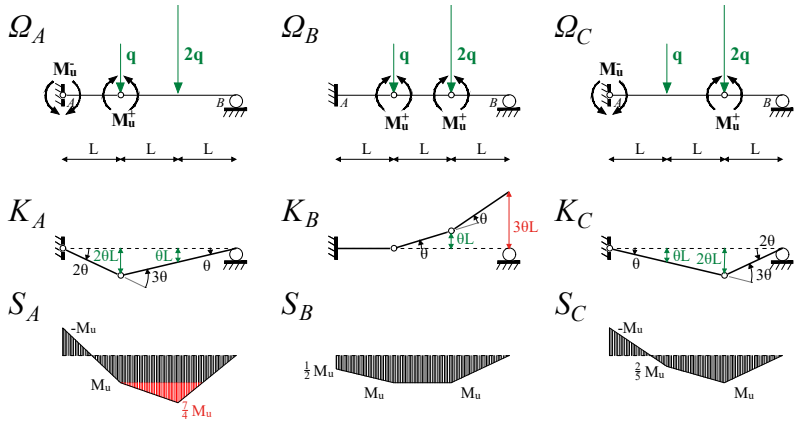

Figure 8 *Complete limit analysis of a statically indeterminate beam.*

1.5 Plastic design

> ***Given a design load case, any statically admissible stress state is a safe plastic solution to the structural design problem.***

This formulation of the lower-bound theorem of plasticity can be considered as the keystone of the plastic approaches of structural design. Its application is conditioned to simplifying assumptions linked to the rheological model of the material and to the fulfillment of the equilibrium and yield conditions. It ensures that, for a material presenting a sufficient ductility (rigid- or elastic- perfectly plastic behaviour), any chosen distribution of stresses in equilibrium with a chosen load case that nowhere exceeds the material specific strength is a suitable solution - even better: a safe solution - for ensuring the stability and strength criteria. These "static" design approaches can only lead to an underestimation of the load bearing capacity of the structure. Therefore, they ensure the safety of a structure through the existence of, at least, one distribution of stresses in equilibrium that abides by the boundary and yield conditions of the building material.

Lower-bound design. The lower-bound theorem can be considered as an outstanding design tool (Zastavni, 2008) since it gives the freedom to the designer to chose one statically admissible stress state, avoiding the need to identify the one actually acting within the structure (Frey, 2000). In hands of talented structural engineers, it has provided the most rapid methods for the initial shaping of structures (Fivet, 2013). The design methodology of the Swiss engineer Robert Maillart for the Salginatoble Bridge can be seen as an exemplary application of this theorem (Fivet and Zastavni, 2012).

Plastic design process. The complexity related to static indeterminacy can usually be avoided by choosing one statically admissible stress state, on which the structural design is based. This stress state is constructed in such a way that it stands in equilibrium with a set of applied loads chosen as design load case (step 1 in **Figure 9**). The magnitude of the internal stresses generated within the different parts of the structure can

be controlled by means of appropriate tools, and the sections of the structural elements can be adapted to correspond to the structural material strength (step 2). Since the chosen stress state in equilibrium with the design loads may correspond to a kinematically indeterminate mechanism, such as in **Figure 9**, the corresponding structure may be unstable. The last step of the design procedure consists in ensuring the stability of the structure against load cases that differ from the design load case, by adding stiffening elements to the structure (step 3).

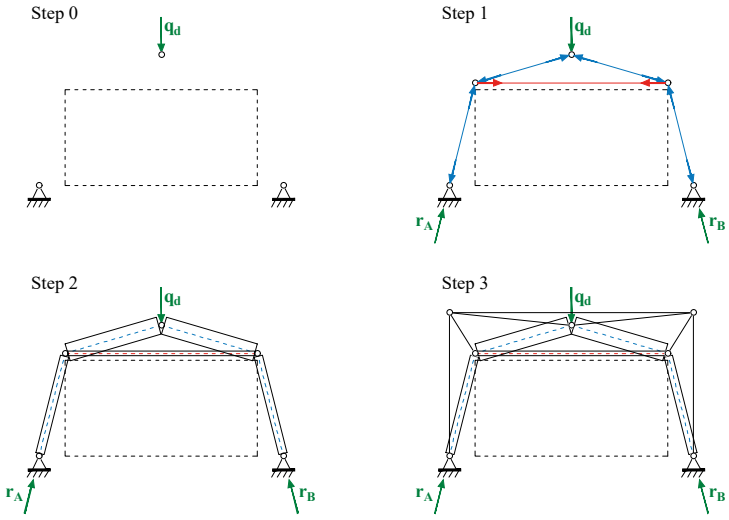

Figure 9 *Structural design process.*

After the design process. However, when it comes to the validation of the solution adopted at the end of the process, the designer may need to evaluate the response of the final proposal with respect to manifold criteria: quantity of construction material, simplicity of the building process, costs, robustness, etc. Each of them requires a different type of analysis. One of those criteria, related to design safety, consists in evaluating the overall strength of the structure by comparing the ultimate load the structure can support to the one the structure is designed for.
Though, because of the static indeterminacy generated by stiffening the

original kinematically indeterminate stress field, the structure usually becomes statically indeterminate. Indeed, taking into account that the stiffening elements of the structure are also able to participate to the overall strength, they have an influence on the global load bearing capacity of the structure **(Fig. 10)**. In addition, the supposed plastic behaviour makes it impossible to determine the actual state of stress acting within the structure. Indeed, the use of the lower-bound theorem for plastic design only ensures the assumed stress field is one of the numerous statically admissible distributions of the stresses within the structural members.

Numerous tools exist for the analysis of structures, depending on the expected outputs. Those tools are not always design-oriented and often necessitate a given geometry and sizing as input data. The information they provide is then subsequent to the design process and often not interactive. If information about the effective load bearing capacity of the structure was available during the design process, it would influence the engineers when making a decision. With this solution they could refine the *dimensioning* towards more efficient solutions.

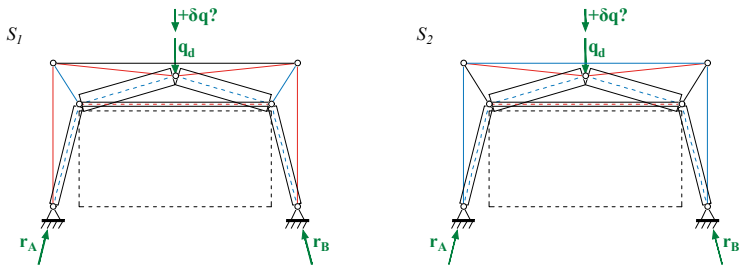

Figure 10 *Influence of the stiffening on the load bearing capacity.*

The next chapter presents one design tool particularly efficient for early stage structural plastic design.

Chapter 2

Strut-and-tie modeling using graphic statics

Modelling the structural behaviour of complex structures by strut-and-tie networks is a common practice in structural engineering, which has been effectively evidenced by several contemporary structural engineers. In the past, the use of the reciprocal diagrams of graphic statics for managing the static equilibrium of these networks revealed being an elegant and efficient method for the design and analysis of many types of structures. Nowadays, parametric tools for constructing and manipulating both form and force diagrams have been developed. Those tools allows a continuous and visual control of the results of the structural analysis as well as for design purposes.

In this chapter, the use of strut-and-ties networks for modeling structural behaviours is explained Then the fundamentals of graphic statics are reviewed from the parallelogram of forces to reciprocal form and force diagrams with some insights on the graphical calculation of elastic deformation. Finally several recent applications for structural design are listed .

2.1 Strut-and-tie networks for structural analysis and design

Methods and tools for structural analysis. In his PhD thesis, Fivet (2013) identifies four partial but complementary aspects that help to identify and classify the numerous tools available for structural analysis and design: the assumed rheological model; representation mode; the required inputs and expected outputs; and the inner solution method. In the previous chapter, simplified hypotheses on the rheological behaviour of the structural material have been adopted, which allow the application of the Theory of Plasticity for both analysis and design. Among the numerous models of representation of the structure and its mechanical behaviour, this dissertation focuses on strut-and-tie models to handle discontinuous stress fields (Marti, 2013; Muttoni et al., 1996) acting within the structure. These networks may be intended as pin-jointed frameworks, or as strut-and-tie models within a continuum of material. The use of strut-and-tie networks goes back to the nineteenth century for the analysis of pin-jointed trusses or suspension bridges (Charlton, 2002) and was extended to study other types of structures showing a plastic behaviour such as reinforced concrete beams (Marti, 2013) or for the computation of the thrust line within masonry structures (Ungewitter and Mohrmann, 1901).

Strut-and-tie modelling and plastic design. Strut-and-tie models are considered by Fivet (2013) as high-level structural abstractions that depict the force path acting inside a structure in the most reduced way. It is composed only of rods in compression - *struts* - or traction - *ties* - linking together pin-jointed nodes on which point forces are applied. They can be used as generic abstractions for many types of structures such as pin-jointed frameworks or beams and frames subjected to bending moments, but also to trace lines of thrust in compression-only structures. More generally, thanks to the lower-bound theorem of plasticity, any continuous structural system made of plastic material (e.g. reinforced concrete) can be modeled by a strut-and-tie network.

Figure 11 shows strut-and-tie network in equilibrium with the applied loads, which may be used to model the stresses distribution within a concrete panel as well as the inner forces acting within the bars of a pin-

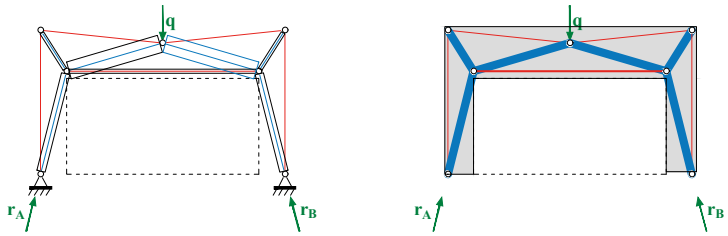

Figure 11 *Strut-and-tie network*

jointed truss or a continuous frame.

This approach initiated by Mörsch (1929) and developed by Muttoni et al. (1996) for reinforced concrete structures, is the theoretical basis for the recent developments achieved in the *Chair of Structural Design* of Prof. Joseph Schwartz at ETH Zürich. Following this approach, the final design is highly dependent on the initial choices made by the designer for establishing the first equilibrium configuration; an adequate choice requires a certain experience and knowledge from the structural engineer.

Graphic equilibrium of strut-and-tie networks. Researchers like Muttoni et al. (1996) or Zastavni et al. (2016) and Deschuyteneer et al. (2018a), have recently shown that strut-and-tie modeling can easily be combined with graphic statics to provide an elegant and efficient method for the design and analysis of reinforced concrete structures. Indeed, the use of reciprocal form and force diagrams gives direct and simultaneous insight on the static behaviour of every structural member. Zastavni (2008) evidenced the use of graphic statics in Maillart's practice for designing bridges and other structures; see Fivet and Zastavni (2012) for a detailed analysis of the design process of the Salginatobel Bridge. Authors like Beghini et al. (2013) and Mazurek et al. (2016) have shown that an optimization process can be applied to the set of graphic statics possible solutions in order to meet specific design requirements, such as the minimization of the volume or weight of building material.

Graphic statics has the great advantage of allowing a permanent control of the operations thanks to the direct, geometric and visual relationship between the form and force diagrams expressing graphically the structure's geometry and its state of stress. These properties are essential in the context of structural design since they help the designer to control the decision-making process, in particular when the structure can be modelled as a strut-and-tie network. The development of graphic statics was made possible thanks to the diffusion, during the first decades of the 19th century, of projective geometry within the schools of engineering, and because efficient tools for calculating the numerous new types of structures like steel trusses or beams were needed. More detailed considerations about the origin of this method, its theoretical development and its applications to design and analysis of various types of structures are discussed in the following section.

2.2 Classical graphic statics

Graphic statics provides graphical procedures that ensure translational and rotational equilibrium's of a set of forces by using two separate polygonal constructions, respectively the form and force diagrams. **Figure 12** illustrates how the static equilibrium of one point is ensured by the principle of the parallelogram and expressed through two different drawings: (1) the resultant (green) of two forces (blue and red) applied on a material point is obtained by the construction of a parallelogram based on these two forces; (2) the opposite of this resultant (green) is consequently in equilibrium with the two applied forces; (3a) rotational equilibrium is ensured by intersecting the action lines of the forces while (3b) translational equilibrium is obtained by ensuring that the three forces form a closed polygon.

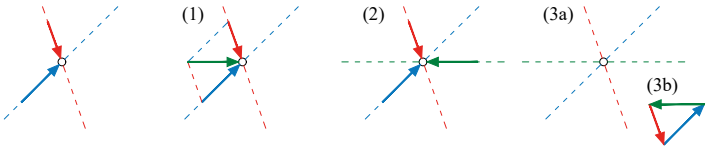

Figure 12 *Graphical equilibrium of a point.*

2.2.1 From parallelogram of forces to form and force diagrams

Premises. Though geometrical considerations were very often used through history to assess the stability of buildings, the introduction by Pierre Varignon (1725) of the concept of funicular polygon in his *Nouvelle Mécanique ou Statique* for modeling the equilibrium of a rope, can be considered as the very first use of graphic statics, since he used a separate construction made of triangles to determine the direction of the segments of the rope **(Fig. 13)**. Even if the idea of achieving the breakdown of forces into component through triangles for explaining equilibrium is due to Stevin (1586), Varignon has been the first indeed to construct consciously two

separated and correlated figures with parallel sides.

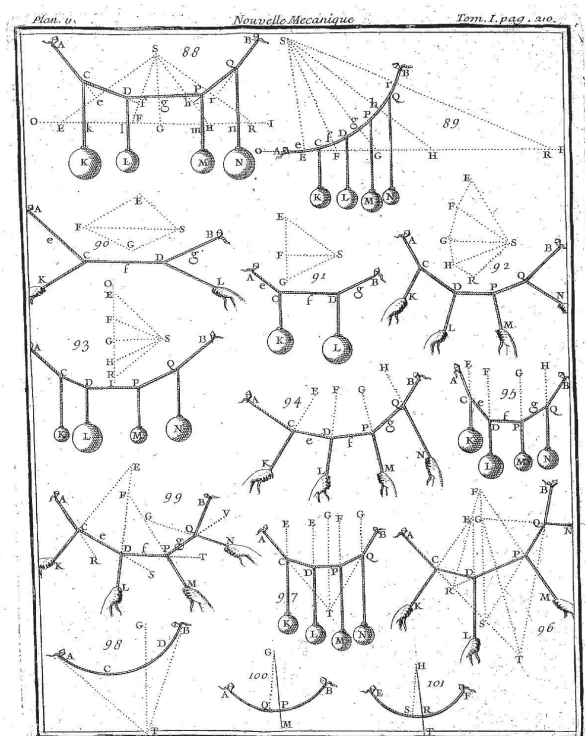

Figure 13 *Static equilibrium of a rope: funicular polygon and force polygon after Varignon (1725, Tome I, p. 210)*

Foundation of a discipline. The publication, more than one century later, of the treaties of Rankine (1864), (Culmann, 1866; 1875) and Cremona (1872), is widely considered as the foundation of the discipline of graphic statics. They have taken advantage of the profound knowledge of descriptive geometry at that time. Indeed, *"Monge managed to elevate descriptive geometry to become the language of the engineer."* (Kurrer, 2008). And in fact, his book *Géométrie descriptive* (Monge, 9495) not only contains theoretical geometric developments but also many practical

case studies useful to develop engineering practice. Note that the use of geometry to solve engineering problems has never been totally lost, nor in the academic context - see for instance the *Calcul graphique à l'usage des ingénieurs* of Masson (1952) - neither in practice (Schwartz, 2012). In particular, Poncelet (1822)'s *Traité des propriétés projectives des figures* had a great influence in the development of Culmann's work on the reciprocal relationships through projective geometry between the *funicular polygon* (*i.e.* the form diagram) and the *polygon of forces* (*i.e.* the force diagram). Culmann's work is most famous for its graphical methodology for determining the static quantities (reaction forces, shear forces, bending moments) in statically determinate beams by using a funicular polygon and a closing line (Culmann, 1880).

Though, at the same period, other scientists used graphic statics for investigating the equilibrium conditions of pin-jointed frameworks. Rankine (1858), for instance, already established the fundamental relationships between the funicular polygon and the force polygon **(Fig. 14)**, which he applied to the analysis of statically determinate trusses:

> *If lines radiating from a point be drawn parallel to the lines of resistance of the bars of a polygonal frame, then the sides of any polygon whose angles lie in those radiating lines will represent a system of forces, which, being applied to the joints of the frame, will balance each other; each such force being applied to the joint between the bars whose lines of resistance are parallel to the pair of radiating lines that enclose the side of the polygon of forces, representing the force in question. A Iso, the lengths of the radiating lines will represent the stresses along the bars to whose lines of resistance they are respectively parallel.*(Rankine, 1858, Theorem, p. 140)

2.2.2 Graphical analysis through reciprocal diagrams

Form and force diagrams as reciprocal figures. The introduction by Maxwell (1864a; 1867) and Cremona (1872) of the concept of reciprocal figures transformed the existing concepts into a universal methodology and a very efficient tool for equilibrium analysis of structures, by modelling their behaviour by pin-jointed networks (Muttoni et al., 1996). **Figure 21** reproduces the reciprocal diagrams from the 1864 paper of James Clerk Maxwell. Each segment in the form diagram **F** represents the action line

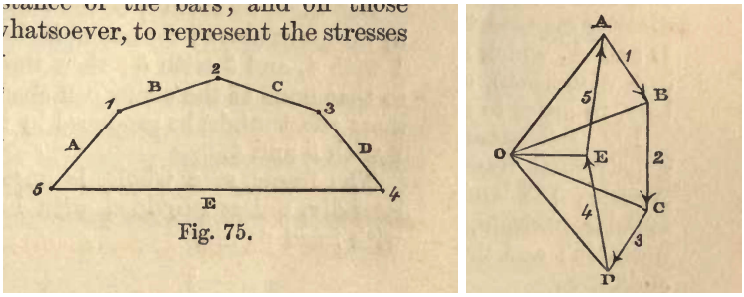

Figure 14 *Polygon of forces and correlated polygonal frame in equilibrium from Rankine (1858, fig. 75 & 75*, p. 139)*

of a force which magnitude is expressed in the reciprocal force diagram $\mathbf{F}^*$ by the length of the corresponding segment. These diagrams abide by two fundamental reciprocal relationship laws expressed hereafter:

> ***Each segment in a diagram is related to one sole segment in its reciprocal diagram, parallel to the latter.***

Maxwell (1867) showed that this property is not applicable to some specific cases, *i.e.* when the form diagram is characterised by a connectivity graph which is not planar (Micheletti, 2008). Since this question is not fundamentally relevant for the present purpose, we refer to Micheletti (2008); D'Acunto et al. (2016); Jasienski et al. (2016) among other for a detailed discussion about *planarity* and its consequences on the construction of the force diagram, especially concerning the issue of extending graphic statics to 3D.

> ***All the segments that meet in a single point in one diagram need to form a closed polygon in its reciprocal.***

This second fundamental relationship ensures that if the structure represented by one of the diagrams respects the rotational equilibrium condition, than the reciprocal expresses the translational equilibrium of the latter's nodes. **Figure 21**-c shows how the original equilibrium is modified by adding two equal and opposite forces or equivalently, by adding a rod **(Fig. 21)**-d-e in both form and force diagrams. It must be underlined that, because of their reciprocity, each of the two diagrams can be considered as a form diagram as well as a force diagram. They constitute

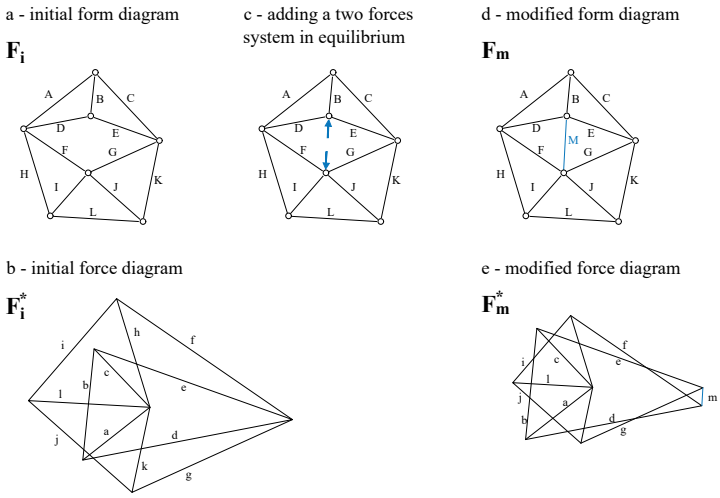

Figure 15 *Reciprocal diagrams inspired from Maxwell (1864a). The axial forces acting in the members (A to L) of the form diagram (1-a) are in equilibrium since the bars (a to l) of the reciprocal force diagram (1-b) form closed polygons. Adding a couple of forces in equilibrium (1-c) to the form diagram is equivalent to add a bar M to it (1-d); the equilibrium in the force diagram (1-e) is modified consequently by adapting the length of the segments (a to m).*

dual structures that provide graphical insight into each other, especially when assessing mechanisms and states of self-stress (Baker et al., 2013). This point will be of great importance in the following dissertation when it comes to evacuating the static and geometric indeterminacy of both form and force diagrams.

Graphical analysis. These fundamental contributions to the discipline of graphic statics have been followed by "myriads of books enhancing the range of applications of graphic statics" (Fivet, 2013): Mohr (1868); Bauschinger (1871); Bow (1873); Lévy (1874a); Du Bois (1875); Eddy (1877); Müller-Breslau (1887); Ritter (1888); Wolfe (1921); Pirard (1950;

1960). Those contributions develop methods for graphical analysis of structures, intended as "the process exposing the causal relationships modelled as functions in the structural system for the purpose of analyzing and synthesizing load bearing systems; it is therefore an intermediary between the work of the engineer and the object of his work, which in this case is present in the form of an idealised structural model." (Kurrer, 2008, p.322)

2.2.3 Elasticity and static indeterminacy

Graphic statics and elastic deflection line. The essential contributions presented in the previous section have been mainly published in a period of the history in which elastic theory prevailed. Indeed, the Navier-Bernouilli beam theory based on the linear proportionality between stress and strain, was particularly suited for the analysis of iron structures (beams, arches, trusses) under service loads. Therefore, the authors of that time attempted to use graphical constructions to determine the elastic deflections occurring within the different types of structures.

Elastic solution for statically indeterminate trusses. Taking advantage of Maxwell's theorem for calculating the displacements of nodes in pin-jointed trusses (Maxwell, 1864b), graphical methods have been developed for the elastic analysis of statically indeterminate trusses. Lander and Cotton (1914), for instance, developed a method based on the compatibility of elastic displacements **(Fig. 16)**. They analyzed rather simple cases but insisted on the great interest of his method for the efficient design of trusses.

Elastic solution for statically indeterminate beams. Culmann (1866) and Mohr (1868) first develop a methodology for tracing the elastic curve of beams by using two successive funicular polygons. They take advantage of the similarity between the bending moment/load double derivative relationship, and the deflection/bending moment one:

$$q(x) = \frac{d^2M(x)}{dx^2} - EI \cdot M(x) = \frac{d^2y(x)}{dx^2} \tag{18}$$

and obtain the elastic curve by tracing a funicular polygon which corresponding "loads" magnitudes are given by the areas of the bending moment diagrams defined by the first funicular polygon **(Fig. 17)**.

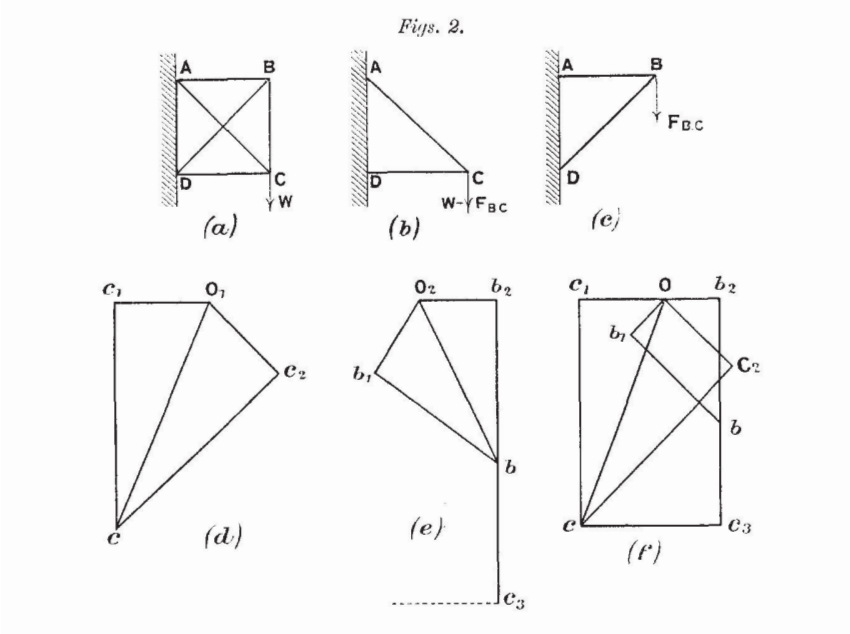

Figure 16 *Graphical procedure for determining the stresses in a statically indeterminate truss. (Lander and Cotton, 1914, p.302)*

Being known the graphical method for determining the deflections, the latter can be controlled in statically indeterminate structure in order to respect the support conditions. Culmann (1866) already used these differential graphical relationships to obtain the correct elastic bending distribution on simple beams by successive attempts (trial and error):

> *(...) it can be seen that between the forces A and B, a bending moment must exist that produces a negative curvature of the beam so that it takes the same direction as the clamped support A. We first give an arbitrary value to this bending moment; we study its influence on the beam; then we correct it in so that the beam axis respect the support conditions.* (Culmann, 1880, p.584, personnal translation)

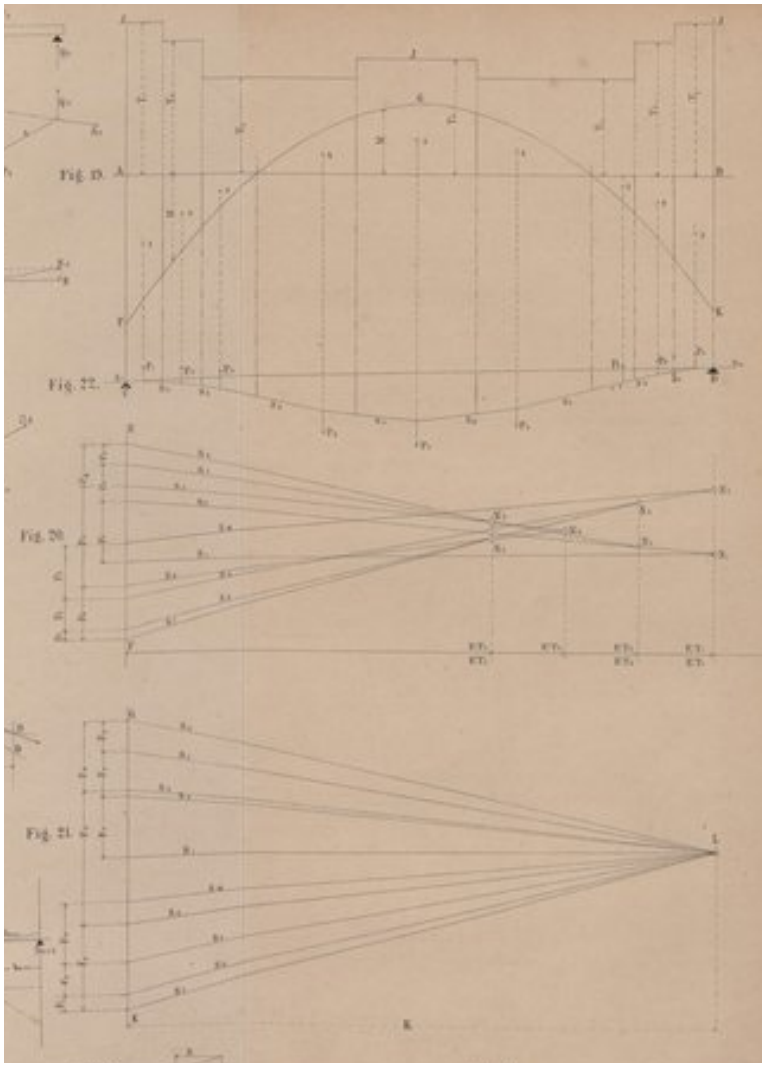

Figure 17 *Graphical procedure for constructing the bending moment diagram and the elastic curve by double integration.(Mohr, 1868, Table XIV, fig.19-22, p.397)*

Following this idea, the authors extended the methodology to more complex cases. Mohr (1868) for instance applied it to continuous beams. Lévy (1874a) proposes an alternative method - the so-called "two moments" method - to the one proposed by Mohr although he recognises the latter as the founder of the graphical strength of materials (Lévy, 1874b, p.viii); Eddy (1877) proposed a slightly different methodology founded on the theorem of "three moments".

Extension to rigid frames. One of the most outstanding and complete text book about graphical analysis was published by Wolfe (1921). It was developed from the notes prepared for his classes at the University of Illinois. His fourth chapter is particularly interesting since it addresses the problem of solving graphically not only statically indeterminate beams but also trusses, rigid frames and arches **(Fig. 18)**.

This book is also particularly interesting since it addresses the problem of applying graphical analysis to structures in masonry or reinforced concrete. The author also insists on the relative freedom of the structural designer:

> *"The designer's work is only half complete when the loads and stresses are found, the choice of sections and the indication of details being a very important part."* (Wolfe, 1921)

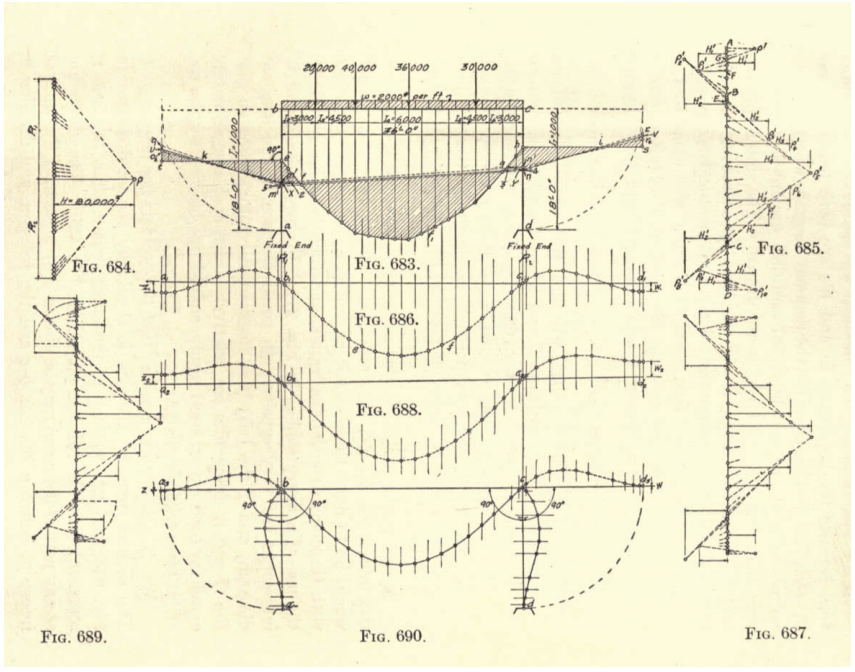

Figure 18 *Graphical procedure for constructing the bending moment diagram and the elastic curve of a statically indeterminate rigid frame. (Wolfe, 1921, p.351)*

2.3 Graphical tools for interactive structural design

Graphical tools for structural analysis. Graphical analysis is an essential part of the teaching of the theory of structures. Indeed, the many advantages this method offers for understanding the structural behaviour of architectural forms has been recognised by numerous authors. Muttoni (2015) for instance recommends the use of graphic statics for teaching structural theory and design within schools of Architecture:

> *[Graphical methods] contributes to intuitive understanding and visualization of [the structural] behavior. They greatly facilitate all statical operations. (...) they have significant advantages over numerical methods in their simplicity, speed, and transparency (...)* (Allen and Zalewski, 2009, p. 12)

It allows reducing *ad minimum* analytic calculations which students in architecture are usually not so familiar with, and to improve their understanding of the conditions of equilibrium within existing structures (Pelsser et al., 2017). This virtue was widely recognised by many engineers and teachers:

> *It is generally possible to solve by graphical methods all statical problems which can be solved analytically, while for certain classes of problems such methods are somewhat simpler and more rapid than analytical methods.* (Spofford, 1928, pp. 337-354)

In addition, it has the advantage to provide continuous and visual control of the results, as already observed by the pioneers:

> *[Graphic statics] gives everyone simple and quick processes, substituting the clever and laborious calculations which our engineers do all the time. These processes also have the valuable advantage of still containing the principle of their own verification, in such a way that, even if they can, like all graphic methods, leave some doubt about a decimal fraction (which does not much matter in this kind of application), they permit to avoid the kind of stupid mistakes found in long arithmetical operations and algebraic formulae where nothing speaks to the*

eyes. (Lévy, 1874a, p. xvi, translation inspired from Fivet (2013))

A last advantage is that graphic statics is suitable for design purposes since it allows a certain indeterminacy and offers a good communication support in the context of a design process:

> *The qualitative evaluation of the forces using an inductive process - for example graphic statics - does not require exact calculation, just practice and experience. This method is understandable to architects too, and offers a good basis for working together.* (Schwartz, 2012, in Flury)

Controllable and interactive tools for structural design. In his thesis, (Fivet, 2013, p.17) highlights the significance of using interactive tools that maximise the structural designers creativity and support their intuition. Arguing on the essential properties - clarity, speed, interactivity - these tools need to provide, Fivet emphasises on the exemplary practice of renowned engineers of the past, such as Robert Maillart (1872-1940) (Bill, 1949; Bryan and Sauer, 1973) whose efficient design methods have been thoroughly studied by Zastavni (2008). Taking advantage of the lower bound theorem of plasticity, design practices using graphic statics have proven to produce high-quality results (Muttoni et al., 1996; Ochsendorf, 2005; Heyman, 2008; Zastavni, 2008).

During the past decades, authors like Block and Ochsendorf (2007); Block (2009); Beghini et al. (2013); Baker et al. (2013) have been developing tools using parametric construction of both diagrams, on which nodes geometrical constraints can be applied . These recent developments offer the opportunity to control the range of possible equilibrium configurations by limiting, for instance, the length of some segments in the force diagram or by constraining the action lines in the form diagram to pass though determined nodes (Fivet and Zastavni, 2013; 2015). As a result, every node in either diagram can be constrained to remain within a graphical region so that it respects the yield conditions of the structure – the equilibrium conditions being automatically respected if we refer to the construction of the reciprocal polygons. This ensures that the conditions of application of the lower-bound theorem of plasticity are respected.

Besides the implementations devoted to didactic purposes, developed at MIT (Greenwold and Allen, 2018, ActiveStatics) and at ETHZ (Van Mele

et al., 2012, eQUILIBRIUM), some recent developments by the Chair of structural Design at ETH Zurich have led to very efficient and interactive tools like Combinatorial Equilibrium Modelling (CEM). For detailed descriptions of this method and of the context of vector-based 3D graphic statics, see Ohlbrock et al. (2016); Jasienski et al. (2016); D'Acunto et al. (2016; 2017); Ohlbrock et al. (2018). Other applications can be found in D'Acunto et al. (2017); Boulic and Schwartz (2018); Enrique and Schwartz (2018); Deschuyteneer et al. (2018a) among others.

Chapter 3

Static indeterminacy and reciprocal diagrams

This chapter consists in a proposal to manipulate statically indeterminate structures by means of graphic statics reciprocal diagrams. Considering the force diagram as a combination of independent stress states, the graphical approach proposed allows to evaluate the structural behaviour of 2D statically indeterminate networks in the context of plastic design and analysis.

First, the concept of static indeterminacy is explained and its consequences related to the structural requirements are outlined. The concept is then translated in terms of combination of independent stress states that can be manipulated using graphic statics reciprocal diagrams. The main theoretical concepts related to the geometric indeterminacy of these reciprocal diagrams are consequently reviewed. Finally, these properties are used to develop a methodology for the graphical limit state analysis of strut-and-tie networks, and several approaches in terms of plastic design are suggested.

3.1 Static indeterminacy in structural design

The former chapter highlighted that graphic statics is a suitable method when dealing with equilibrium problems, but becomes rapidly intricate when involving the computation of structures' deformation. Indeed the construction rules of the reciprocal diagrams ensure the static equilibrium of any part of the structure, but give no rule for choosing between one stress distribution or another when the structure is statically indeterminate, *i.e.* when the force diagram presents a certain degree of geometric indeterminacy. We have seen that fascinating methods have been developed during the past two centuries for tracing the elastic deflections and consequently determining the elastic distribution of stresses in structures like trusses and beams. This peculiar solution to the equilibrium problem is highly dependent on the assumptions made on the mechanical behaviour of the building material, but also on the physical conditions during the set up of the structure.

Though, when thinking in terms of design, these difficulties disappear: static indeterminacy indeed gives some latitude to the structural designer for finding a suitable equilibrium, taking into account architectural or technical requirements. However, when it comes to the analysis of existing structures, this is an evident drawback since the method requires from the structural engineer to identify how the structure can reach its ultimate carrying capacity before calculating it; for wide or complex structures, this is often not an easy matter. As highlighted in the first chapter, the Theory of Plasticity offers a partial answer to this question when seeking to determine the load bearing capacity of given structures, as well as in design context.

The role of static indeterminacy. Structural engineers often have to deal with statically indeterminate structures. A *statically indeterminate structure* is defined as *a structure for which the conditions of static equilibrium are not defined unequivocally.* In design phases, static redundancy may be desirable for several reasons related to the improvement of the structural behaviour or in response to architectural requirements:

– **stiffness**: at service state, the static indeterminacy usually reduces deflections within the structure, because of the extra supports or

extra links generated between the structural parts;

- **strength**: the distribution of the internal forces is modified by the overabundant supports or internal linkages, in such a way that it usually reduces the value of the maximum internal forces;
- **robustness**: since robustness can be considered as a form of insensitivity to local failure, the capacity of a structure to redistribute stresses in case of damage is an important robustness criterion (Deschuyteneer et al., 2015). The ability of finding alternative stress states is strongly linked to a structure's static indeterminacy, since it means that some linkages are not strictly necessary for the overall equilibrium of the structure, but must be useful in case of damage within other parts of it.

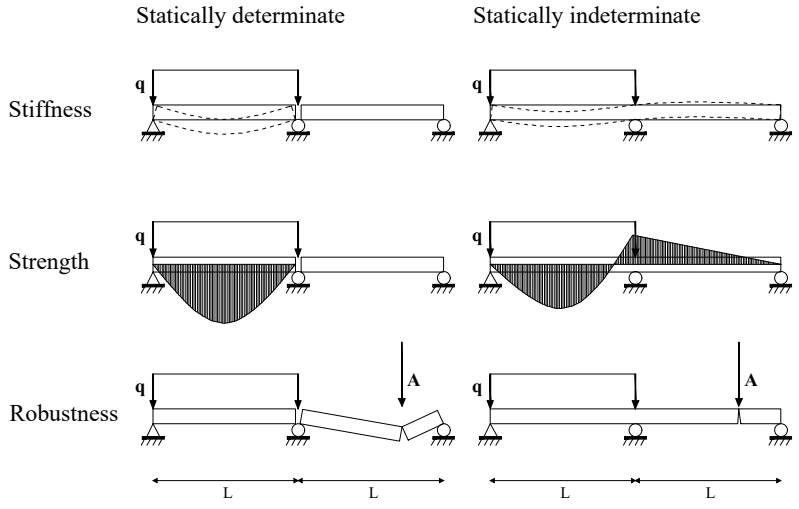

Figure 19 *Comparison between statically determinate and corresponding continuous beam on three supports.*

Figure 19 illustrates these three concepts with the simple case of a beam on three support. The behaviour of a statically determinate articulated beam is compared with the one of a statically indeterminate continuous

beam. The behaviour of the latter can be considered more satisfactory, since

- stiffness is improved, as vertical deflections are limited;
- strength is improved, as the maximum magnitude of the bending moment is reduced by redistributing it on both beams;
- robustness is ensured, as the structure is kept stable in case of accidental damage.

Static indeterminacy may also not result from structural design choices, but rather from technological or constructive reasons that may arise after the initial design phase. In that case, structural engineers must be able to analyze the modified situation in order to propose a refined design.

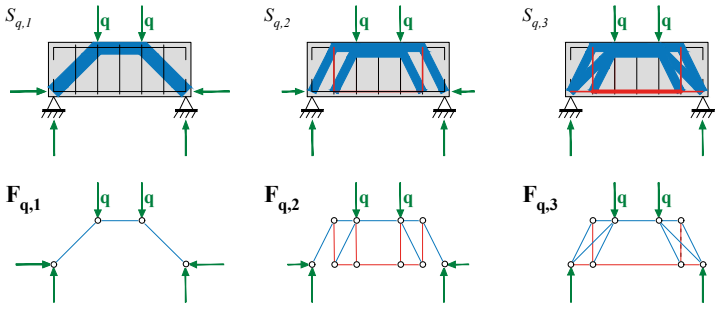

Figure 20 *Three admissible stress fields acting within the same reinforced concrete beam. In blue: concrete struts in compression; in red: steel rebars in tension.*

Multiplicity of admissible stress states. The consequence of static indeterminacy is that it is generally impossible to know the actual state of stress acting within the members that constitute a structure. Indeed, stresses acting within the different parts of the structural model cannot be determined by equilibrium considerations only. Generally speaking, this means that various stress distributions may be found, while respecting equilibrium, boundary and yield conditions. This property is illustrated in **Figure 20**, which shows three simplified stress fields that can occur

within the same reinforced concrete beam following the methodology proposed by Muttoni et al. (1996). The compression struts in concrete are represented by blue-hatched areas, while the tensile forces acting in the rebars are represented by red lines. Each of these fields is in equilibrium with the external loads. If the struts and ties are sized in such a way to avoid violating the yield conditions, then they all are statically admissible stress states. This means that it is impossible to determine which one is effective within the structure in service.

Under service loading, assuming an elastic behaviour of both concrete and steel, compatibility conditions may be set on strains in order to determine the corresponding distribution of stresses. However, these conditions are not always easy to fix, since they may depend on initial conditions: history of loading, initial deformations, residual stresses, etc. Furthermore, considering the inelastic behaviour of reinforced concrete at yielding, it is in general impossible to determine the actual distribution of stresses within a statically indeterminate structure when the yield stress is reached in some of the structural members.

3.2 Static indeterminacy as a combination of independent stress states

Static indeterminacy due to stress states. This indeterminate distribution of stresses may be considered as a linear combination of various independent stress states. Therefore the following concepts are defined:

Stress state S_q a distribution of stresses within the structure, in equilibrium with the applied loads;

Self-stress state S_x a distribution of stresses within the structure, in equilibrium with itself. *Self-stress states* can only occur in statically indeterminate structures. The number of independent *self-stress states* is equal to the number of internal static indeterminacy of the structure.

Since stress states are generated by equilibrium considerations only, and because of the linearity of the vector addition that rules classic mechanics, stress states and self-stress states can be linearly combined together to give another stress state while keeping unchanged the conditions of equilibrium with the applied loads. This is illustrated in **Figure 21**, where stress state S_{q0} is transformed by combining it with self-stress state S_1. The magnitude of the compression force acting within the diagonal struts is reduced by the tension force acting within these struts in the self-stress state, while the magnitude of the tensile stress within the rebars is modified. The combination of S_{q0} and S_1 gives another stress state, identical to those S_{q3} of **Figure 20**.

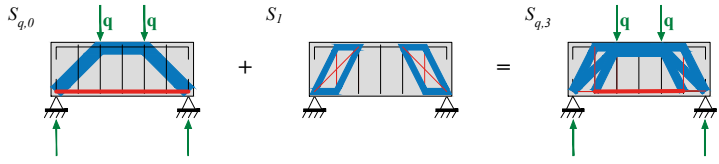

Figure 21 *Combination of a stress state with a self-stress state, giving another stress state in equilibrium with the external loads.*

Generally speaking, for a given external equilibrium configuration, any stress state can be obtained by combining a fundamental stress state and a series of self-stress states without modifying the external equilibrium.

Reciprocal diagrams for representing stress states. The geometry of any stress state can be represented in a form diagram $\mathbf{F_q}$ corresponding to the strut-and-tie model. The magnitude of the forces acting within structural members are represented in the reciprocal force diagram $\mathbf{F_q^*}$ **(Fig. 22)**.

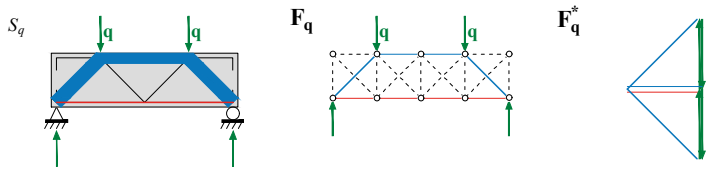

Figure 22 *Reciprocal diagrams* $\mathbf{F_q} - \mathbf{F_q^*}$ *representing the stress state within a reinforced concrete beam.*

In the same way, any *self-stress state* is characterised by a strut-and-tie model, which geometry is represented in a form diagram $\mathbf{F_x}$, and which forces magnitudes acting within its members are represented in the reciprocal force diagram $\mathbf{F_x^*}$.

Influence of self-stress states on structural behaviour. A self-stress state can be generated in many different ways during the history of loading of the structure: differential heating, displacements of the supports due to settlements, residual stresses, etc. A classical type of self-stress states is illustrated in **Figure 23**, obtained by applying a pretension force $\mathbf{p}$ along a diagonal cable. When removing the external forces, compression stresses within the concrete strut $\mathbf{p}^-$ ensure the equilibrium of the tension force $\mathbf{p}$ acting in the cable. The magnitude of these stresses are represented by the segments $\mathbf{p}^*$ and $\mathbf{p}^{-*}$ in the force diagram $\mathbf{F_0^*}$. Since no external load is applied on the structure, the reciprocal diagrams $\mathbf{F_0}$ and $\mathbf{F_0^*}$ represent a basic self-stress state.

Consider now another equilibrium, obtained by compressive forces acting in vertical and horizontal concrete struts and by a tensile force acting in

the diagonal stirrup like in **Figure 24**. Depending on the chosen magnitude of the pre-tensioning force, different self-stress states can be obtained. Translated in terms of graphic statics, this means that different force diagrams can be drawn, similar one to another but at different scales **(Fig. 24)**.

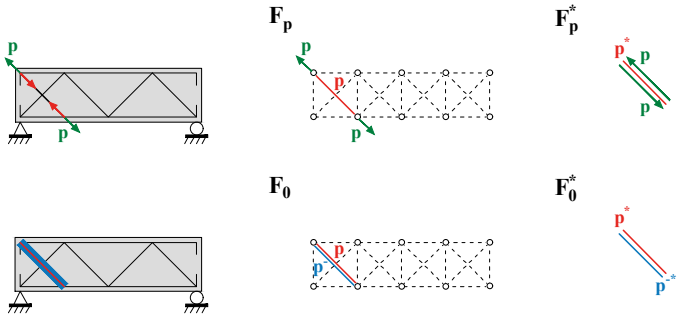

Figure 23 *Self-stress state generated by pre-tensioning within a reinforced concrete beam.*

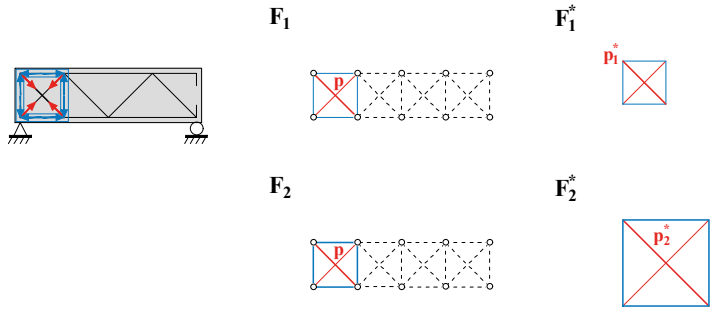

Figure 24 *Self-stress state in equilibrium with the pre-tensioning.*

When combining the stress state $\mathbf{F_q}$-$\mathbf{F^*_q}$ generated by the external loads and the self-stress state $\mathbf{F_x}$-$\mathbf{F^*_x}$, it produces stress state $\mathbf{F_{q+x}}$-$\mathbf{F^*_{q+x}}$, which depends on the magnitude chosen for the pre-tensioning force $\mathbf{p^*_x}$ **(Fig. 25)**.

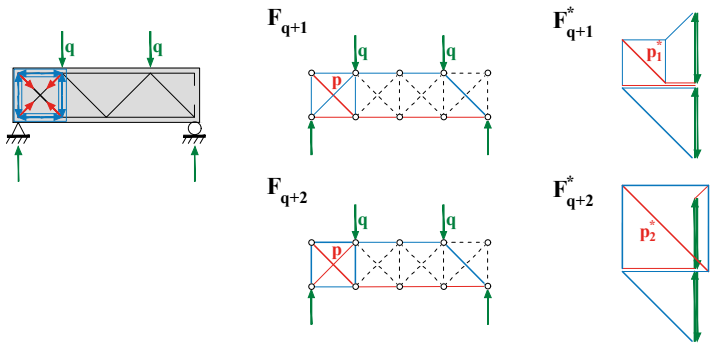

Figure 25 *Combination of a stress state due to the applied loads and a self-stress state at two different scales.*

It is useful to find out rules for dealing with reciprocal diagrams in case of geometric or static indeterminacy. The next section outlines some of them in term of independent self-stress states.

3.3 Geometrical freedom of force diagrams

Maxwell rigidity number for reciprocal figures. Reciprocal diagrams constitute dual structures that provide graphical insight into each other, especially when assessing kinematic mechanisms and states of self-stress (Mitchell et al., 2016; Micheletti, 2008; McRobie et al., 2016; Konstantatou et al., 2018). For networks with an underlying planar graph, this assessment can be done considering the Maxwell rigidity number N for 2D structures as modified by Calladine (1978):

$$N = 2v - b - 3 = m - s \tag{19}$$

with

$\boldsymbol{v}$ the number of vertices,

$\boldsymbol{b}$ the number of bars,

$\boldsymbol{m}$ the number of kinematic mechanisms,

$\boldsymbol{s}$ the number of independent self-stress states.

For the reciprocal diagrams $\mathbf{F} - \mathbf{F}^*$ of **Figure 26**, we have $v = 5$, $v^* = 6$ and $b = b^* = 9$. Since $\mathbf{F}$ has an underlying planar graph we have:

$$N = 2 \cdot 5 - 9 - 3 = -2 \tag{20}$$

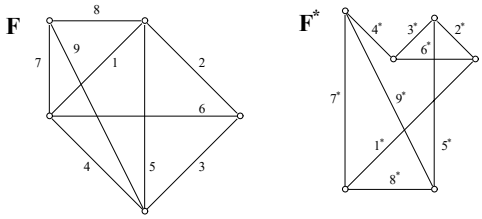

Figure 26 *Reciprocal diagrams* $\mathbf{F} - \mathbf{F}^*$.

The rigidity number N of one of the dual figures and the one N^* of its reciprocal are related by (Micheletti, 2008):

$$N + N^* = -2 \tag{21}$$

Therefore, the Maxwell rigidity number N^* of the reciprocal diagram $\mathbf{F}^*$ should be equal to zero, in order to respect Equation 21. This is indeed the case since:

$$N^* = 2 \cdot 6 - 9 - 3 = 0 \tag{22}$$

Kinematic mechanisms and states of self-stress in reciprocal diagrams. Looking at diagram $\mathbf{F}$ presented in **Figure 26**, in which there is no kinematic mechanism, a rigidity number $N = -2$ indicates that there are two independent states of self-stress. These are intended as a system of forces acting within the bars, that are in equilibrium with themselves, and which magnitudes can be scaled *ad infinitum*. This concept is further developed in the next section of this dissertation.

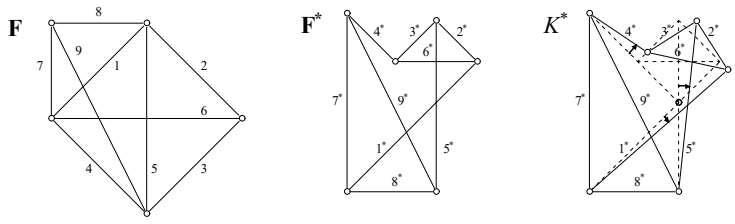

Figure 27 *Kinematic mechanism within* $\mathbf{F}^*$.

On diagram $\mathbf{F}^*$ of **Figure 26**, for which $N^* = 0$, only one kinematic mechanism can be developed. This kinematic mechanism K^* is represented in **Figure 27**. Consequently, there must be only one possible independent state of self-stress. Indeed, considering $\mathbf{F}^*$ as a form diagram, there is only one possible geometry for its reciprocal $\mathbf{F}$ because each vertex of $\mathbf{F}^*$ connects exactly with three bars.

Self-stress states and geometrical freedom of the reciprocals. The degree of static indeterminacy of a given 2D network **F** without internal mechanism can usually be identified. Each of these degrees of static indeterminacy can be correlated to an independent self-stress state of **F**. Considering **F** in **Figure 28** as a form diagram, *i.e.* as a representation of the structure's geometry, each state of self-stress corresponds to a degree of internal static indeterminacy of this diagram. Consequently, it corresponds to a degree of freedom in the reciprocal force diagram $\mathbf{F}^*$.

These degrees of freedom consist in particular transformations of the force diagram $\mathbf{F}^*$ that are equivalent to offsets (Mitchell et al., 2016; McRobie et al., 2016), *i.e.* to the scaling of one part of the force diagram without modifying the lengths of the other bars. In these transformations, all the bars keep their direction unchanged.

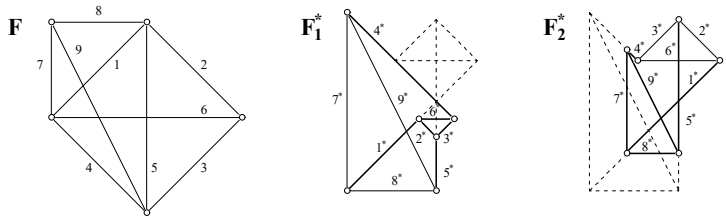

Figure 28 *Two independent offsets of* $\mathbf{F}^*$.

Figure 28 shows how the lengths of bars $7^*, 8^*, 9^*$ are not modified when applying an offset operation on bars $2^*, 3^*, 6^*$ of $\mathbf{F_1^*}$. In the same way, the lengths of bars $7^*, 8^*, 9^*$ in $\mathbf{F_2^*}$ can be scaled without any influence on the lengths of bars $2^*, 3^*, 6^*$. $\mathbf{F}^*$ thus presents two geometrical degrees of freedom corresponding to the independent self-stress states that may act within **F**.

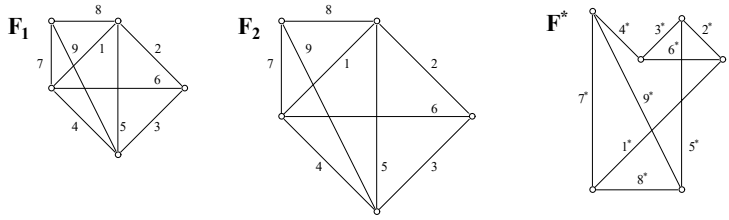

Figure 29 *One only possible offset for* $\mathbf{F}$.

Since $\mathbf{F}^*$ is characterised by a sole independent self-stress state, $\mathbf{F}$ presents only one degree of freedom corresponding to its entire scaling **(Fig. 29)**.

Reciprocal diagrams for independent self-stress states. The properties of reciprocal diagrams constitute the basis of the methodology proposed in the next section, for dealing with static indeterminacy within reciprocal diagrams.

A first insight into the proposed methodology is illustrated by considering the 2D network analysed previously **(Fig. 30)**. From the initial structure two independent states of self-stress can be created by imposing successively null forces in bars $7^*, 8^*, 9^*$ and $2^*, 3^*, 6^*$ respectively. Each of these in dependent stress states is characterised by reciprocal form and force diagrams, respectively $\mathbf{F_1} - \mathbf{F_1^*}$ and $\mathbf{F_2} - \mathbf{F_2^*}$. Each self-stressed force diagram can be traced at an independent scale. When assembling these two states of self-stress, the resulting force diagram $\mathbf{F}^*$ has two degrees of freedom that are related to two independent offsets.

The same kind of analysis is applied to a network with three independent stress states **(Fig. 31)**. Maxwell's rigidity number N can be easily calculated: $N = 2 \cdot 6 - 12 - 3 = -3$. Since there are no mechanisms, three independent self-stress states can be found; they are depicted in **Figure 30** by the couples of reciprocal diagrams $\mathbf{F_1} - \mathbf{F_1^*}$, $\mathbf{F_2} - \mathbf{F_2^*}$ and $\mathbf{F_3} - \mathbf{F_3^*}$.

If one of the self-stress states is fixed, the force diagram $\mathbf{F}^*$ has one degree of freedom less. This diagram can be transformed by modifying the scale of the remaining self-stress states. Thanks to these transformations,

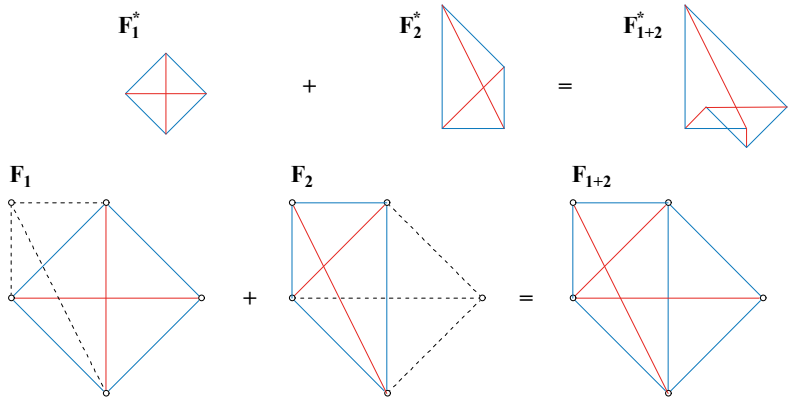

Figure 30 *Network with two independent self-stress states. The complete reciprocal diagrams* $\mathbf{F} - \mathbf{F}^*$ *are obtained by assembling the independent diagrams* $\mathbf{F_1} - \mathbf{F_1^*}$ *and* $\mathbf{F_2} - \mathbf{F_2^*}$.

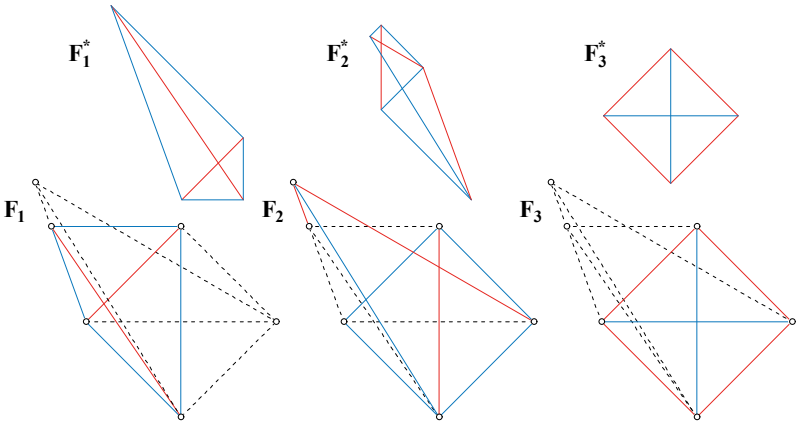

Figure 31 *Network with three independent self-stress states.*

all the possible geometrical configurations of $\mathbf{F}^*$ can be explored. The methodology is developed in the next section for the limit state analysis of statically indeterminate strut-and-tie networks.

3.4 Limit state analysis using reciprocal diagrams

Limit state analysis for statically indeterminate structures. It has been emphasised in the previous section that, when dealing with statically indeterminate structures, one unique stress state may not be found. Indeed, global equilibrium considerations are not sufficient since the stress state depends of the relative magnitude of the self-stress states, which are not affecting external equilibrium. It should be noted, though, that plastic theory provides a theoretical framework and effective tools to evaluate the validity of stress states when the structure has reached its ultimate limit state, *i.e.* at collapse.

When the necessary conditions of ductility are fulfilled for applying plastic theory, the lower-bound theorem of plasticity ensures that any stress state in equilibrium with the external loads respecting yield and boundary conditions, is a suitable stresses distribution. Furthermore, it allows to know the stress distributions that may lead to collapse, as well as the identification amongst them of a lower-bound value for the magnitude of applied loads. This means that the lower-bound theorem can be applied in the case of a linear combination of a stress state and self-stress states, providing each of them is in equilibrium and that the resultant stress state does not violates the yield conditions in any part of the structure.

The approaches for solving structural problems that respect equilibrium and yield conditions are known as *static approaches*, in opposition with the so-called *kinematic approaches* based on the study of kinematic mechanisms, for which the yield condition may not be respected. **Table 1** from Chapter 1 resumes these conditions.

Yield conditions in force diagrams. Since graphic statics construction rules ensure that equilibrium conditions are respected, the lower-bound theorem of plasticity may be applied for the limit state analysis of strut-and-ties networks. Taking advantage of reciprocal diagrams $\mathbf{F} - \mathbf{F}^*$ properties, this is equivalent to perform a static limit analysis on the force diagram $\mathbf{F}^*$. Indeed, equilibrium being ensured, it is easy to impose the respect of yield conditions by limiting bars' lengths in $\mathbf{F}^*$.

Being

- $\mathbf{f_b}$ the segment in $\mathbf{F}$ representing the geometrical properties of the internal force acting in bar b;
- $\mathbf{f_b^*}$ the segment in $\mathbf{F}^*$ representing the mechanical properties of the internal force acting in bar b;
- f_b [kN] the magnitude of the force acting in bar b and $\mathrm{f_b^*}$ [m] the corresponding length in $\mathbf{F}^*$ at scale s^*;
- $f_{u,b}$ [kN] the magnitude of the ultimate plastic normal force that can be supported by bar b and $\mathrm{f_{u,b}^*}$ [m] the corresponding limit length in $\mathbf{F}^*$;
- s [m/m] the drawing scale of $\mathbf{F}$;
- s^* [kN/m] the drawing scale of $\mathbf{F}^*$ so that $\mathrm{f_b^*} \cdot s^* = f_b$;

the yield condition can be expressed as follows:

$$\mathrm{f_b^*} \leq \mathrm{f_{u,b}^*} \qquad \forall b \tag{23}$$

It follows that the limit state analysis of a strut-and-tie network consists in analyzing all the possible configurations of the force diagram $\mathbf{F}^*$ that respect Equation 24, and in finding the one corresponding to the highest magnitude of the applied loads. In Chapter 4, this methodology will be applied to pin-jointed trusses. Before that, the following paragraphs highlight how limit analysis can be performed by graphical manipulation of self-stress states in the force diagram.

Limit states by manipulating force diagrams. The methodology is illustrated by a very simple example, in which two self-stress states are successively applied to **Figure 26**'s form diagram $\mathbf{F}$. These two self-stress states, already identified in the previous section, have been represented by two pairs of reciprocal diagrams $\mathbf{F_1} - \mathbf{F_1^*}$ and $\mathbf{F_2} - \mathbf{F_2^*}$ **(Fig. 30)**. Transforming this situation into the one represented in **Figure 32**, self-stress state $\mathbf{F_2} - \mathbf{F_2^*}$ is turned into a stress state produced by three external forces in equilibrium $\mathbf{q_1}$, $\mathbf{q_2}$ and $\mathbf{q_3}$. The corresponding form and force diagrams $\mathbf{F_q}$ and $\mathbf{F_q^*}$ are drawn at scales s and s^* respectively. The magnitude of the external loads q_i is obtained from $\mathbf{F_q^*}$:

$$q_i = s^* \cdot \mathrm{q_i^*} \tag{24}$$

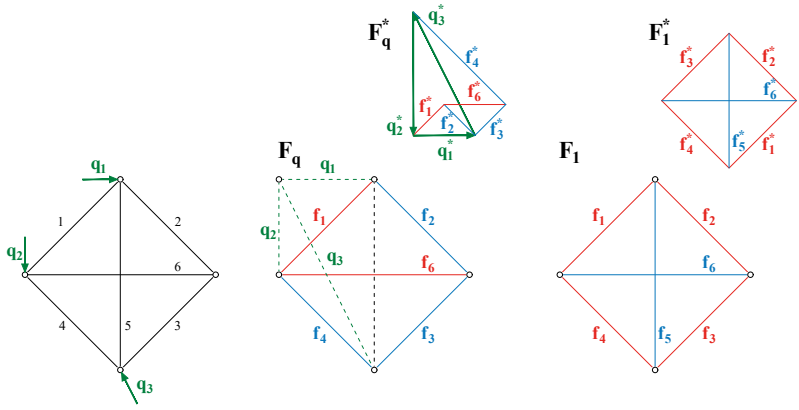

Figure 32 *Two independent stress states acting inside of the same network.* $\mathbf{F_q}$-$\mathbf{F_q^*}$ *is produced by the external loads;* $\mathbf{F_1}$-$\mathbf{F_1^*}$ *corresponds to a self-stress state.*

The reciprocal diagrams $\mathbf{F_1}$ and $\mathbf{F_1^*}$ are then constructed in **Figure 32**. They correspond to a self-stress state drawn at an arbitrarily chosen scale.

Force polygons $\mathbf{F_q^*}$ of the given external stress state and $\mathbf{F_1^*}$ of the self-stress state are combined into one sole force diagram $\mathbf{F}^*$ with one geometric degree of freedom. This degree of freedom is correlated to the relative scale between $\mathbf{F_q^*}$ and $\mathbf{F_1^*}$. Considering $\mathbf{F_q^*}$ as fixed, and λ_1 as the scale factor applied to $\mathbf{F_1^*}$:

$$\mathbf{F}^* = \mathbf{F_q^*} + \lambda_1 \cdot \mathbf{F_1^*} \tag{25}$$

Figure 33 shows two possible geometries for the force diagram $\mathbf{F}^*$, correlated to two different scaling factors $\lambda_{1,1}$ and $\lambda_{1,2}$.

Linear combination of independent force diagrams. More generally speaking, force diagram $\mathbf{F}^*$ can be seen as a linear combination of stress states, each of them corresponding to a degree of freedom in the force

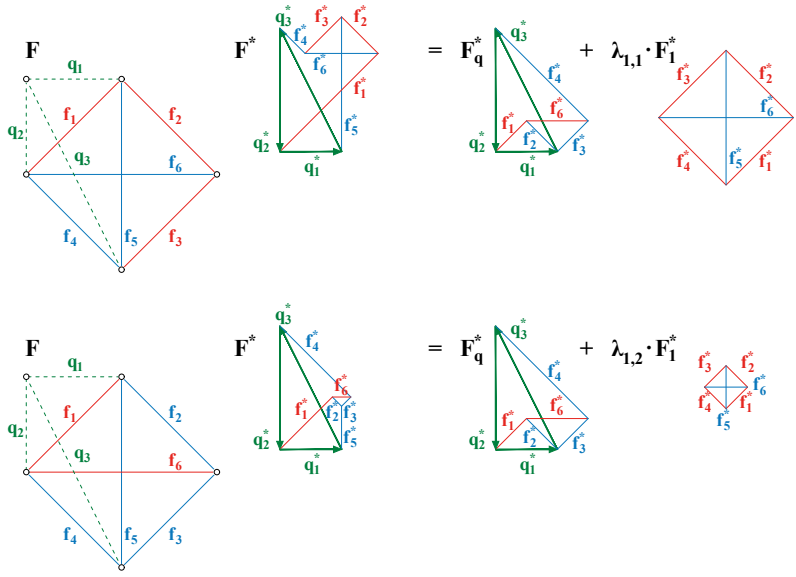

Figure 33 *Construction of the global force diagram* $\mathbf{F}^*$*, by combining the force diagram of the external forces* $\mathbf{F}^*_\mathbf{q}$ *with the one of the self-stress state* $\mathbf{F}^*_\mathbf{1}$ *for two different scale factors.*

diagram (or equivalently to a degree of static indeterminacy of the form diagram). One of these degrees of freedom of the force diagram $\mathbf{F}^*$ is given by the magnitude of the applied loads. In terms of graphic statics, this means applying a scale factor λ^*_q to the force diagram $\mathbf{F}^*_\mathbf{q}$ **(Fig. 34)**, *i.e.* scaling the entire force diagram $\mathbf{F}^*$ (D'Acunto et al., 2016; Jasienski et al., 2016).

$$\mathbf{F}^* = \lambda^*_q \cdot \mathbf{F}^*_\mathbf{q} + \sum_{i=1\rightarrow|N|} \lambda_i \cdot \mathbf{F}^*_\mathbf{i} \tag{26}$$

When looking to achieve a limit state analysis on a structure subjected to a given system of loads in equilibrium $\mathbf{q}$, we try to determine the load factor λ_u that needs to be applied to $\mathbf{q}$ in order to obtain the ultimate limit state, such that:

$$\{\mathbf{q}\}_\mathbf{u} = \lambda_u \cdot \{\mathbf{q}\} \tag{27}$$

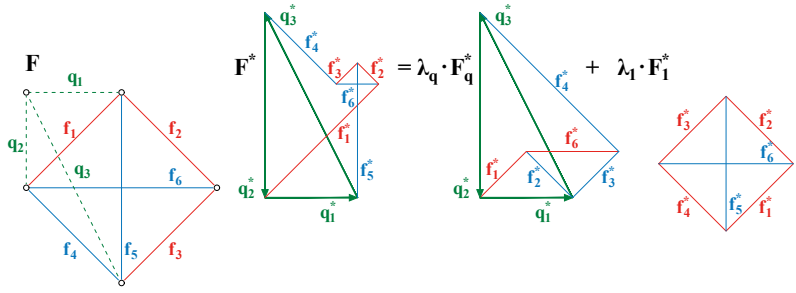

Figure 34 *Construction of the global force diagram* $\mathbf{F}^*$ *by linear combining the force diagrams of two independent stress states* $\mathbf{F}^*_\mathbf{q}$ *and* $\mathbf{F}^*_\mathbf{1}$.

In terms of graphic statics, this is applying a scale factor λ^*_u to $\mathbf{F}^*_\mathbf{q}$ so that it produces the collapse force polygon $\mathbf{F}^*_\mathbf{u}$. When combined with the independent stress states $\mathbf{F}^*_\mathbf{i}$ drawn at scale λ^*_i, equation 26 then becomes:

$$\mathbf{F}^*_\mathbf{u} = \lambda^*_u \cdot \mathbf{F}^*_\mathbf{q} + \sum_{i=1 \rightarrow |N|} \lambda^*_i \cdot \mathbf{F}^*_\mathbf{i} \tag{28}$$

Application of the lower-bound theorem. Considering now the lower-bound theorem of plasticity and its consequences (Eq. 16), we can determine the collapse load factor λ^*_u as the highest scale factor λ^*_q that can be applied to $\mathbf{F}^*_\mathbf{q}$ so that yield conditions are respected. This means:

$$\lambda^*_u = max\{\lambda^*_q\} : \mathrm{f}^*_\mathrm{i} \leq \mathrm{f}^*_\mathrm{u} \ \forall i \tag{29}$$

In order to make this formulation more explicit, the following concepts are defined:

***limit stress state*,** a stress state for which the magnitude of the ultimate plastic normal force $f_{u,b}$ is reached in such an amount of bars that it transforms the structure into a mechanism;

limit force diagram $\mathbf{F}^*_\mathbf{s}$**,** a force diagram that corresponds to a limit stress state and that respects the yield conditions;

limit load factor λ^*_s**,** a scale factor λ^*_q that corresponds to a limit state.

For a given structure subject to a specific load case, there are several possible limit stress states, *i.e.* several limit force diagrams $\mathbf{F^*_{s,l}}$, any of them being correlated to a specific limit load factor $\lambda^*_{s,l}$. Considering these limit cases only, Equation 29 thus becomes:

$$\lambda^*_u = max_l\{\lambda^*_{s,l}\} : \mathrm{f^*_b} \leq \mathrm{f^*_{u,b}}\ \forall b \tag{30}$$

Consequently, the ultimate force polygon $\mathbf{F^*_u}$ can be identified among all the limit state polygons $\mathbf{F^*_{s,l}}$:

$$\mathbf{F^*_u} = \mathbf{F^*_{s,u}} : \lambda^*_{s,u} = max_l\{\lambda^*_{s,l}\}\ \forall l \tag{31}$$

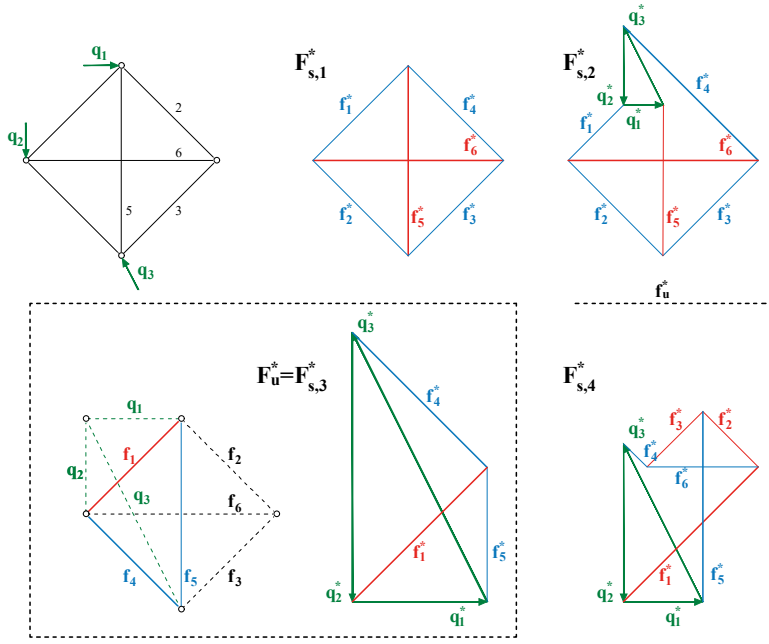

Figure 35 *Four limit force diagrams* $\mathbf{F^*_{s,1\to4}}$ *corresponding to four different values for the load factor* $\lambda^*_{s,1\to4}$

Considering the network of **Figure 35**, a limit stress state is obtained when the distribution of forces is such that the yield stress is reached in

two bars of the network because it turns the structure into a mechanism. For the simplicity of the analysis, this yield stress is set equal for all the bars of the network. It is represented by length $\mathrm{f}_{\mathrm{u}}^{*}$ in the force diagram $\mathbf{F}^{*}$.

Force diagram $\mathbf{F}_{\mathbf{s,1}}^{*}$ of **Figure 35** is as a limit force diagram, since the ultimate normal force f_u is reached in two bars (5 and 6). Indeed, $\mathrm{f}_{5}^{*} = \mathrm{f}_{6}^{*} = \mathrm{f}_{\mathrm{u}}^{*}$. Since there is no external force needed to reach this limit state, the associated load factor $\lambda_{s,1} = 0$. The other limit force diagrams $\mathbf{F}_{\mathbf{s,l}}^{*}$ are drawn in **Figure 35**. Each of them corresponds to a specific limit load factor $\lambda_{s,l}^{*}$. The collapse load factor λ_{u}^{*} is the biggest one among them, corresponding here to $\mathbf{F}_{\mathbf{s,3}}^{*}$:

$$\lambda_{u}^{*} = max_{l}\{\lambda_{s,l}^{*}\} = \lambda_{s,3}^{*} \tag{32}$$

Ratios between lengths in the force diagram. It can be convenient to express the collapse load factor with respect to the relative magnitude of q and f_u. This is done by defining $\rho_{s,l}^{*}$ as the ratio of the length $\mathrm{q}_{\mathrm{s,l}}^{*}$ in $\mathbf{F}_{\mathbf{s,l}}^{*}$ corresponding to a limit stress state, and $\mathrm{f}_{\mathrm{u}}^{*}$, the length representing the ultimate normal force at scale s^{*}. Lengths q^{*} and $\mathrm{f}_{\mathrm{u}}^{*}$ being fixed, this ratio $\rho_{s,l}^{*}$ is proportional to the limit load factor $\lambda_{s,l}^{*}$:

$$\rho_{s,l}^{*} = \frac{\mathrm{q}_{\mathrm{s,l}}^{*}}{\mathrm{f}_{\mathrm{u}}^{*}} = \lambda_{s,l}^{*} \cdot \frac{\mathrm{q}^{*}}{\mathrm{f}_{\mathrm{u}}^{*}} \qquad \forall l \tag{33}$$

The collapse load factor λ_{u}^{*} can consequently be determined from the collapse force diagram $\mathbf{F}_{\mathbf{u}}^{*}$, identified thanks to Equation 28:

$$\lambda_{u}^{*} = max_{l}\{\lambda_{s,l}^{*}\} = max_{l}\{\rho_{s,l}^{*}\} \cdot \frac{\mathrm{f}_{\mathrm{u}}^{*}}{\mathrm{q}^{*}} \qquad \forall l \tag{34}$$

Applied to **Figure 35**, Equation 34 can be rewritten as:

$$\lambda_{u}^{*} = \rho_{s,3}^{*} \cdot \frac{\mathrm{f}_{\mathrm{u}}^{*}}{\mathrm{q}_{\mathrm{1}}^{*}} = \frac{\sqrt{2}}{2} \cdot \frac{\mathrm{f}_{\mathrm{u}}^{*}}{\mathrm{q}_{\mathrm{1}}^{*}} \tag{35}$$

Next section gives some insight into its possible application in terms of structural design.

3.5 Designing with indeterminate force diagrams

Design freedom due to static indeterminacy. As previously pointed out, static indeterminacy plays an important role in structural design. Because strut-and-tie modelling is fundamentally devoted to plastic design, a methodology has been proposed in Section 3.3 to manage this question using geometrically indeterminate force diagrams, which degree of geometric freedom is related to the number of independent self-stress states that may coexist within the structure. Besides the potentialities offered for limit state analysis (Section 3.4), geometric freedom within force diagrams is also particularly attractive in the context of structural design. Indeed, it gives the designer additional freedom for choosing a structural solution that responds to the prerequisites, above all when the design constraints are to an extent that strut-and-tie network geometry cannot be modified.

Design strategies. Various types of strategies have been developed for plastic design, depending on the problem statement as well as on the designer's methodology. For instance, following Billington (1997), Zastavni (2008) interprets Robert Maillart's design method as an additive process involving specific answers to distinct structural questions. The design strategy is mostly directed at the shaping of the structure (Zastavni et al., 2014). The geometry of the strut-and-tie model (for arch bridges: the compressive funicular polygon) is resulting from this process. In a different context, Muttoni et al. (1996) propose a method for *dimensioning* reinforced concrete structures for which the overall geometry is given. The design statge then consists in choosing a statically admissible distribution for the stresses, in which related strut-and-tie models are successively refined to match with the yield conditions.

Focusing now on the possibilities offered by the aforementioned methodology, various design strategies can be identified, three of them being outlined hereafter. These strategies consist in modifying the self-stress states in order to adapt the stress distribution to different criteria.

(a) Prevention of yielding. Self-stress states can be used to redistribute stresses when they exceed material strength in some parts of the structure. Considering for instance the statically indeterminate structure of **Figure 36**, in which concrete rods $\mathbf{f_1}$ and $\mathbf{f_2}$ are yielded, the stress state can be modified by adding two self-stress states, reducing the magnitude of the force transmitted within the corresponding struts. This results in shortening $\mathbf{f_1^*}$ and $\mathbf{f_2^*}$ so that their length in $\mathbf{F^*_{(a)}}$ does not exceed $\mathbf{f_u^*}$. Thus, the yield stress is not reached in any of the concrete struts.

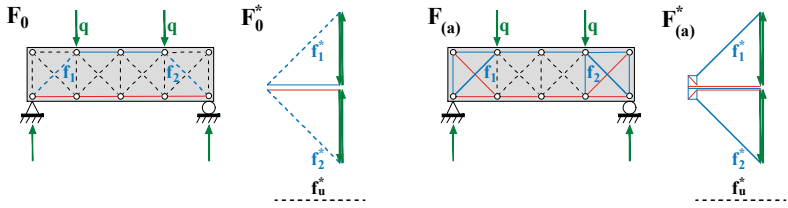

Figure 36 *Prevention of yielding by modifying* $\mathbf{F_0^*}$ *into* $\mathbf{F^*_{(a)}}$ *with two symmetric self-stress states.*

(b) Optimised distribution of stresses. The same methodology can be used to aim for homogeneous stress distribution. Considering the structure of **Figure 37**, forces acting in concrete rods $\mathbf{f_1}$ and $\mathbf{f_2}$ can be reduced to those of the horizontal strut $\mathbf{f_0}$. This results in equalising length of $\mathbf{f_1^*}$ and $\mathbf{f_2^*}$ to those of $\mathbf{f_0^*}$ in $\mathbf{F^*_{(b)}}$.

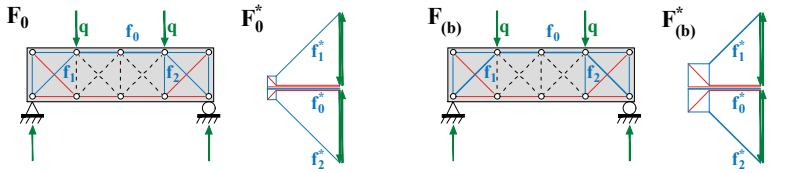

Figure 37 *Optimization of the stress distribution in the concrete rods by modifying the magnitude of the self-stress states.*

(c) Increase of the load bearing capacity. Thanks to self-stress states, the structure's load bearing capacity can be increased. In other words, it is possible to add a stress state to the structural system, generated by an increment $\delta\mathbf{q}$ of the applied load. The addition of both $\mathbf{q}$ and $\delta\mathbf{q}$ without yielding is made possible thanks to the modification of the self-stress states. The resulting stress state $\mathbf{F}_{(c)}$-$\mathbf{F}^*_{(c)}$, in equilibrium with the increased applied loads, is such that stresses never exceed material strength. In this way, the structure's load bearing capacity of is increased by its static indeterminacy.

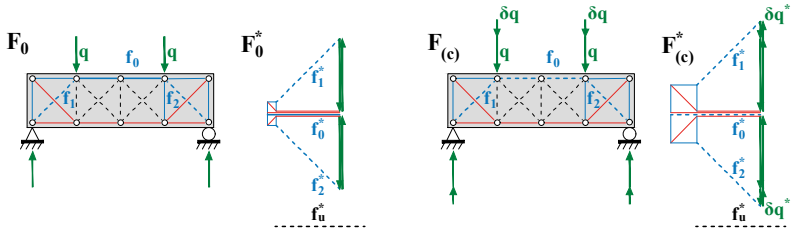

Figure 38 *Increase of the load bearing capacity of the structure by increasing the magnitude of the self-stress states.*

The role of *dimensioning*. These three strategies for redistributing stresses thanks to self-stress states are only one aspect of the structural design process. They must be accompanied by a correct and design-oriented sizing of the structural elements, as a function of the stress the designer wants to put in. However, working on both aspects (stress distribution and sizing) may provide the structural engineer a greater freedom as well as a better confidence in the decision-making process for the *dimensioning* of structures.

The issue of robustness. As mentioned in the introductory section of this chapter, one of the key issues in structural design is the question of robustness. Intended here as the capacity of a structure to find alternative paths for the stresses, robustness is consequently deeply related to the structure's static indeterminacy. The aptitude to manipulate indeterminacy through self-stress states puts the designer on the trail for a better

robustness-oriented design attitude. The work initiated in this direction by Deschuyteneer et al. (2015) and Zastavni et al. (2016) is very promising.

Despite the great potentiality of the method in term of design, this dissertation is dedicated to the question of the graphical limit state analysis of statically indeterminate structures by means of reciprocal diagrams. Hence the exclusive focus on this question for the three last chapters. Next chapter is specifically dedicated to the limit state analysis of pin-jointed trusses.

Chapter 4

Pin-jointed trusses

The objective of this chapter is to implement graphical limit state analysis on pin-jointed trusses.

After recalling the fundamental assumptions adopted for this type of structures , the methodology is performed on simple trusses before a six-steps optimization procedure is proposed. As a result of this procedure of limit analysis, the collapse load factor is obtained for several case studies. This chapter ends with some perspectives towards an extended use of parametric force diagrams for analysis as well as for design purposes.

4.1 Working hypotheses

In this chapter, we apply the graphical limit state analysis procedure to a specific type of structures called pin-jointed trusses, or simply trusses. These well known structures are supposed to respect several hypotheses, which allow to simplify their structural behaviour (Frey, 2000):

- they are composed by a series of rectilinear bars;
- these bars are jointed together by perfectly articulated nodes (pin-jointed);
- the external loads may only consist in point forces applied on the nodes.

As a consequence, the action line of the internal force acting within a bar is parallel to the direction of the bar (the line of action's eccentricity can be neglected). Therefore, the strut-and-tie network, which model the structural behaviour, has the exact shape of the truss itself.

Even if those assumptions may not be perfectly fitting the constructive reality, this has usually no consequence on the global behaviour (Latteur, 2016).

Apart from these hypotheses, the assumptions that allow the application of the plastic theorems must be added (Section 1.2). These are summarised hereafter for the case of pin-jointed trusses.

- The structural material behaves like a elastic-perfectly plastic material. For steel trusses, this hypothesis is very close to the reality; for other materials (e.g. construction wood) this assumption must be discussed (Trautz and Koj, 2009). In any case, it is supposed that the bars can stand large plastic deformations before rupture **(Fig. 1)**.
- Each bar is supposed to be sized in such a way that buckling and other instabilities cannot occur before the yield stress is reached.

In addition, it is assumed for the following paragraphs that each bar can support the same ultimate yield force f_u, no matters it is in compression or in traction.

4.2 Complete graphical limit state analysis

In this section, the graphical methodology proposed in Chapter 3 is applied to the complete limit state analysis of pin-jointed trusses.

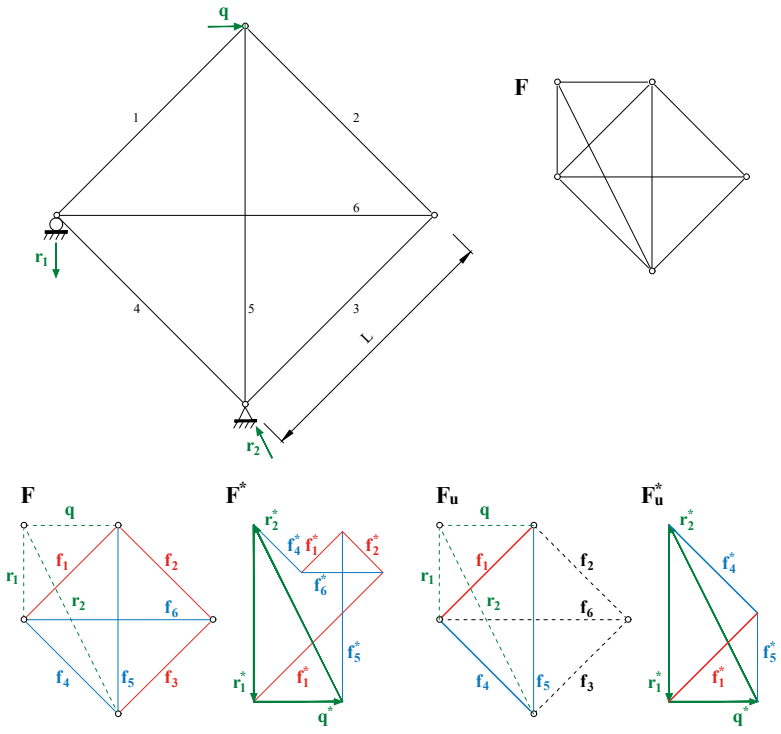

Figure 39 *Graphical limit state analysis of a statically indeterminate pin-jointed truss.*

The basic truss network of **Figure 39** is first considered. The structure being externally statically determinate, the applied load $\mathbf{q}$ generates determinate reaction forces $\mathbf{r_1}$ and $\mathbf{r_2}$. This pin-jointed truss is actually equivalent to the form diagram **F** analysed in **Figure 35**.

A kinematic limit analysis is applied on all the kinematically admissible mechanisms using the Principle of Virtual Works (Rondeaux et al., 2017). All these mechanisms are represented in **Figure 40** and the corresponding ratios $\rho_{k,m}$ of the magnitude of the applied force $q_{k,m}$ that provokes this mechanism, to the ultimate normal force f_u are listed in **Table 2**.

They are calculated by equating the work done by $\mathbf{q}$ in the displacement of its application point in the direction of the force, the work of the other external forces (reaction forces) being null:

$$\delta W_{ext} = \mathbf{q} \cdot \delta_{\mathbf{q}} \tag{36}$$

The work done by the internal stresses can be calculate considering that only axial forces act in pin-jointed networks and that the elastic strains in the bars can be neglected compared to the plastic ones occurring in the plasticised bars, so that:

$$\delta W_{int} = \sum_{\beta} f_u \cdot \delta l_\beta \tag{37}$$

The magnitudes of $\mathbf{q}$ and $\mathrm{f_u}$ being fixed, this ratio $\rho_{k,m}$ is proportional to the load factor $\lambda_{k,m}$:

$$\rho_{k,m} = \frac{q_{k,m}}{f_u} = \lambda_{k,m} \cdot \frac{q}{f_u} \ \forall m \tag{38}$$

Comp. mech.	ρ_k	Comp. mech.	ρ_k	Comp. mech.	ρ_k
K_{12}	$\sqrt{2}$	K_{13}	$\sqrt{2}$	K_{14}	$\frac{\sqrt{2}}{2}$
K_{15}	$1+\frac{\sqrt{2}}{2}$	K_{16}	$1+\frac{\sqrt{2}}{2}$	K_{23}	–
K_{24}	$\sqrt{2}$	K_{25}	$1+\frac{\sqrt{2}}{2}$	K_{26}	–
K_{34}	$\sqrt{2}$	K_{35}	$\frac{1+\sqrt{2}}{2}$	K_{36}	–
K_{45}	$\frac{1+\sqrt{2}}{2}$	K_{46}	$1+\frac{\sqrt{2}}{2}$	K_{56}	1

Table 2 *Kinematic load factors relative to 15 kinematically compatible mechanisms. In bold: collapse mechanism and corresponding ratio ρ.*

To identify the collapse mechanism and the corresponding collapse load factor λ_u, we may take advantage of the lower-bound theorem of plasticity:

$$\lambda_u = min_m\{\lambda_{k,m}\} = min_m\{\frac{q_{k,m}}{q}\}\ \forall m \tag{39}$$

Because of the proportionality between $\lambda_{k,m}$ and $\rho_{k,m}$, Equation 39 is equivalent to:

$$\rho_u = min_m\{\rho_{k,m}\} = min_m\{\frac{q_{k,m}}{f_u}\}\ \forall m \tag{40}$$

In case of **Table 2**, the lowest value for $\rho_{k,m}$ is identified for the collapse mechanism K_{14}, where bars 1 and 4 are plasticised. For this mechanism:

$$\lambda_u = \rho_u \cdot \frac{f_u}{q_1} = \frac{\sqrt{2}}{2} \cdot \frac{f_u}{q_1} \tag{41}$$

This value being exactly the same as the one obtained using the collapse force diagram $\mathbf{F}^*_\mathbf{u}$ where $\mathrm{f}^*_1 = \mathrm{f}^*_4 = f^*_u$, the three theorems of limit analysis expressed by Equation 4 are verified. Through this dissertation, comparisons between static and kinematic approaches are used to confirm the results obtained by applying the proposed graphical methodology to the various case studies.

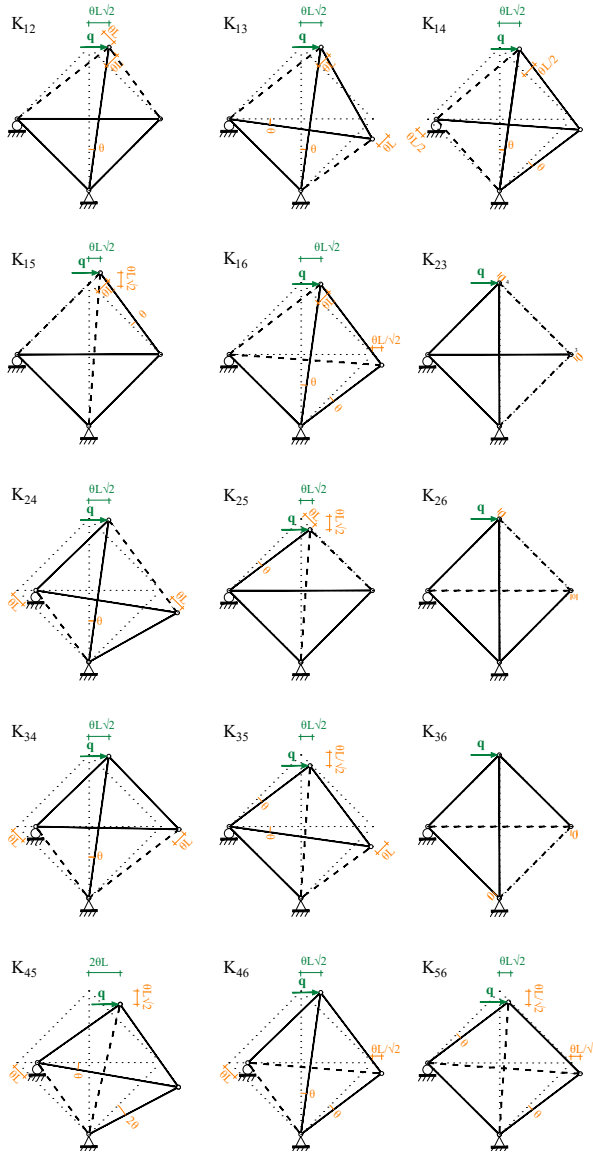

Figure 40 *Kinematically compatible mechanisms for the pin-jointed truss of* ***Figure 39****.*

The same methodology is applied to a truss two times statically indeterminate (**Fig. 41**). The form diagram of this truss is equivalent to the one analysed in **Figure 31**, which Maxwell's rigidity number $N = -3$. Indeed, self-stress states $\mathbf{F_1} - \mathbf{F_1^*}$ and $\mathbf{F_2} - \mathbf{F_2^*}$ of **Figure 31** can be considered as external stress state due to the applied load $\mathbf{q}$ and to excess reaction force $\mathbf{f_{e1}}$ respectively.

Figure 41 shows the three independent pairs of reciprocals diagrams $\mathbf{F_q} - \mathbf{F_q^*}$, $\mathbf{F_{e1}} - \mathbf{F_{e1}^*}$ and $\mathbf{F_2} - \mathbf{F_2^*}$.

The three force diagrams are then assembled in one sole force diagram $\mathbf{F}^*$ on which a geometrical limit state analysis is applied. In this case, a collapse mechanism can be formed if two or three bars have yielded. Six different configurations for the force diagram can be found in which this limit is reached; these diagrams are represented in **Figure 42**. Since the structure has one external degree of static indeterminacy, the reaction forces may have different magnitudes and constitute one degree of freedom of the force diagram $\mathbf{F}^*$; the second one being cause by the internal static indeterminacy of the pin-jointed network.

Among the six limit force diagrams $\mathbf{F^*_{s,1\to 6}}$ in **Figure 42**, it is easy to observe that both limit force diagrams $\mathbf{F^*_{s,5}}$ and $\mathbf{F^*_{s,6}}$ present the highest length for the applied force $\mathbf{q}^*$, so that both of them can be considered as the collapse force diagram. Actually, this can be explained by the fact that the collapse mechanism is produced by yielding of only two bars, 1 and 2; so it doesn't really matter which one of the other bar is also yielded since the magnitude of collapse load $\mathbf{q_u}$ is fixed by the magnitude of $\mathbf{f_1}$ and $\mathbf{f_2}$ that have yielded:

$$\mathrm{q_u^*} = \mathrm{f_1^*} \cdot \sqrt{2} = \mathrm{f_2^*} \cdot \sqrt{2} = \mathrm{f_u^*} \cdot \sqrt{2} \tag{42}$$

Or equivalently:

$$\lambda_u^* = \rho_{s,5}^* \cdot \left(\frac{f_u}{q}\right) = \rho_{s,6}^* \cdot \left(\frac{f_u}{q}\right) = \sqrt{2} \cdot \left(\frac{f_u}{q}\right) \tag{43}$$

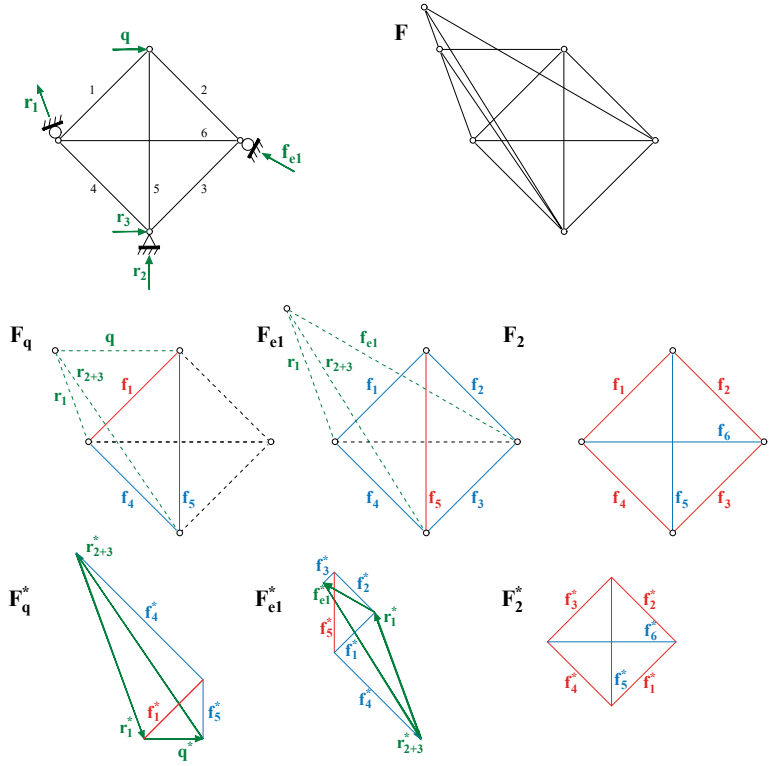

Figure 41 *Pin-jointed truss with three independent stress states. The three pairs of form and force diagrams are respectively due to the external load* $\mathbf{q}$ $(\mathbf{F_q} - \mathbf{F^*_q})$*, to an excess reaction force* $(\mathbf{F_{e1}} - \mathbf{F^*_{e1}})$ *and to an internal indeterminacy* $(\mathbf{F_2} - \mathbf{F^*_2})$

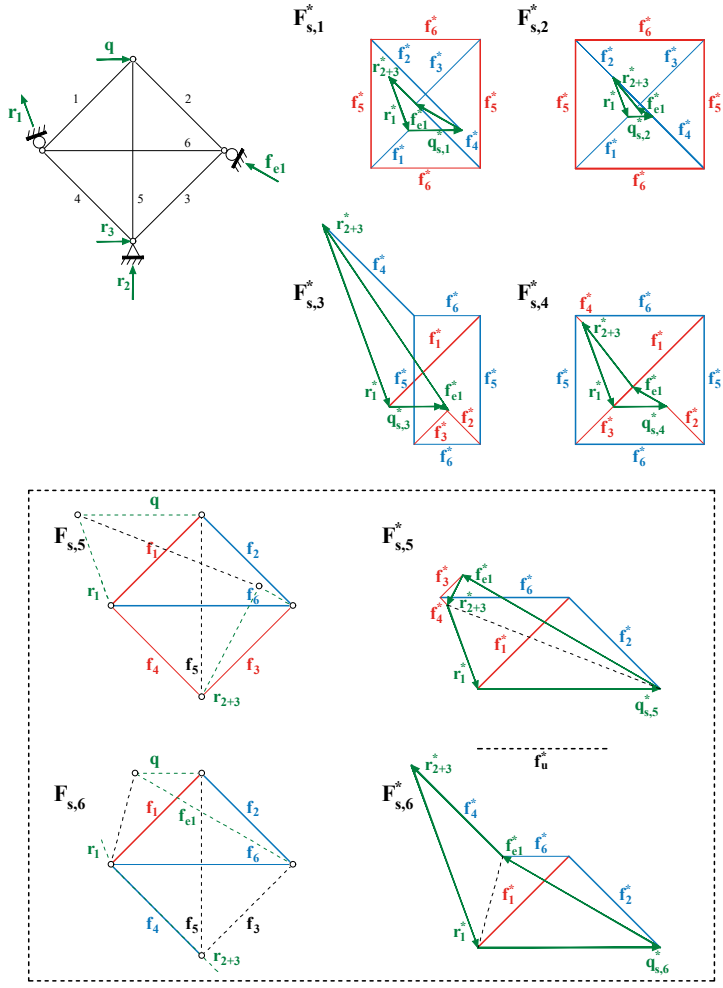

Figure 42 *Full graphic static limit state analysis of the network, with six limit force diagrams* $\mathbf{F^*_{s,1\to 6}}$. *Diagrams* $\mathbf{F^*_{s,5}}$ *and* $\mathbf{F^*_{s,6}}$ *are two possible collapse diagrams since they both present the highest length for the applied load vector* $\mathbf{q}^*$.

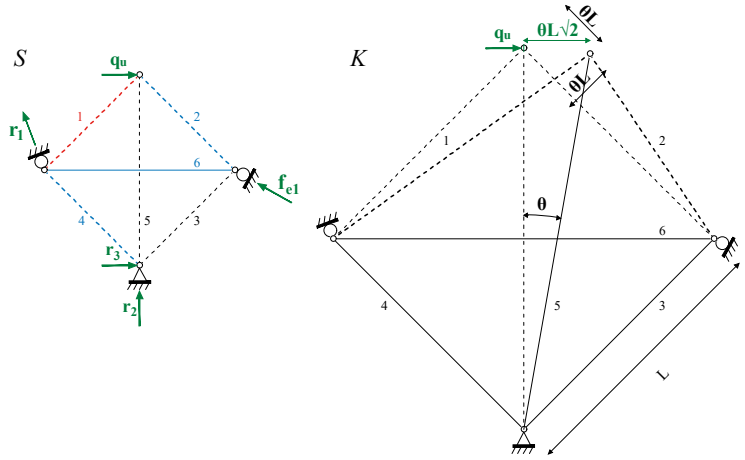

Figure 43 *Kinematic analysis on the collapse mechanism.*

In order to confirm this result, a kinematic analysis has been done on this structure for a collapse mechanism occurring when bars 1, 2, and 4 have yielded. **Figure 43** illustrates this kinematic analysis on the chosen collapse mechanism: assuming a rotation θ of bar 5 and the consecutive displacement of the application point of $\mathbf{q}$ in the direction of the force, the work of the external forces is only due to $\mathbf{q}$ since all the other external forces are reaction forces on non moving points:

$$\delta W_{ext} = \mathbf{q_u} \cdot \delta \mathbf{u_q} \tag{44}$$

The work done by the internal stresses can be calculated considering the plastic strains in the yielded bars 1 and 2, so that:

$$\delta W_{int} = f_1 \cdot \delta l_1 + f_2 \cdot \delta l_2 \tag{45}$$

Since the magnitude of the force acting in bars 1 and 2 is equal to $\mathrm{f_u}$, equating these two quantities gives the magnitude of $\mathbf{q_u}$:

$$\mathrm{q_u} \cdot \theta L\sqrt{2} = \mathrm{f_u} \cdot \theta L + \mathrm{f_u} \cdot \theta L \rho_k \leftrightarrow \frac{\mathrm{q_u}}{\mathrm{f_u}} = \sqrt{2} \tag{46}$$

When looking to the collapse force diagram $\mathbf{F_u^*}$ of **Figure 42**, the same ratio between the length of $\mathbf{q_u^*}$ and the length of $\mathbf{f_1^*}$ and $\mathbf{f_2^*}$ can be found:

$$\rho_s^* = \frac{q_u^*}{f_u^*} = \sqrt{2} \tag{47}$$

Since both ratio's ρ_s^* and ρ_k obtained respectively by the graphical methodology and by the kinematic analysis are equal, the theorems of limit analysis then ensure that the collapse load factor λ_u can be calculated as:

$$\lambda_u = \rho_k \cdot \left(\frac{f_u}{q}\right) = \sqrt{2}\left(\frac{f_u}{q}\right) \tag{48}$$

4.3 Optimization procedure on the force diagram

For high degrees of static indeterminacy, or when the amount of bars increases, it becomes more and more inconvenient to analyse all the limit stress states for determining the collapse one among them. Indeed, this would mean to draw as much limit force diagrams $\mathbf{F^*_{s,j}}$ as there are possible limit states. In order to avoid it, a systematic methodology is proposed in this section for determining automatically the limit load acting on a given 2D statically indeterminate network. It takes advantage of the fact that any degree of static indeterminacy of a structure corresponds to a degree of freedom of its correlated force diagram $\mathbf{F}^*$. Considering these degrees of freedom as geometric parameters of $\mathbf{F}^*$, this procedure is developed for internally statically indeterminate structures (Rondeaux et al., 2017) as well as for externally ones (Rondeaux et al., 2018a) in collaboration with ETH Zurich. These two procedures are assembled here in one sole procedure including both internal and external static indeterminacy.

Systematic procedure for constructing a parametric force diagram.

- **Step 1** - The degrees of external and internal static indeterminacy of a structure subjected to a given loading $\{\mathbf{q}\}$, is obtained by counting the number n_i of independent self stress states and the number n_e of independent external stress states due to the excess reaction forces with respect to a statically determinate configuration. Considering that the structure presents no kinematic indeterminacy, this corresponds to the opposite of Maxwell rigidity number N for the form diagram $\mathbf{F}$: $n_e + n_i = -N$. An extra stress state due to the applied forces must be considered, so that there are $n_i + n_e + 1$ independent stress states.

- **Step 2** - The $n_i + n_e + 1$ associated force diagrams are drawn at arbitrary scales. We use the following notations for them:

  1. $\mathbf{F^*_i}$ is the force diagram related to the ith self-stress state: $i \in \{1; n_i\}$;
  2. $\mathbf{F^*_{ej}}$ is the force diagram related to the jth unknown external stress state: $j \in \{n_i + 1; n_i + n_e\}$;
  3. $\mathbf{F^*_q}$ is the force diagram related to the given external loads.

– **Step 3** - The independent force diagrams $\mathbf{F_i^*}$, $\mathbf{F_{ej}^*}$ and $\mathbf{F_q^*}$ are assembled into one single force diagram $\mathbf{F}^*$, by performing a vector addition of the corresponding vectors.

– **Step 4** - Considering a fixed length for the vector $\mathbf{q}^*$ corresponding to the given loading, each degree of freedom of the force diagram $\mathbf{F}^*$ is detected, which corresponds to an offset of one of the independent force diagrams $\mathbf{F_i^*}$ or $\mathbf{F_{ej}^*}$ (Mitchell et al., 2016). $\mathbf{F}^*$ can consequently be transformed into a parametric force diagram $\mathbf{F_p^*}$, in which each degree of freedom depends on a parameter x_i or x_{ej} defined as the position of the node P_i^* or P_{ej}^* respectively, along the line of action of one of the internal forces $\mathbf{f_i^*}$ or excess reaction forces $\mathbf{r_j^*}$. Since the positions of all the other nodes of $\mathbf{F_p^*}$ can be deduced from x_i or x_{ej} by geometrical constructions, the variation of the x_i and x_{ej} describes the overall geometric transformation of $\mathbf{F_p^*}$.

– **Step 5** - As the length of $\mathbf{q}^*$ is kept constant, corresponding to the given magnitude of the applied load $\mathbf{q}$, maximizing its magnitude $|\mathbf{q}|$ is equivalent to maximizing the ratio between $|\mathbf{q}|$ and the magnitude $\mathrm{f_u}$ of the admissible normal force in the bars. In terms of graphic statics, this is equivalent to maximizing the ratio between the length of $\mathbf{q}^*$ and the one of the longest $\mathbf{f_i^*}$ in the force diagram $\mathbf{F}^*$.
An optimization process is consequently applied on the values of the x_i and $x_{e,j}$ in order to minimise the length of the $\mathbf{f_i^*}$. Out of this step, the collapse force diagram $\mathbf{F_u^*}$ is obtained.

The optimization functions that are dealt with in this graphical procedure are in general non-linear. A global optimization algorithm such as an evolutionary algorithm, can be used in the first place in order to locate an intermediate solution close to the global optimum. Afterwards, provided that the function is continuous, the optimization problem can be solved using a gradient-based algorithm. The algorithms used to solve the optimization problems treated in this section and in the followings are the ones included in the Grasshopper plugin Goat (Flöry et al., 1990), which relies on the *NLopt* library (Johnson, 1990).

– **Step 6** - The last step consists in applying a scale factor to the entire collapse force diagram $\mathbf{F^*_u}$. This factor is defined as:

$$\lambda_u = \frac{s^*_u}{s^*} \quad : \quad max_i\{\mathrm{f}^*_\mathrm{i}\} \cdot \lambda_u = \mathrm{f}^*_\mathrm{u} \tag{49}$$

It transforms $\mathbf{F^*_u}$ into $\lambda_u \mathbf{F^*_u}$ in which length of the longest bar is exactly equal to f^*_u, the length corresponding to the admissible normal force f_u. This scaling is equivalent to apply to $\mathbf{q}$ a collapse load factor λ_u:

$$q \cdot \lambda_u = \mathrm{q}^* \cdot s^* \cdot \lambda_u = \mathrm{q}^*_\mathrm{u} \cdot s^* = q_u \tag{50}$$

This transformation is equivalent to read $\mathbf{F^*_u}$ at a scale s^*_u:

$$\mathrm{q}^* \cdot s^*_u = \mathrm{q}^* \cdot \lambda_u \cdot s^* = \mathrm{q}^*_\mathrm{u} \cdot s^* = q_u \tag{51}$$

Application to a truss two times statically indeterminate. This procedure is illustrated in **Figure 44** for the very simple network already used in the previous section. This structure presents one internal and one external degrees of static indeterminacy (Step 1), corresponding respectively to a self-stress state $\mathbf{F^*_1}$ and to a stress state $\mathbf{F^*_{e1}}$ produced by $\mathbf{f^*_{e1}}$ (Step 2). These two force diagrams has to be combined with $\mathbf{F^*_q}$, the one due to the external given load $\mathbf{q}^*$. Combining these three force diagrams produces the complete force diagram $\mathbf{F}^*$ (Step 3). To transform it into a parametric force diagram $\mathbf{F^*_p}$, the position of points P^*_{e1} and P^*_1 is chosen along the direction of $\mathbf{f^*_{e1}}$ and $\mathbf{f^*_6}$ respectively (Step 4). The optimization process on $\mathbf{F^*_p}$ produces the collapse force diagram $\mathbf{F^*_u}$ in which $\mathbf{f^*_1}$, $\mathbf{f^*_2}$ and $\mathbf{f^*_4}$ have reached the same length $\mathrm{f}^*_\mathrm{max}$ (Step 5). Scaling this diagram by a scale factor λ_u so that $\lambda_u \cdot \mathrm{f}^*_\mathrm{max} = \mathrm{f}^*_\mathrm{u}$ gives the actual collapse force diagram $\mathbf{F^*_u}$ at the chosen scale s^* (Step 6).

This force diagram $\mathbf{F^*_u}$ is identical to the one obtained in **Section 4.2** by a complete limit state analysis of the same structure.

In the next section, the proposed methodology is applied to several case studies. The results are systematically compared to the ones obtained by applying a kinematic analysis to the corresponding collapse mechanism.

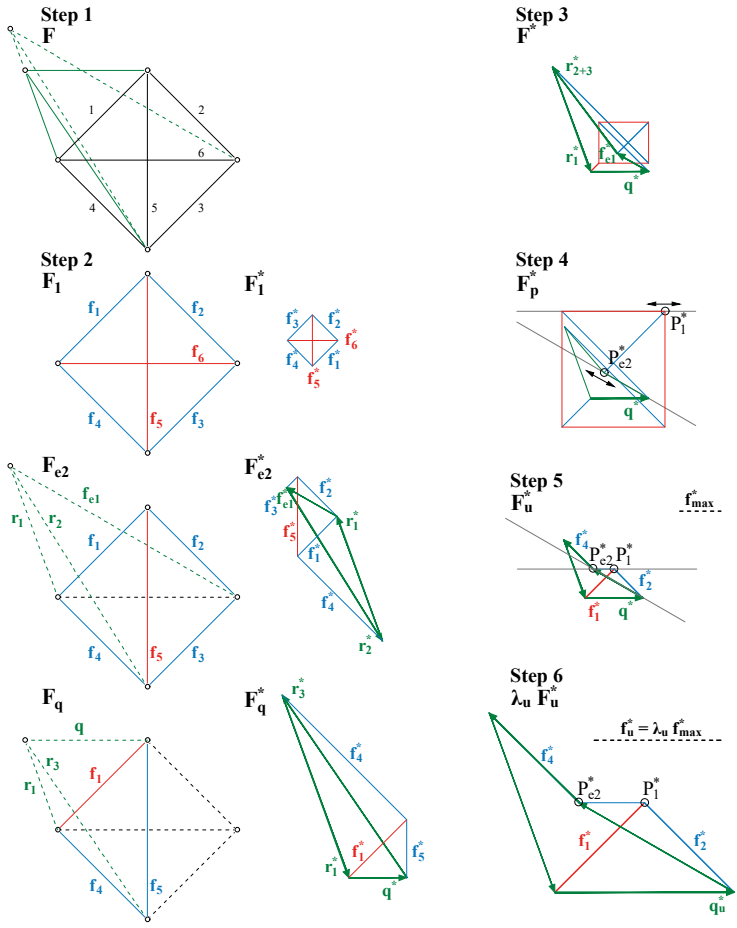

Figure 44 *Six-steps procedure for determining the load factor of a pin-jointed network under given loading* $\mathbf{q}$.

4.4 Case studies: internally and externally statically indeterminate trusses

The graphical procedure described in the previous section is applied to several 2D pin-jointed trusses. Some of these case studies are taken from papers presented in IASS annual symposiums Rondeaux et al. (2017; 2018a). The results are confronted to the ones obtained by a kinematic limit state analysis.

Case study 1A

Following this graphical procedure, we first define the form $\mathbf{F_q}, \mathbf{F_1}$ and force $\mathbf{F_q^*}, \mathbf{F_1^*}$ diagrams of the two independent stress states of the given network. The reciprocals diagrams $\mathbf{F_q}$ and $\mathbf{F_q^*}$ are related to the stress state generated by the three external forces; the ones $\mathbf{F_1}$ and $\mathbf{F_1^*}$ to the self stress state. The diagrams are drawn using arbitrary scale factors within the digital CAD environment *McNeel Rhinoceros*. Then, we assemble $\mathbf{F_q^*}$ and $\mathbf{F_1^*}$ and, using the parametric tool *Grasshopper*, we construct a parametric force diagram $\mathbf{F_p^*}$ where the external loads are fixed. Here we define the position of node P^* along the line of $\mathbf{f_5^*}$ in $\mathbf{F_p^*}$ as the parameter of the optimization process. In this process, we minimize the highest of the absolute magnitudes $\mathrm{f_i^*}$ of the force vectors in $\mathbf{F_p^*}$. The collapse form $\mathbf{F_u}$ and force $\mathbf{F_u^*}$ diagrams are obtained, with the identification of the collapse load $\mathbf{q_u^*}$ and of the yielded bars $\mathbf{f_1^*}$ and $\mathbf{f_4^*}$ for which $\mathrm{f_1^*} = \mathbf{f_4^*} = \mathrm{f_u^*}$. The solution found gives a ratio $\frac{\mathrm{q_u^*}}{\mathrm{f_u^*}} = \rho_u = 0.707$. The comparison with the results obtained by both complete static and kinematic analyses shows that the same collapse force diagram $\mathbf{F_u^*}$ and the same value for $\rho_u = \frac{\sqrt{2}}{2}$ are obtained. Therefore, we can deduce geometrically the collapse load factor:

$$\lambda_u^* = \frac{\sqrt{2}}{2} \frac{\mathrm{f_u^*}}{\mathrm{q^*}} \tag{52}$$

Case study 1B

The graphic procedure is also applied to a similar network with two external static redundancies, as detailed in **Figure 46**.
The two excess reaction forces $\mathbf{f_{e1}}$ and $\mathbf{f_{e2}}$ are chosen as parameters of the

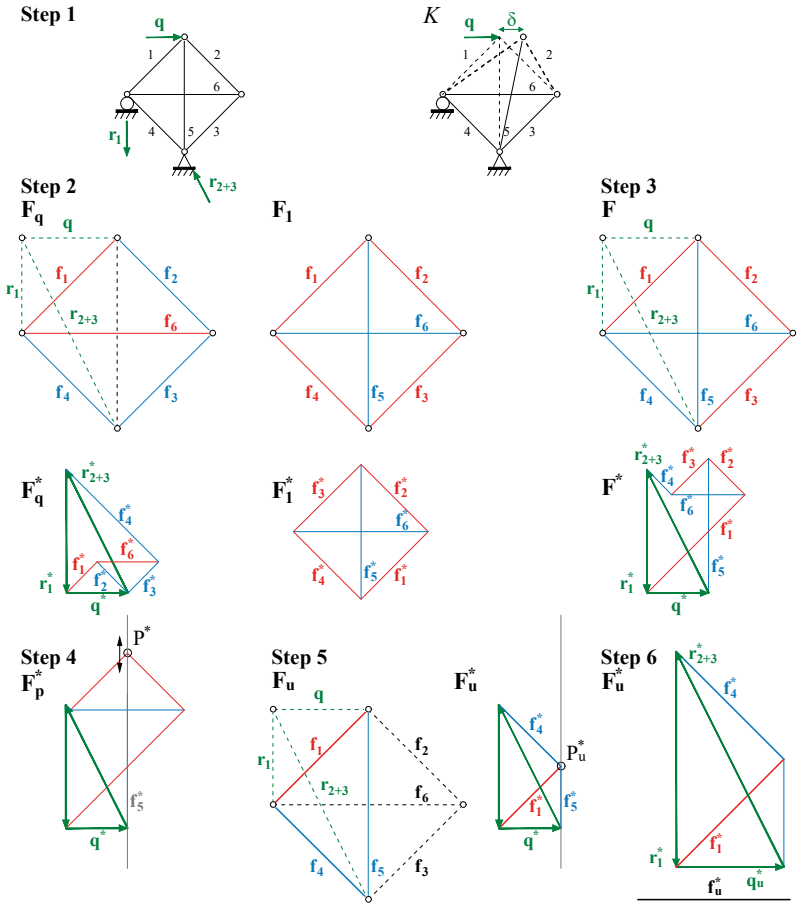

Figure 45 *Application of the proposed graphical procedure for the limit analysis of a network with one degree of internal static indeterminacy: form diagrams* $\mathbf{F_q^*}$, $\mathbf{F_1}$ *and reciprocal force diagrams* $\mathbf{F_q^*}$, $\mathbf{F_1^*}$ *of the independent stress states; parametric force diagram* $\mathbf{F_p^*}$*; collapse form diagram* $\mathbf{F_u}$ *with identification of the yielded bars* $\mathbf{f_1}$ *and* $\mathbf{f_4}$*; collapse force diagram* $\mathbf{F_u^*}$ *with identification of the collapse load* $\mathbf{q_u^*}$ *so that* $f_1^* = f_4^* = f_u^*$.

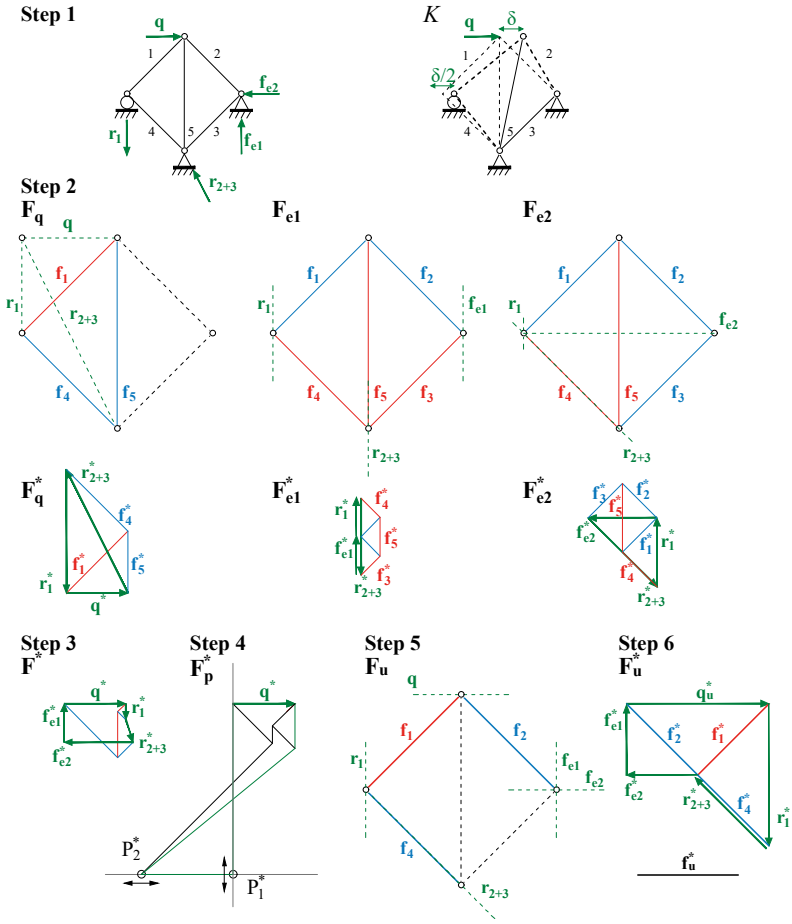

Figure 46 *Application of the proposed graphical procedure for the limit analysis of a network with two degrees of external static indeterminacy: form diagrams* $\mathbf{F_q^*}$, $\mathbf{F_{e1}}$, $\mathbf{F_{e2}}$ *and reciprocal force diagrams* $\mathbf{F_q^*}$, $\mathbf{F_{e1}^*}$, $\mathbf{F_{e1}^*}$ *of the independent stress states; assembled force diagram* $\mathbf{F^*}$*; parametric force diagram* $\mathbf{F_p^*}$*; collapse form diagram* $\mathbf{F_u}$ *with identification of the yielded bars* $\mathbf{f_1}$, $\mathbf{f_2}$ *and* $\mathbf{f_4}$*; collapse force diagram* $\mathbf{F_u^*}$ *with identification of the collapse load* $\mathbf{q_u^*}$*. Bars in compression are depicted in blue, the ones in tension in red.*

static indeterminacy. The $2+1=3$ independent form and force diagrams are built and assembled in a complete force diagram $\mathbf{F}^*$. In the parametric force diagram $\mathbf{F^*_p}$, the variable positions of point P_1^* and P_2^* respectively along the line of action of reaction forces $\mathbf{f_{e1}}$ and $\mathbf{f_{e2}}$ respectively are chosen as parameters. The form and force collapse diagrams $\mathbf{F_u}$ and $\mathbf{F^*_u}$ are obtained after the optimization process. The collapse force diagram $\mathbf{F^*_u}$ is scaled in order to obtain the magnitude q^*_u of the applied load $\mathbf{q}$ leading to collapse:

$$\mathrm{q}^*_\mathrm{u} = \mathrm{f}^*_\mathrm{u} \cdot \sqrt{2} \tag{53}$$

with f^*_u the yield normal force that can be undertaken by the structural members. The analysis of the collapse form and force diagrams $\mathbf{F_u}$ and $\mathbf{F^*_u}$ reveals that yielding occurs in bars 1, 2 and 4. Considering these bars as being plasticized, the *Principle of Virtual Works* can also be applied to the corresponding collapse mechanism, which is also depicted in **Figure 46**:

$$\mathbf{q_u} \cdot \delta = \mathbf{f_u} \cdot \left(\delta \frac{\sqrt{2}}{2} + \delta \frac{\sqrt{2}}{4} + \delta \frac{\sqrt{2}}{4} \right) = \mathbf{f_u} \cdot \sqrt{2} \tag{54}$$

As both results are equal, this proves that the exact magnitude of the collapse load factor has been found using the graphic procedure:

$$\lambda^*_u = \frac{\mathrm{f}^*_\mathrm{u}}{\mathrm{q}^*} \sqrt{2} \tag{55}$$

Following the procedure described in **Section 3.3**, we analyzed some 2D networks with higher degrees of static indeterminacy. For each case study we first detect the degree of static indeterminacy of the structure and build up the form and force diagrams for every independent state of stress of the structure. We then assemble a parametric force diagram and eventually run the optimization process to obtain the collapse force diagram $\mathbf{F^*_u}$. From this, we can obtain by simple measurements the ratio's ρ^*_u.

Case study 2

In the case study shown in **Figure 47**, a structure with two degrees of internal static indeterminacy is taken into consideration, corresponding to two independent self-stress states $\mathbf{F_1}$-$\mathbf{F_1^*}$ and $\mathbf{F_2}$-$\mathbf{F_2^*}$. The parametric force diagram $\mathbf{F_p^*}$ is optimized with respect to the positions of the nodes P_1^* and P_2^*. The collapse force diagram $\mathbf{F_u^*}$ is obtained and the resulting collapse load factor can be compared to the ones calculated by applying a complete kinematic limit analysis on the corresponding collapse mechanism; both approaches give the same result:

$$\lambda_u = \lambda_s^* = \lambda_k = 1.762 \cdot \left(\frac{\mathrm{f_u}}{\mathrm{q}} \right) \tag{56}$$

Case study 3

In the second example illustrated in **Figure 48**, the same optimization procedure is applied on the positions of three nodes (P_1^*, P_2^*,P_3^*) of $\mathbf{F_p^*}$ to obtain $\mathbf{F_u^*}$. Once again, the collapse load factor obtained with the proposed graphical methodology is equal to the kinematic one calculated with a complete kinematic limit analysis:

$$\lambda_u = \lambda_s^* = \lambda_k = 1.155 \cdot \left(\frac{\mathrm{f_u}}{\mathrm{q}} \right) \tag{57}$$

Case study 4

As a fourth case study, the proposed graphical limit state procedure is applied to the structure of **Figure 49**, for three different support conditions. The network is internally statically determinate and presents some excess reaction forces at the supports. The form and force diagrams $\mathbf{F_u} - \mathbf{F_u^*}$ depicted in **Figure 49** are the ones corresponding to collapse. The length corresponding to the collapse load $|q_u^*|$ can be measured on the three $\mathbf{F_u^*}$.

The ratios $\rho_u^* = \frac{|q_u^*|}{|f_u^*|}$ obtained for the three support conditions are respectively equal to 0.333, 0.5 and 0.707, with the corresponding yielded bars depicted in bold in the figure. In practice, this type of results can give insight on the best support configuration to be implemented when designing a truss. This corresponds to the third case in the present study, as it allows the highest magnitude for the applied load $\mathbf{q}$.

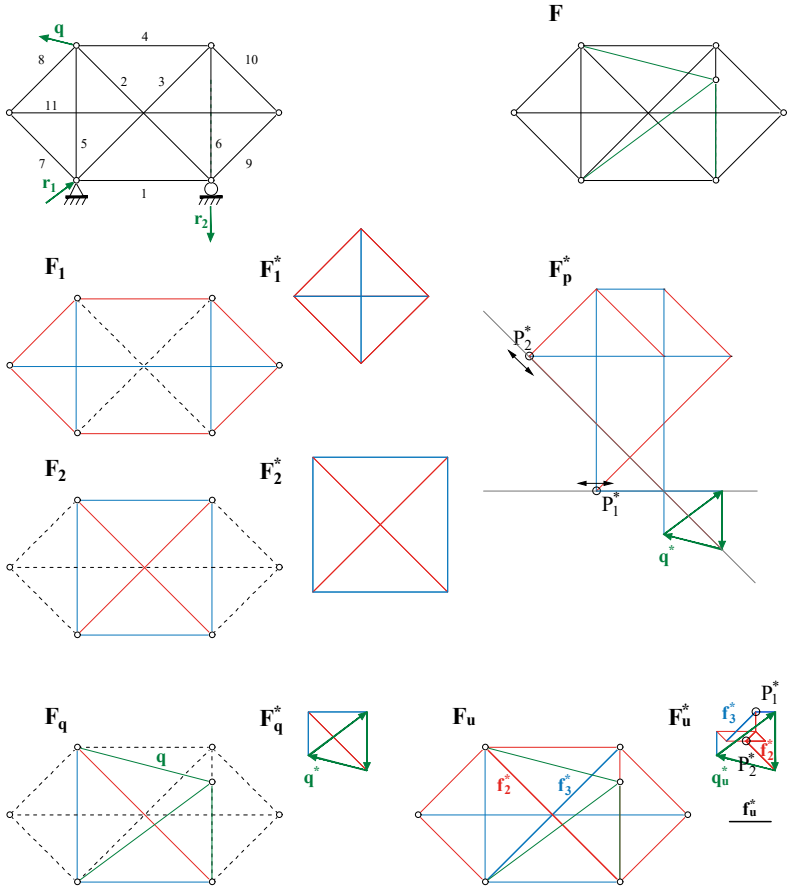

Figure 47 *Application of the graphical procedure for the limit state analysis of a network with two degrees of internal static indeterminacy.*

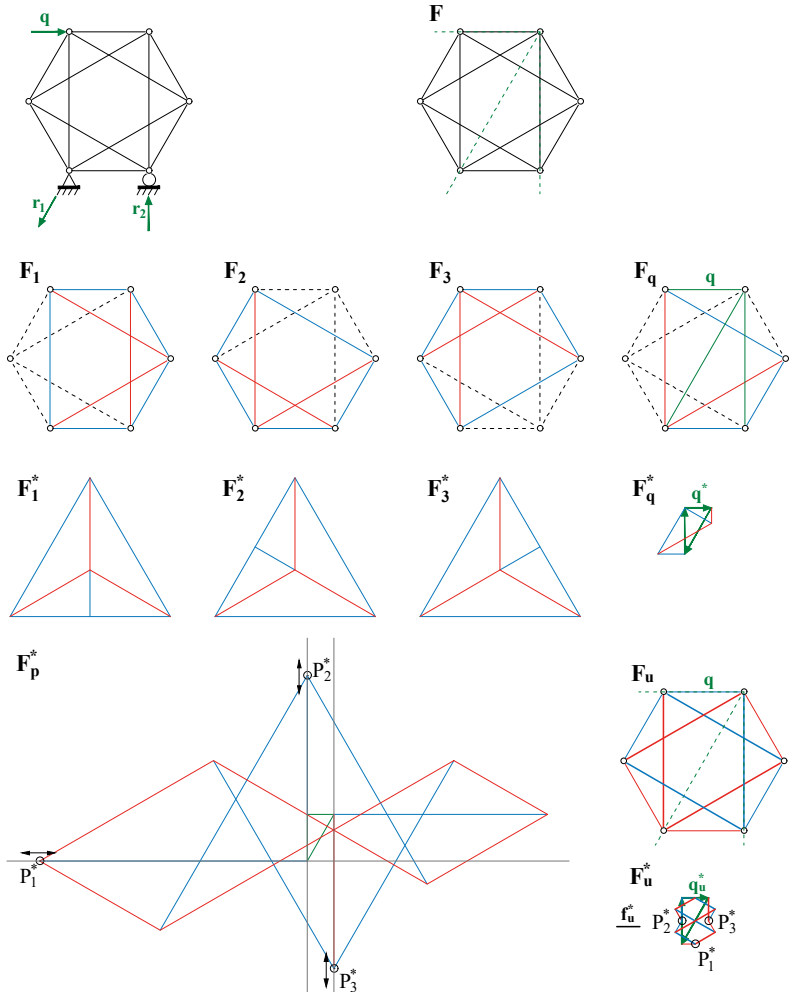

Figure 48 *Application of the graphical procedure for the limit state analysis of a network with three degrees of internal static indeterminacy.*

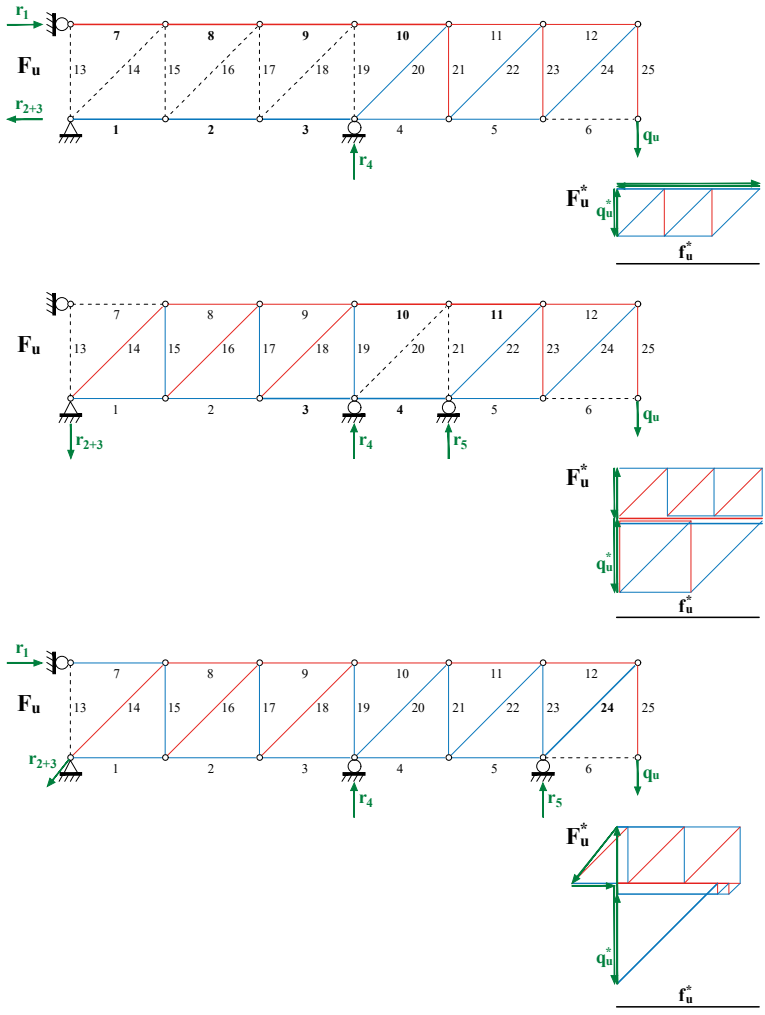

Figure 49 *Graphic limit state analysis of a pin-jointed framework externally statically indeterminate with three different support conditions. The three collapse force diagrams* $\mathbf{F_u^*}$ *present ratio's* $\rho_u^* = 0.333$, 0.5 *and* 0.707 *respectively. The corresponding yielded bars are depicted in bold in the form diagrams* $\mathbf{F_u}$.

4.5 Perspectives

Various perspectives in the development of this research on limit state analysis of pin-jointed networks can be expected, which are emphasised in the following paragraphs.

(a) Admissible geometrical domains. In his PhD thesis, Fivet (2013) introduces a geometrical support for computer-aided structural design, called "constraint-based graphic statics". Basically, he proposes to support the design process thanks to an interactive visual environment, in which the admissible positions of the vertices of both form and force diagrams are described by geometrical admissible domains. These graphical regions give the designer the possibility to describe, constrain and modify the static equilibrium according to various requirements. Moreover they inform the users on the scope of possibilities for the structural design.

One type of constraints that can be applied for defining these domains is related to the strength of the structural members. In the context of this dissertation, this constraint corresponds to limit the length of each segment of the force diagram to a value corresponding to the ultimate normal force of the corresponding bar. Therefore, it is possible to plot the admissible domain for the position of any vertex of the force polygon. Obviously, the domains of the different points interact with each other since, generally speaking, the positions of the vertices of the force diagram are not independent.

For example, **Figure 50** shows the domain D_P^* of point P^* that characterise the geometrical freedom of $\mathbf{F}^*$ when the origin of $\mathbf{q}^*$ is fixed. This domain is the set of the locations for P^* such as to respect the equilibrium and yield conditions. This domain is called "statically admissible" since it corresponds to the respect of the equilibrium and yield conditions of the lower-bound theorem of Plasticity.

Therefore, D_P^* can be analyzed in terms of limit states. Each of the vertices $P_{s,x}^*$ of the boundary of this domain is a location of P^* that produces a statically admissible limit state $S_{s,x}$. All the limit force diagrams are represented in **Figure 50** with the corresponding position of P^*; e.g. $P_{s,3}^*$

and $P^*_{s,7}$ are the positions of P^* that correspond to the collapse states of the truss Ω.

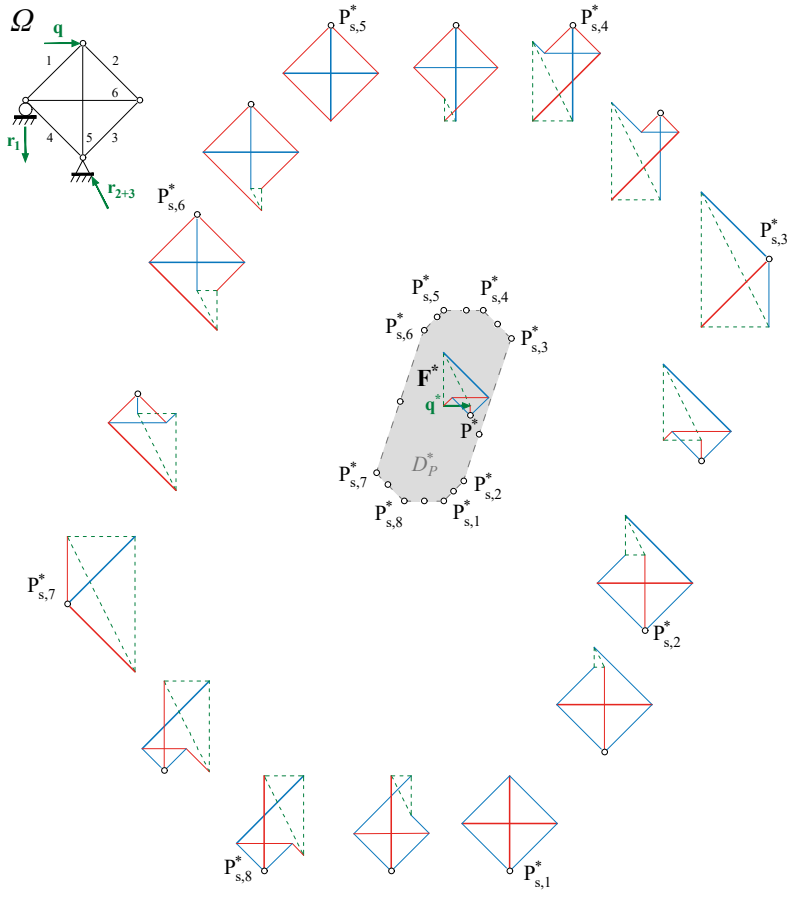

Figure 50 *Statically admissible domain D^*_P of point P^*.*

Further analysis of the properties of these domains would be of interest. Indeed, following the idea of Zastavni et al. (2015) and Deschuyteneer et al. (2015), these domains can be used to evaluate constitutive elements

of structural robustness. It is expected that the development of new tools can better inform the structural designer on the possible plastic redistribution of the stresses in the structure.

In the same vein, the application to reinforced concrete structures has been initiated by Deschuyteneer et al. (2018a) and offers numerous perspectives of development for design purposes.

(b) Interactive and 3D structural design. The application of the method to complex and real case studies would require an automation of the process. The principal question is the one of the systematic construction of the force diagram. This question has been resolved for 3D networks by researchers as Ohlbrock et al. (2018) from ETh Zurich. In collaboration with them, an attempt has already been made with success for applying the graphical limit state analysis to some basic structure. Further work would be needed to apply the methodology to design situations.

Chapter 5

Beams

In his dissertation, Fivet (2013, pp 287-288) outlined that constraint-based graphic statics is adequate in the context of preservation assessment "for structures with a plastic behaviour (such as reinforced concrete) (...) and also that "strut-and-tie networks are very well suited for use and abstractions of the stability of a very wide range of structures (...)". He mentioned, among others, the case of the Euler-Bernouilli beams subject to bending. Indeed, taking advantage of the relationship between bending moment diagrams and funicular polygon - see for instance Pirard (1950, pp 186-189) -, Fivet (2013) highlights "how bending moments can be controlled by purely geometric means with constraint-based graphic statics". He uses for this purpose an example from Zastavni (2008, appendix 4), a clamped horizontal beam with uniform inertia subject to two vertical loads. Using the lower-bound theorem of plasticity for design purposes, he deduces easily an optimum distribution of bending moments for which two plastic hinges are developed in order for a mechanism to exist.

This chapter begins with a reminder on the link between funicular polygon and bending moments. A methodology is developed for analyzing the collapse conditions using graphical constructions only. We first establish some basic principles concerning funicular polygons. Then we develop more explicitly the link to the theorems of plasticity in order to achieve a complete limit state analysis of that kind of structures by means of graphic constructions only. This method is further developed in order to integrate the concept of *admissible geometrical domain*. Its application to case studies proves that the results obtained are comparable to the ones found in the literature (Hodge, 1959; Horne, 1979; Heyman, 2008). Finally, we outline the potential developments of this method for the analysis and design of more complex structures (frames, continuous beams, etc.) by means of *admissible geometrical domains* (Deschuyteneer and Zastavni, 2017).

5.1 Bending and funicular polygons

Despite the controversial - and fascinating! - discussions around the confusion induced in many engineers' mind by Henri Navier's formulation of the mathematical elastic theory of elastic beams under bending loads (Schwartz, 2010; Rinke and Schwartz, 2010), bending moment is an essential concept when dealing with elastic but also with plastic bending. Indeed, for beams or frames under bending the plastic yield conditions are expressed in terms of full plastic moment M_u acting in the yielded cross sections. Considering the fundamental definition of bending moment $\mathbf{M}$ as the resultant vector moment of the stresses acting in a cross section, it follows that this moment must be in rotational equilibrium with the external forces applied on each fragment of the structure defined by the specific cross section. Therefore, it has to be such that the bending moment is the exact opposite of the momentum produced by the resultant of the external forces on the fragment. It follows that the bending moment is equivalent to the vector product of the resultant force vector $\mathbf{q_R}$ by the vector $\mathbf{d_G}$ describing the position of this force from the center of gravity G of the cross section

$$\mathbf{M} = \mathbf{q_R} \times \mathbf{d_G} \tag{58}$$

In terms of graphic statics, the magnitude of the resultant force $\mathbf{q_R}$ is obtained by measured its length q_R^* at scale s^* in the force diagram $\mathbf{F}^*$; and the magnitude of the projection of the position vector $\mathbf{d_G}$ perpendicularly to the line of action of $\mathbf{q_R}$ by measuring its segment at scale s in the form diagram $\mathbf{F}$. The length of this projection is referred as ν in **Figure 51**. Since these two lengths are perpendicular, the magnitude of the bending moment M is obtained by their scalar product multiplied by the scales s and s^* of the form and force diagrams respectively. Equation 59 expresses this relationship between bending moment and the lengths measured on the reciprocal diagrams.

$$M = (\mathrm{q}_\mathrm{R}^* \cdot s^*) \cdot (\nu \cdot s) \tag{59}$$

We may prefer, for practical reasons, to use an horizontal projection of the position vector $\mathbf{d_G}$ and a projection of $\mathbf{q_R^*}$ perpendicular to the latter. The length of this projection is referred as H^* in **Figure 52**. This may be done since the properties of vector product imply that any perpendicular

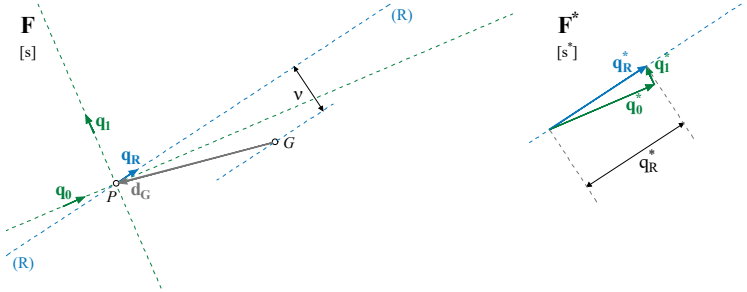

Figure 51 *Two external forces* q_0^* *and* q_1^* *and their resultant* q_R^* *in* $\mathbf{F}^*$ *have action lines* q_0, q_1 *and* q_R *respectively in* $\mathbf{F}$. *The moment of* q_0 *and* q_1 *- or equivalently of* q_R *with respect to* G *in given by* $M = q_R^* \cdot s^* \cdot \nu \cdot s$, *with* s^* *and* s *the scales of* $\mathbf{F}^*$ *and* $\mathbf{F}$ *respectively.*

projections of $\mathbf{q_R^*}$ and $\mathbf{d_G}$ will give the same magnitude for $\mathbf{M}$, so that we may choose any perpendicular directions for these projections. Defining:

- $\mu^{(X)}$ length of the the parallel projection of $\mathbf{d_G}$ in $\mathbf{F}$ along the direction X, and
- $H^{*(X)}$ the length of the orthogonal projection of $\mathbf{q_R^*}$ with this direction X in $\mathbf{F}^*$,

we can generalise Equation 59 in the following way:

$$M = H^{*(X)} \cdot s^* \cdot \mu^{(X)} \cdot s \tag{60}$$

We consider now a direction for (X) parallel to the action line of $\mathbf{q_R^*}$. Being (R) this direction, the value of M is indeterminate since μ have an infinite length in $\mathbf{F}$ and H^* is reduced to zero in $\mathbf{F}^*$. The solution for solving this particular case is to use two fictive forces equivalent to $\mathbf{q_R}$. Let $\mathbf{f}^*$ and $\mathbf{f_1^*}$ be these forces in $\mathbf{F}^*$, and $\mathbf{f}$ and $\mathbf{f_1}$ their action lines in $\mathbf{F}$ respectively. Since $\mathbf{q_R^*}$, $\mathbf{f}^*$ and $\mathbf{f_1^*}$ form a close triangle in $\mathbf{F}^*$, they must meet in one same point in $\mathbf{F}$. This point may be chosen anywhere on the action line of $\mathbf{q_R}$. **Figure 53** shows two distinct positions for this meeting point P along $\mathbf{q_R}$. The components of these fictive forces parallel to direction (R) have the same magnitude, that can be measured by the length $H^{*(R)}$ in $\mathbf{F}^*$. They consequently form a couple of forces

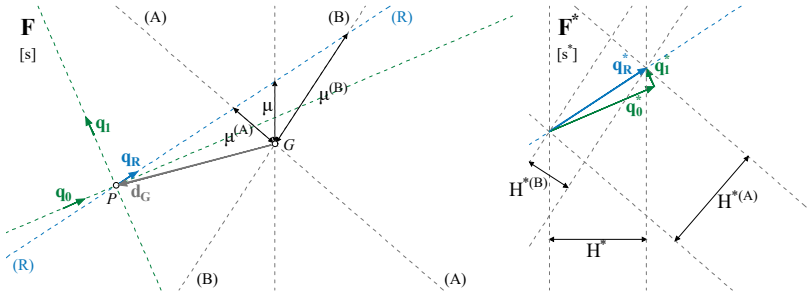

Figure 52 *Various projections of* $\mathbf{d_G}$ *and* $\mathbf{q^*_R}$ *leading to the same value of the moment of* $\mathrm{q_R}$ *with respect to* G.

of equal magnitude but opposite sense, with parallel action lines, both perpendicular to (R). Therefore, their level arm is the distance $\mu^{(R)}$ in $\mathbf{F}$ between the points where the action lines of $\mathbf{f}$ and $\mathbf{f_1}$ meet the parallel to (R) through G. **Figure 53** shows in detail this procedure.

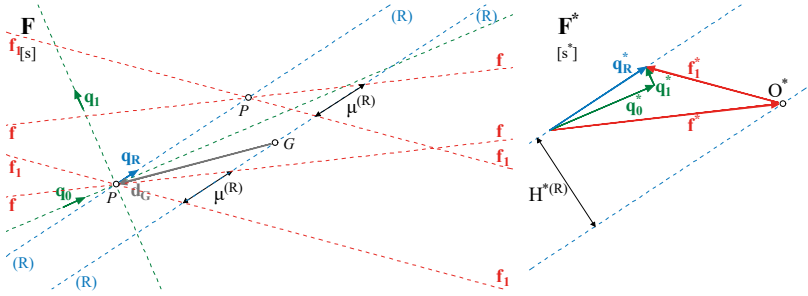

Figure 53 *Two fictive forces* $\mathbf{f}^*$ *and* $\mathbf{f}^*_\mathbf{1}$ *in equilibrium with* $\mathbf{q^*_R}$. *The moment of* $\mathbf{q_R}$ *with respect to* G *in given by* $M = H^{*(R)}s^* \cdot \mu^{(R)}s$, *with* s^* *and* s *the scales of* $\mathbf{F}^*$ *and* $\mathbf{F}$ *respectively.*

This substitution of the resultant force $\mathbf{f_R}$ by two equivalent fictive forces is the basic principle for constructing funicular polygons: given a system of forces $\{\mathbf{q_i}\}$ in equilibrium, a system of fictive pairs of forces can be adjunct to the system so that to form bars in equilibrium with the external system

of forces **(Fig. 54)**. All these bars must meet in one sole point in $\mathbf{F}^*$, which is called the *pole* of the funicular polygon and noted O^*.

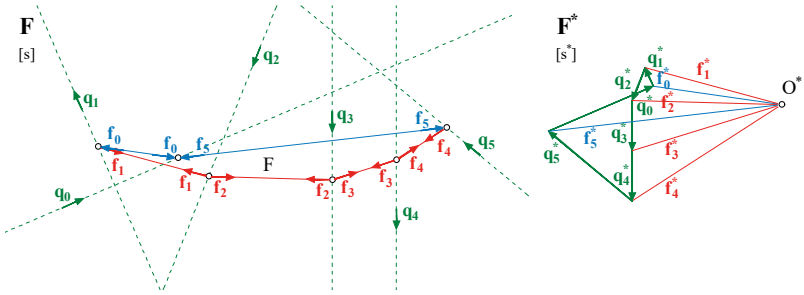

Figure 54 *The funicular polygon* F *in* **F** *is in rotational equilibrium with a system of six external forces* $\{\mathbf{q_{0\to5}}\}$ *in equilibrium. In* $\mathbf{F}^*$*, the tensile (red) and compressive (blue) funicular rays meeting in pole* O^* *are in translational equilibrium with the system of external forces* $\{\mathbf{q_{0\to5}}\}$.

As expressed by Timoshenko and Young (1945), a funicular polygon may be regarded as a system of hinged (fictive) bars creating an arch – or, inverted, a string – that is in equilibrium under the action of the applied and reaction forces **(Fig. 55)**. It is constructed similarly to reciprocal figures in the case of pin-jointed frameworks: any three bars meeting in a same point in the form diagram **F** must form a closed triangle in the force diagram $\mathbf{F}^*$.

Applying graphic statics to structures under bending requires the use of funicular polygons because of the (semi-)parallelism between all the external forces applied on the structural members. In order to express the fact that the bending moment is acting within a specific section of a free body in equilibrium, we use pairs of fictive forces from the funicular polygon that are equivalent to the applied forces on the free body. The horizontal projections of each pair of forces form a couple of forces in rotational equilibrium with the external forces applied on the free body. The distance μ measured on the form diagram **F** between the two action lines of these forces multiplied by the magnitude of these forces horizontal component H^* gives the magnitude of this couple, and thus of the bend-

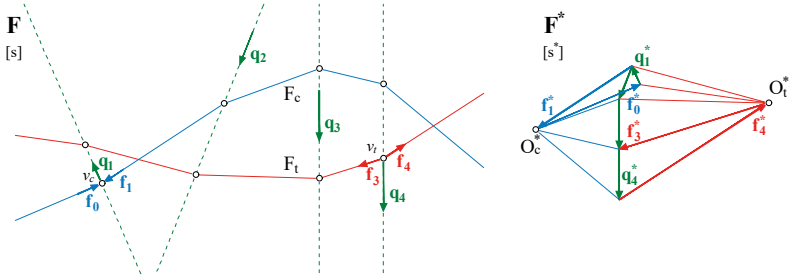

Figure 55 *In* **F***: two funicular polygons in equilibrium with four external forces (green): a tensile polygon* $\mathrm{F_t}$ *(red) and a compressive polygon* $\mathrm{F_c}$ *(blue); funicular forces* $\mathbf{f_0}$ *and* $\mathbf{f_1}$ *are in equilibrium with* $\mathbf{q_1}$*,* $\mathbf{f_3}$ *and* $\mathbf{f_4}$ *with* $\mathbf{q_4}$*. In* $\mathbf{F}^*$*: tensile (red) and compressive (blue) funicular rays in equilibrium with the external forces, meeting in poles* O_t^* *and* O_c^* *respectively*

ing moment. Since the pole O^* is defined as the intersection point of all the funicular forces within the force diagram $\mathbf{F}^*$, H^* is actually the distance between O^* and the vertical line of the external forces. **Figure 56** illustrates this methodology.

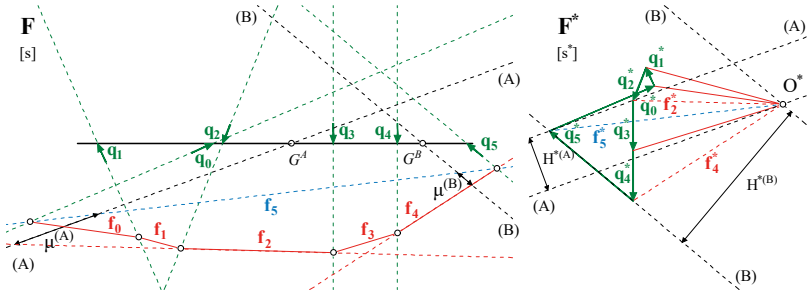

Figure 56 *Graphical determination of the bending moment acting in sections* G^A *and* G^B*:* $M^A = \mu^{(A)} s \cdot H^{*(A)} s^*$*;* $M^B = \mu^{(B)} s \cdot H^{*(B)} s^*$*.*

Therefore, the bending moment in graphic statics results from a couple of forces whose magnitudes are given in the force diagram $\mathbf{F}^*$ and whose lever arm is measured in the form diagram $\mathbf{F}$. Similarly, externally applied couples like the one applied on the clamped end A of the cantilever beam subject to a single force $\mathbf{q}$ in **Figure 57** can also be expressed by two forces $\mathbf{m}^+$ and $\mathbf{m}^-$ separated by a distance μ_A in $\mathbf{F}$, so that

$$M_a = \mathrm{m}^{+*} \cdot \mu_A \cdot s^* s = \mathrm{m}^{-*} \cdot \mu_A \cdot s^* s \tag{61}$$

In function of the chosen position for the pole O^*, the length of H^* may vary, keeping the Equation 61 valid. In **Figure 57**, two different locations of the pole, O_1^* and O_2^*, generate two different values for μ_A, respectively μ_{A1} and μ_{A2}. Equation 61 ensures that the magnitude M_A of the bending moment at the clamped end, resulting from the product of the perpendicular distances μ_1 and H_1^* (respectively μ_2 and H_2^*), remains constant, independently of the arbitrarily chosen position for the pole of the force diagram. Equation 62 expresses this equality.

$$(ss^*) \cdot \mu_1 \cdot H_1^* = (ss^*) \cdot \mu_2 \cdot H_2^* = M \tag{62}$$

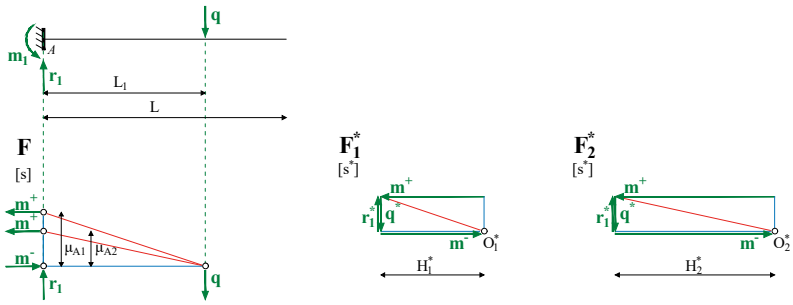

Figure 57 *Graphical construction of the bending moment for a clamped beam.*

5.2 Statically admissible limit states of funiculars polygons

In this section, we analyze beams subject to bending at collapse using graphic statics reciprocal diagrams. As shown in the previous section, these diagrams have the particularity to be fully described by the position of one specific node of the force diagram $\mathbf{F}^*$ known as the *pole of the funicular polygon* and referenced as O^* in $\mathbf{F}^*$. Therefore, the limit state analysis of this type of structure is strongly linked to peculiar positions for O^* and to the analysis of its *admissible geometrical domain* $\mathbf{D}^*$.
The construction rules of these specific reciprocal diagrams ensure the global equilibrium of the structure under the action of all the forces acting on it, as well as the local equilibrium of all its parts. It means that the first condition for having a *Statically Admissible Field* is completed. Providing the yield conditions are respected means here the limitation of the magnitude of bending moments in any section of the beam:

$$\mathrm{M} \leq \mathrm{M_u} \tag{63}$$

where $\mathrm{M_u}$ is the magnitude of the full plastic moment leading to the formation of a plastic hinge in the corresponding beam cross sections. Expressed in terms of graphic statics, and in the particular case of funicular reciprocal diagrams, this means that, for a given value of H^* in $\mathbf{F}^*$, the funicular polygon F in the form diagram $\mathbf{F}$ must be contained within certain boundaries. In the case of a beam showing constant geometrical and material properties along his axis for instance, this is equivalent to enclosing F in-between two straight lines parallel to the beam axis at a distance μ_u chosen as to correspond to the magnitude of $\mathrm{M_u}$: being s and s^* the scale factors of the form diagram $\mathbf{F}$ and force diagrams $\mathbf{F}^*$ respectively, the distance μ_u between the beam's axis and these two straight-lines can be determined as follows:

$$\mu_u = \frac{\mathrm{M_u}}{s \cdot s^* \cdot H_u^*} \tag{64}$$

with H_u^* an arbitrarily chosen value for H^* in $\mathbf{F}^*$. This concept can be extended to any type of beam presenting a varying bending capacity all along its axis: a maximum admissible value $\mu_u(x)$ can be defined for each

cross section x in order to respect the yield condition expressed in Equation 63. **Figure 58** shows these boundaries with $\mu_u(x)$ varying along the axis of the beam following the variation of the plastic modulus $W = \frac{bh^2(x)}{4}$ of the plain rectangular cross section.

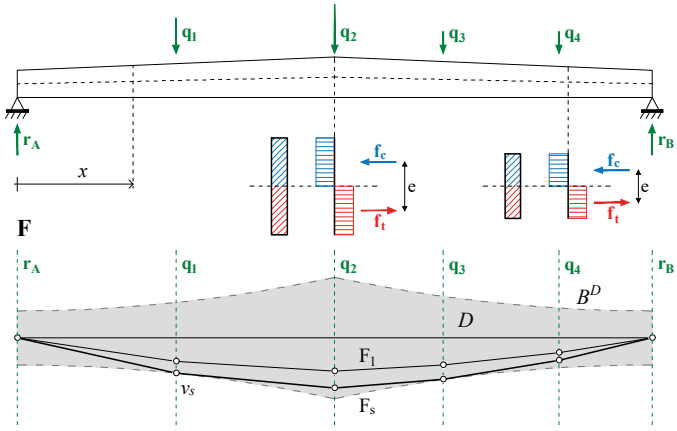

Figure 58 *Form domain D of a beam with variable rectangular cross section, delimited by the form boundary B^D. An admissible force polygon* F *and a limit force polygon* $\mathrm{F_s}$.

Actually, considering the fundamental assumption that shear and axial forces have no effect upon the carrying capacities of beams, so that the resistance of a section is exclusively given by the full plastic moment M_u, these boundaries described in $\mathbf{F}^*$ by the distance μ_u define the yield surface for each section of a beam in perfectly plastic material.

We define the following concepts and the associated notations:

Form domain D**,** a form diagram geometric admissible domain for the funicular polygon;

Form boundary B^D**,** the boundary of D;

Admissible polygon F**,** a funicular polygon that lies entirely inside of the *form domain*; and

Limit polygon $\mathrm{F_s}$**,** an admissible polygon that is in contact with the form boundary in such a way to correspond to a series of plastic hinges that transforms the structure into a mechanism.

Limit pole O_s^***,** a pole corresponding to a *limit polygon*.

We illustrate these concepts in **Figure 58** with an *admissible polygon* $\mathrm{F_1}$ lying entirely inside the *form domain* D . Since the formation of one plastic hinge would transform the beam into a three hinges mechanism, $\mathrm{F_s}$ is a *limit polygon* that reaches the *form boundary* B^D in its vertex v_s.

At limit state, the funicular polygon is such that it reaches the *form boundary* B^D in such a number of sections to transform the structure into a mechanism; it follows that each statically admissible collapse mechanism is related to one specific limit polygon $\mathrm{F_{s,j}}$. For each of them, the - unstable - equilibrium is unequivocally defined and the reciprocal force diagram $\mathbf{F}^*$ can be drawn so that to form a *statically admissible field*. Since any *limit polygon* $\mathrm{F_{s,j}}$ is unequivocally correlated to a pole $O^*_{s,j}$ in the force diagram $\mathbf{F}^*$, it follows that any statically admissible limit state can be described through the specific location of the corresponding pole. More precisely, this specific position is uniquely define relatively to a fixed point of $\mathbf{F}^*$, that may be chosen as one of the vertices of the applied loads $\mathbf{q}^*$. Since μ_u and H_u have been fixed as to respect Equation 64, all these poles must be situated on a vertical line in $\mathbf{F}^*$ at a distance H^*_u from the action line of the applied forces. For a statically determinate structure as in **Figure 59**, this position for O^* is unique, and the magnitude of the applied force $\mathbf{q}^*$ defines the orientation of the rays of the funicular polygon. The limit state is attained when these rays are so as to correspond to the limit funicular polygon $\mathrm{F_s}$.

In this limit situation, the applied loads are so that they transform the structure into a mechanism; their magnitude is measured in $\mathbf{F^*_s}$ and the corresponding load factor can be calculated as the ratio of q_u to q. Equivalently, because of the similar triangles relationships existing between the form and force diagrams, this ratio is equivalent to the one of μ_u to μ, so that:

$$\lambda_u = \frac{q_u}{q} = \frac{\mu_u}{\mu} = 1 + \frac{\Delta\mu}{\mu} \tag{65}$$

When it comes to statically indeterminate structures, this limit state may not be unique, and a complete limit state analysis is needed. Using the

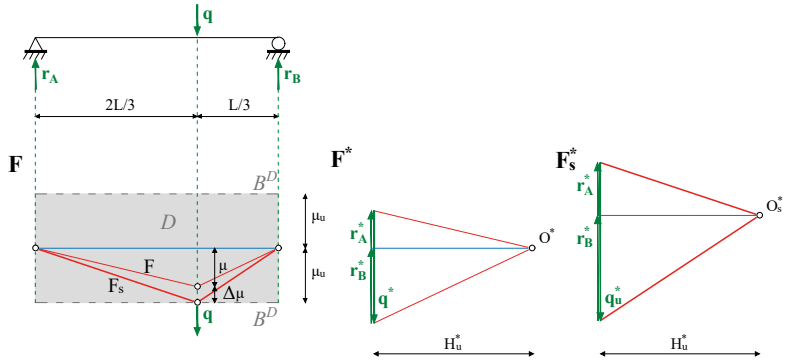

Figure 59 *In* **F***: an admissible polygon* F *and a limit polygon* F_s *for the simply supported beam AB. Their corresponding force diagram* F^* *and* F_s^* *respectively, for a fixed value of* H_u^*

example suggested by Fivet (2013) following Zastavni (2008), this methodology is applied on the clamped beam of **Figure 60**. Two plastic hinges are needed to transform the structure into a mechanism, which may be situated at the clamped end of the beam or on the action line of one of the two applied forces $\mathbf{q_1}$ and $\mathbf{q_2}$. Among the three possible combinations of two distinct plastic hinges, there are three possible limit polygons $F_{s,1}$, $F_{s,2}$ and $F_{s,3}$, corresponding to three possible mechanisms, and consequently two associated force diagrams $\mathbf{F^*_{s,1}}$, $\mathbf{F^*_{s,2}}$ and $\mathbf{F^*_{s,3}}$. The fourth combination of plastic hinges - clamped end and $\mathbf{q_1}$ - may not be taken into consideration as a possible limit state, since it produces a funicular polygon F_0 that violates the yield condition since it goes out of the *form domain* where it intersects with the action line of $\mathbf{q_2}$. The associated force diagrams $\mathbf{F^*_0}$ may consequently not be considered as a possible limit case for $\mathbf{F}^*$.

The length H_u^* being fixed as to respect Equation 64, we can immediately identify which one of the two limit force diagrams presents the highest magnitude for the applied forces. Comparing it to the actual magnitude of the applied forces gives the value of the two correlated static load factors:

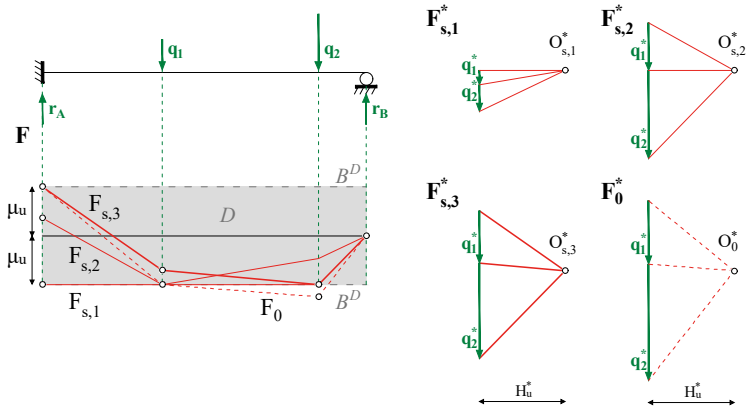

Figure 60 *Three possible limit polygons* $\mathrm{F}_{s,1\to3}$ *and their corresponding force polygons* $\mathbf{F^*_{s,1\to3}}$ *for the statically indeterminate beam* AB. F_0 *is not an admissible polygon since it does not respect the yield condition;* $\mathbf{F^*_0}$ *is consequently not a statically admissible distribution.*

$$\lambda^*_{s,j} = \frac{\{\mathbf{q}\}^*_{s,j}}{\{\mathbf{q}\}^*} \tag{66}$$

As a consequence from the lower-bound theorem of limit analysis:

$$\lambda^*_{s,u} = max_j \left\{\lambda^*_{s,j}\right\} = \lambda^*_{s,3} \tag{67}$$

In that way, it is possible to obtain the collapse load factor for a beam subject to a given loading inducing bending. However, for more complex cases it can be very inconvenient to have to draw separately every limit reciprocal polygons in order to make a full static limit state analysis. In the next subsection, we develop a methodology for obtaining all the possible limit state force diagrams and recognizing among them the collapse one using geometrical admissible domains in the force diagram $\mathbf{F}^*$.

Constructing one sole force diagram $\mathbf{F}^*$. In order to overcome this difficulty of having a series of different limit force diagrams, we consider the relationships between the reciprocal diagrams that will allow us to draw one sole force diagram which scale s^* will be used as an indicator of the structural safety.

Let us first consider the fundamental relationship expressed by Equation 64. Since a limit state is characterised by a full plastic moment M_u being produced in the sections where the corresponding limit polygon reaches the form boundary:

$$\mathrm{M_u} = \mu_u \cdot s \cdot \mathrm{H_j^*} \cdot s_j^* \tag{68}$$

Where, $\mathrm{H_j^*}$ is the horizontal projection of the funicular rays in $\mathbf{F}^*$ which correspond to a limit polygon $\mathrm{F_j}$, and s_j^* the drawing scale of the force diagram so that Equation 68 is respected for fixed values of μ_u and s. It follows that any force diagrams $\mathbf{F_j^*}$ must respect the following relationship:

$$\mathrm{H_j^*} \cdot s_j^* = \mathrm{H_u^*} \cdot s^* = \frac{\mathrm{M_u}}{\mu_u \cdot s} = cst \tag{69}$$

The product $\mathrm{H_j^*} \cdot s_j^*$ being a constant value, maximizing one of its two components is equivalent to minimizing the other one. Considering this property, the fundamental equation of static limit state analysis may be adapted in two different ways. Let us first consider a fixed scale s^* of the force diagram chosen so that Equation 69 is respected. Then any force vector $\mathbf{q}$ must be represented in $\mathbf{F}^*$ by $\mathbf{q}^*$ so that:

$$\mathbf{q} = \mathbf{q}^* \cdot s^* \tag{70}$$

At a limit state j, the external forces $\{\mathbf{q}\}_{s,j}$ must be so as to correspond to a limit polygon $\mathrm{F_{s,j}}$ and must be represented in $\mathbf{F}^*$ by a set of vectors $\{\mathbf{q}\}_{s,j}^*$ so that $\mathrm{H_j^*} = \mathrm{H_u^*}$. The magnitude of these forces is then given by:

$$\{\mathrm{q}\}_{s,j} = \{\mathrm{q}\}_{s,j}^* \cdot s^* \tag{71}$$

Applying then the lower-bound theorem of limit analysis on all the possible limit cases, we obtain a lower-bound value for $\{\mathbf{q}\}_u$:

$$\{\mathbf{q}\}_{s,u} = max_j \left\{\{\mathbf{q}\}_{s,j}\right\} = max_j \left\{\{\mathbf{q}\}_{s,j}^* \cdot s^*\right\} = s^* \cdot max_j \left\{\{\mathbf{q}\}_{s,j}^*\right\} \tag{72}$$

This methodology is the one we have used in the previous section for determining the collapse load factor for the structure in **Figure 60**.
Considering now that instead of drawing all the limit state force diagrams at the same scale s^*, we fix the length of the applied external forces $\{\mathbf{q}\}^*$ in $\mathbf{F}^*$ as to respect equation 70. Keeping this set of forces $\{\mathbf{q}\}^*$ constant, then all the $\{\mathbf{q}\}_{s,j}^*$ have the same lengths $\{\mathbf{q}\}^*$ but each of them must be

considered as drawn at a specific scale factor $s^*_{s,j}$. Equation 75 is then transformed as follows:

$$\{\mathbf{q}\}_{s,u} = max_j \left\{\{\mathbf{q}\}_{s,j}\right\} = max_j \left\{\{\mathbf{q}\}^* \cdot s^*_{s,j}\right\} = \{\mathbf{q}\}^* \cdot max_j \left\{s^*_{s,j}\right\} \quad (73)$$

Since at the limit state the scale factor $s^*_{s,j}$ must be so to respect Equation 68, Equation 76 can be written in the following form:

$$\{\mathbf{q}\}_{s,u} = \{\mathbf{q}\}^* \cdot max_j \left\{\frac{M_u}{\mu_u \cdot s \cdot H^*_{s,j}}\right\} = \{\mathbf{q}\}^* \cdot \frac{M_u}{\mu_u \cdot s} \cdot \frac{1}{min_j \left\{H^*_{s,j}\right\}} \quad (74)$$

where $H^*_{s,j}$ measures the specific distance between the pole $O^*_{s,j}$ and the applied forces $\{\mathbf{q}\}^*$. This means that the limit state leading to collapse is the one for which the pole $O^*_{s,j}$ is the closest of the applied forces. Indeed, the corresponding scale s^*_u for the force diagram is is so that $s^*_u = max_j \left\{s^*_{s,j}\right\}$, so that $\{\mathbf{q}\}_{s,u} = \{\mathbf{q}\}^* \cdot s^*_u$.

This is illustrated in **Figure 61** using the same example as for the previous methodology. The comparison between the various distances $H^*_{s,j}$ gives immediately the minimum one: $H^*_{s,3}$.

We can now use this property for qualifying the collapse load factor in a very simple way. Indeed, the lower-bound theorem of plasticity can be expressed as follows:

$$\lambda_u = \frac{\{\mathbf{q}\}_u}{\{\mathbf{q}\}} \geq \lambda^*_{s,j} = \frac{\{\mathbf{q}\}^*_{s,j}}{\{\mathbf{q}^*\}} \ \forall j \quad (75)$$

Defining $\lambda^*_{s,u}$ so that:

$$\lambda^*_{s,u} = max_j \{\lambda^*_{s,j}\} \quad (76)$$

Therefore, if considering all the possible statically admissible limit states:

$$\lambda_u = \frac{\{\mathbf{q}\}_u}{\{\mathbf{q}\}} \geq \frac{max_j \left\{\{\mathbf{q}\}_{s,j}\right\}}{\{\mathbf{q}\}} = \frac{max_j \left\{\{\mathbf{q}\}^* \cdot s^*_{s,j}\right\}}{\{\mathbf{q}\}^* \cdot s^*} = \frac{\{\mathbf{q}\}^* \cdot max_j \left\{s^*_{s,j}\right\}}{\{\mathbf{q}\}^* \cdot s^*} \quad (77)$$

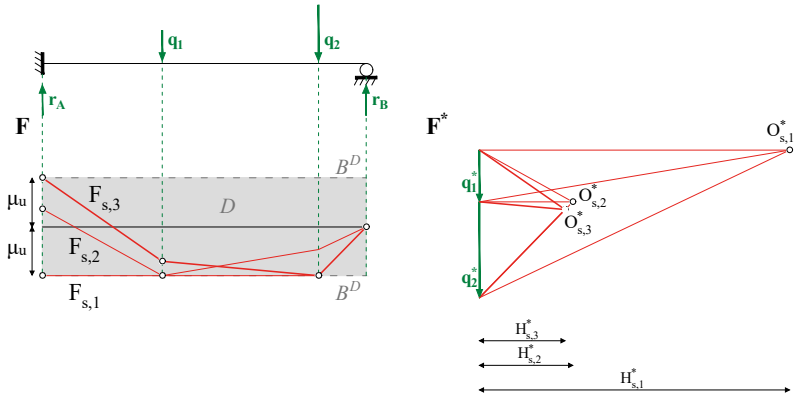

Figure 61 *In* **F***: three limit polygons* $\mathrm{F_{s,1\to 3}}$ *for the statically indeterminate beam AB. In* $\mathbf{F}^*$*: three limit poles* $O^*_{s,1\to 3}$ *corresponding to the limit polygons. For fixed external forces, each of them is characterised by the horizontal distance* $H^*_{s,1\to 3}$*.*

And finally, combining equations 74, 75 and 77:

$$\lambda^*_{s,u} = \frac{M_u}{\mu_u \cdot s \cdot s^*} \cdot \frac{1}{min_j \left\{H^*_{s,j}\right\}} = \frac{\mathrm{H^*_u}}{min_j \left\{\mathrm{H^*_{s,j}}\right\}} \tag{78}$$

The value $\lambda^*_{s,u}$ is a lower-bound value for λ_u obtained using exclusively graphical means, which is exactly equal to λ_u if all the possible limit state have been considered.

5.3 Admissible geometrical domains

In the previous section, we have been mainly interested in constructing the reciprocal diagrams (funicular polygon and force polygon) for limit states of the structure, and getting out of their analysis a lower bound value λ_u^* for the collapse load factor λ_u. Each of these limit states is defined by a limit polygon, *i.e.* a funicular polygon which apexes reach the form boundaries in the sections where a plastic hinge is formed in the corresponding kinematically admissible mechanism. Being fixed the external forces in the force polygon $\mathbf{F}^*$, we have seen that any pair of limit diagrams may be unequivocally described by the specific location of its limit pole O_s in $\mathbf{F}^*$.
Though, beside these limit poles corresponding to limit states, we can identify a set of other locations for the pole, which characteristics are such that the corresponding admissible reciprocal diagrams do not correspond to limit states. This occurs when the funicular polygon do not reach the form boundaries in a sufficient number of sections to correspond to a mechanism.
We define the following concepts:

Force domain D^***,** geometric admissible domain in the force diagram for the pole O^* so that it corresponds to an *admissible polygon*;

Force boundary B_D^***,** the polygonal envelope of D^*.

Considering that this force boundary plays the same role as a global yield surface for the entire beam, it is very intuitive to suppose that the limit poles must be situated on the *force boundary*. The following developments aim to develop a construction procedure for this force boundary defining the admissible domain for the pole.

The line of poles. For constructing this *force boundary* we make use of a geometrical property of funicular polygons, expressed as the following theorem by Timoshenko and Young (1945, p.22):

> ***"If, for a given system of forces in a plane, any two funicular polygons are drawn for two different poles O and O', corresponding sides of these polygons will***

meet in points that lie on a straight line parallel to the line OO' joining the two poles."

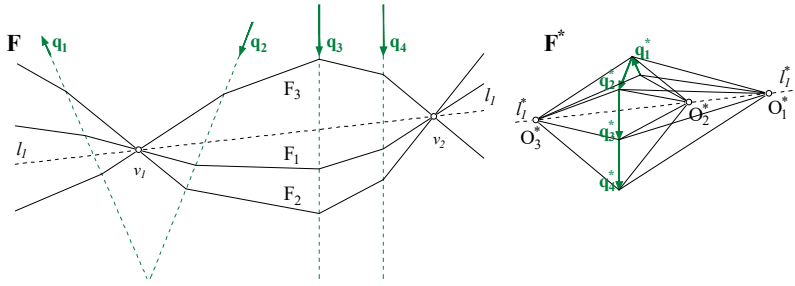

Figure 62 *Three funicular polygons* $\mathrm{F}_{1\to3}$ *meeting in points* v_1 *and* v_2 *are related respectively to poles* $O^*{}_1 \to 3$ *lying on a straight line* l_1^* *in* $\mathbf{F}^*$ *parallel to the one* l_1 *joining* v_1 *and* v_2 *in* $\mathbf{F}$.

According to this theorem, any funicular polygon passing by two chosen points v_1 and v_2 of $\mathbf{F}$ have a pole O^* lying on a straight line of $\mathbf{F}^*$ parallel to the line joining v_1 and v_2 **(Fig. 62)**. This line in $\mathbf{F}^*$ is called a *line of poles* l^*.

Another fundamental property of reciprocal diagrams can be derived from the previous theorem that will be helpful for the construction of the pole admissible domains. Figuring out a funicular polygon passing through three fixed points v_A,v_B and v_C, the three different closing lines $l_{1\to3}$ joining two of the three fixed points, form a closed triangle in $\mathbf{F}$ **(Fig. 63)**. Since these three straight lines close one same polygon, their parallels in $\mathbf{F}^*$, $l^*_{1\to3}$ meet in one same point identified as the pole O^* of the polygon.

So, the general property of reciprocal figures that ensures that:

All the segments that meet in one sole point in one diagram form a closed polygon in its reciprocal

can be extended to closing lines of funicular polygons. In the particular case of three segments, this property is reversible and symmetric:

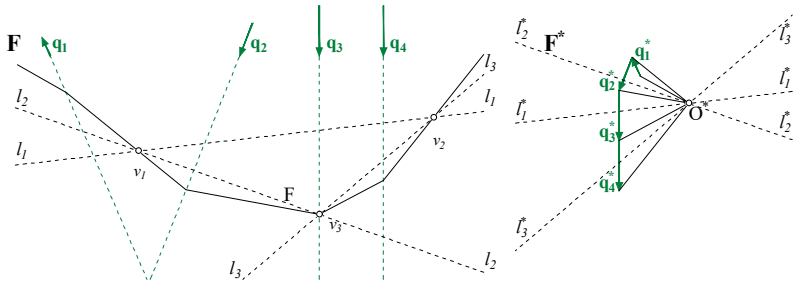

Figure 63 *$l_{1\to3}$ close* F *in* **F** *so that $l^*_{1\to3}$ meet at O^** $\mathbf{F}^*$.

Any three segments of a same forming a closed triangle in one diagram meet in one sole point in the other.

Transposed to closing lines of funicular polygons for our purposes:

Any three closing lines joining three points of a same funicular polygon meet in one same pole in the force diagram.

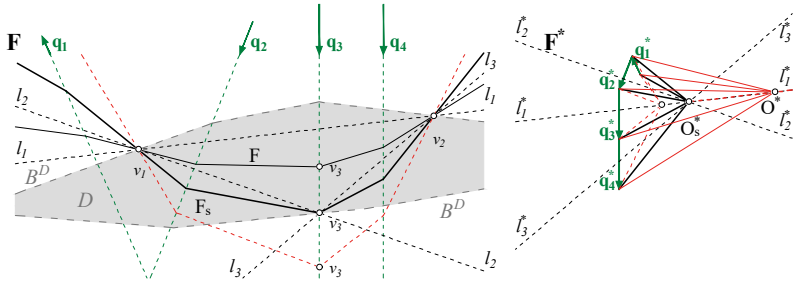

Figure 64 *In* F*: limit polygon* $\mathbf{F_s}$ *with three closing lines l_1, l_2, l_3, each one joining two vertices on B^D. In* F^**: limit pole O^*_s and admissible positions for O^* along the three lines of poles.*

Thinking now in terms of limit polygons, the three points may be chosen where the funicular polygon meets the form boundaries. In that case, the lines of poles parallels to the three closing lines, meet at the limit pole O_s^* in $\mathbf{F}^*$ **(Fig. 64)**. In that way, the limit pole bounds the admissible positions for the pole along each line of poles so that it corresponds to admissible polygons.

Statically determinate beam. It is straightforward to apply the properties exposed above to the funicular polygons characterizing the simply supported isostatic beam of **Figure 65**. Since the bending moment must be null at both ends of the beam, any statically admissible funicular polygon must pass by both points v_1 and v_2. Let us call l the horizontal line joining these two points v_1 - v_2. We can draw a random admissible polygon F and deduce the corresponding position of its pole O in $\mathbf{F}^*$. Drawing the line of poles l^* parallel to l and passing by O, this is the locus of the possible positions for the pole. In order to respect the yield condition, *i.e.* keeping the whole funicular polygon inside of the form domain D, the pole O^* may slide along l^* until the position O_s is reached. For this specific position, the limit polygon $\mathrm{F_s}$ meets the form boundary B_D in v_s. Provided that the force diagram is read with a scale s_s^* so that $H_s^* \cdot s_s^* = H_u^* \cdot s^*$, the product $H_s^* \cdot \mu_u \cdot s_s^* \cdot s = M_u$ gives the magnitude of the full plastic moment which is obtained in the section of the beam where the external load $\mathbf{q}$ is applied. The force domain for O^* is consequently the half horizontal line going rightwards from O_s^*.

Because of the axial symmetry of the form domain along the beam axis - we have supposed that the beam's cross section can undertake indifferently a positive or negative plastic bending moment - exactly the same analysis can be achieved using compressive funicular polygon instead of tensile ones. **Figure 65** shows three funicular polygons: one of them (dashed blue lines) is not a admissible polygon since it is not entirely contained within the form domain; a second one F is an admissible polygon (continuous blue lines); the third one F_s is a limit polygon (continuous bold blue lines). Each of them correspond to a specific location of the pole O^* along l^*. The force domain for O^* is consequently the half horizontal line going leftwards from O_s^*.

For statically determinate structures as the simply supported beam, these results may be obtained by using equilibrium relationships only, in such a

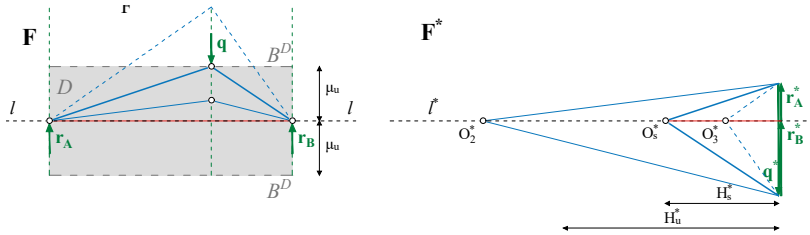

Figure 65 *Limit analysis of a statically determinate beam.*

way that limit state analysis is not very relevant. Since there is only one possible collapse mechanism corresponding to a bending moment distribution that respects equilibrium and yield conditions. Consequently, there is one sole location O_s^* for the pole that corresponds to a limit polygon $\mathrm{F_s}$ in **F**. This may not be the case for statically indeterminate structures since equilibrium considerations only cannot give sufficient information to describe the inner distribution of forces inside the beam. Therefore, the following paragraphs are dedicated to the description of a graphical procedure for generating the force boundary of any statically indeterminate beam subject to bending.

Statically indeterminate beam. Indeed, μ_u being fixed, the formation of plastic hinge in specific sections of the beam defines the location of the corresponding vertex of the funicular polygon on the form boundary B^D. Since a beam reaches a limit state as soon as a certain number of sections are yielded, this is equivalent to define specific locations for the corresponding vertices of the funicular polygon. Analyzing all the possible combinations of these locations is equivalent to make a full static limit state analysis of the structure. In order to explain the procedure, we use the example of the beam clamped in A and simply supported in B.

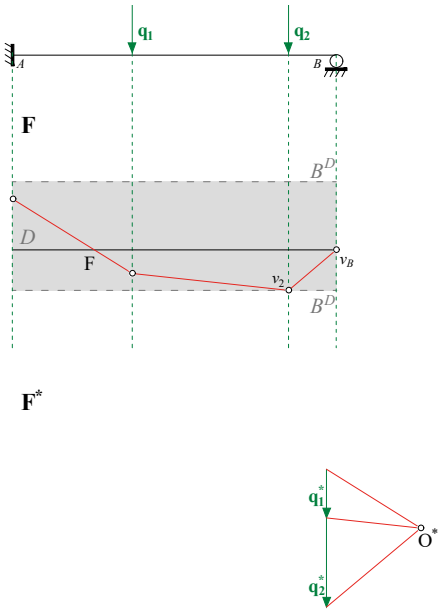

Figure 66 *Constructing D^* - One tensile admissible polygon* F *(red) for a statically indeterminate beam AB and its corresponding pole O^* in* $\mathbf{F}^*$*. The location of v_B in* **F** *is fixed to respect the support condition.*

Figure 66 shows this beam subject to two external loads $\mathbf{q_1}$ and $\mathbf{q_2}$, its corresponding form domain D and its asymmetric boundaries B^D. Considering a reinforced concrete beam, this asymmetry may result from a higher reinforcement on the upper side than on the lower one. In order to respect the support conditions at B, the location of v_B must be fixed along the beam's axis. The yield condition imposes that any admissible funicular polygon F must stay enclosed within D. This is the case for F which vertex v_2 lies on the form boundary, all its other vertices being contained within D.

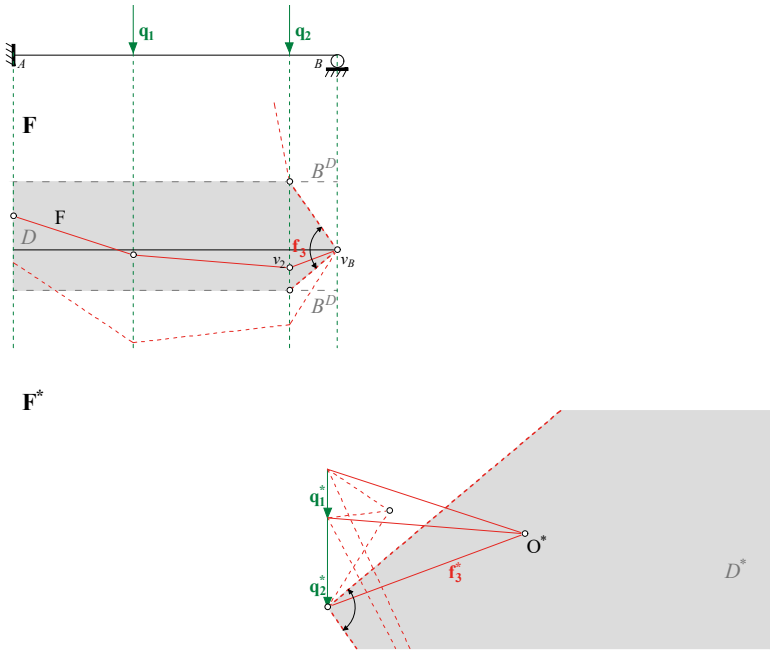

Figure 67 *Constructing D^* - In* **F***: admissible directions for* $\mathbf{f_3}$ *in order to keep v_2 within D; In* $\mathbf{F}^*$ *corresponding force domain D^* for the pole O^**

A necessary geometrical condition for F being an admissible polygon is that v_2 lies within the form boundary; this is equivalent to limit the direction of $\mathbf{f_3}$ around v_B in **F** in between the direction of two straight lines joining v_B and the meeting points of the line of action of $\mathbf{q_2}$ with the form boundaries B^D. This is consequently reducing the form domains D as indicated in **??**. The corresponding geometrical constraint in the form diagram $\mathbf{F}^*$ is that the pole O^* must be located within the force domain D^* which boundaries are the straight lines parallel to the ones joining joining v_B and the limit locations for v_2 in **F**.

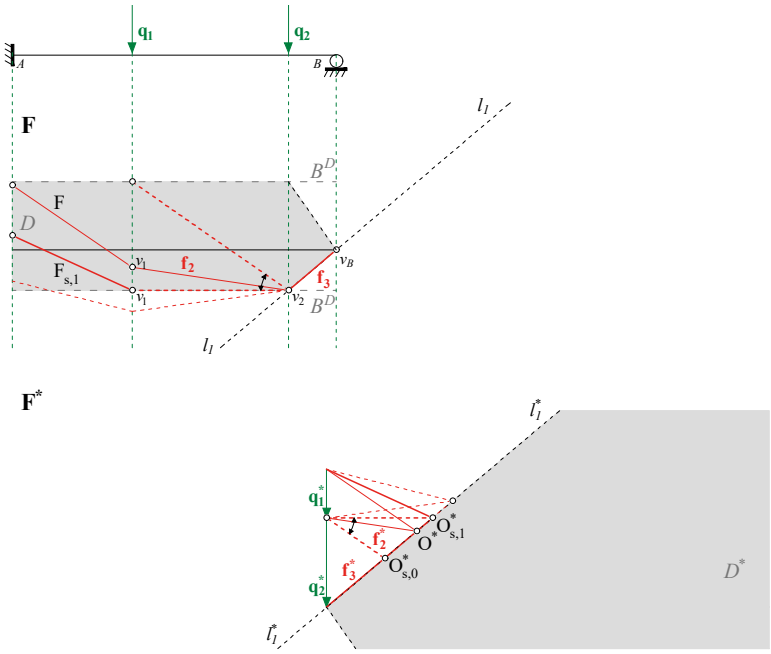

Figure 68 *Constructing D^* - Three funicular polygons passing by both points v_2 and v_B: an admissible polygon* F *(red continuous lines), a limit polygon* $\mathrm{F_s}$ *(red bold lines) and a funicular polygon that does not respect the yield conditions (red dashed lines). The respective locations for the pole corresponding to these three polygons along the line of poles l_1^* are indicated in* $\mathbf{F}^*$.

These geometric conditions in $\mathbf{F}$ and $\mathbf{F}^*$ are obviously not sufficient to ensure that the funicular polygon respects the yield conditions since they provide no control on the location of its other vertices v_1 and v_A. Considering now the direction of bar $\mathbf{f_3}$ being fixed in the limit position indicated in **Figure 68**, a complementary geometrical condition in $\mathbf{F}$ is that the direction of the funicular ray $\mathbf{f_2}$ is as to keep the vertex v_1 within the form domain D. Since the direction of $\mathbf{f_3}$ is fixed, let l_1 be the closing line of the funicular polygons joining the given vertices v_2 and v_B of F. The aforementioned theorem then ensures that the pole O^* must be lying on the pole line l_1^* parallel to l_1. The condition on the direction of $\mathbf{f_2}$ being

equivalent to limit the direction of $\mathbf{f_2^*}$ in $\mathbf{F}^*$, this delimits a set of admissible locations for O^* on l_1^* in between two limit positions $O_{s,0}$ and $O_{s,1}$ for the pole. A pole situated on l_1^* but outside the segment delimited by these two limit poles would correspond to a funicular polygon that is not entirely lying within the form boundary D **(Fig. 68)**.

This second geometric constraint on O^* is still not sufficient, since it does not ensure that the last vertex v_A lies inside the form domain. Furthermore, it is only valid for a fixed closing line l_1 and its corresponding line of poles l_1^*. Therefore, defining the entire admissible force domain for O^* would imply considering all the inter-dependencies between the various conditions on the three rays of the funicular polygon. This may become more and more intricate when the number of geometric conditions on the funicular rays grows. Though, Fivet (2013) has proven that one can deal with these constraints inter-dependencies and their dynamic handling using a limited set of geometrical constraints. In order to facilitate the analysis and to make it more systematic, we need to consider the objective of the present dissertation, which is to define an admissible domain for the pole that takes into account all the statically admissible fields, and particularly the ones corresponding to static limit states. In the case of the clamped beam AB, the degree of static indeterminacy is equal to one, so that the formation of two plastic hinges is necessary to transform it into a three hinges mechanism. Therefore, a limit polygon must reach the form boundary in two different points in order to correspond to a static limit state. Considering the three funicular polygons represented in **Figure 68**, we can analyze them from a limit state point of view: the first one F is an admissible polygon since it lies entirely within D; the second one $\mathrm{F_{s,1}}$ is a limit polygon since its vertices v_1 and v_2 both lie on the form boundary B^D; the third one is not an admissible polygon since it does not respect the yield conditions, *i.e.* being entirely enclosed within D.

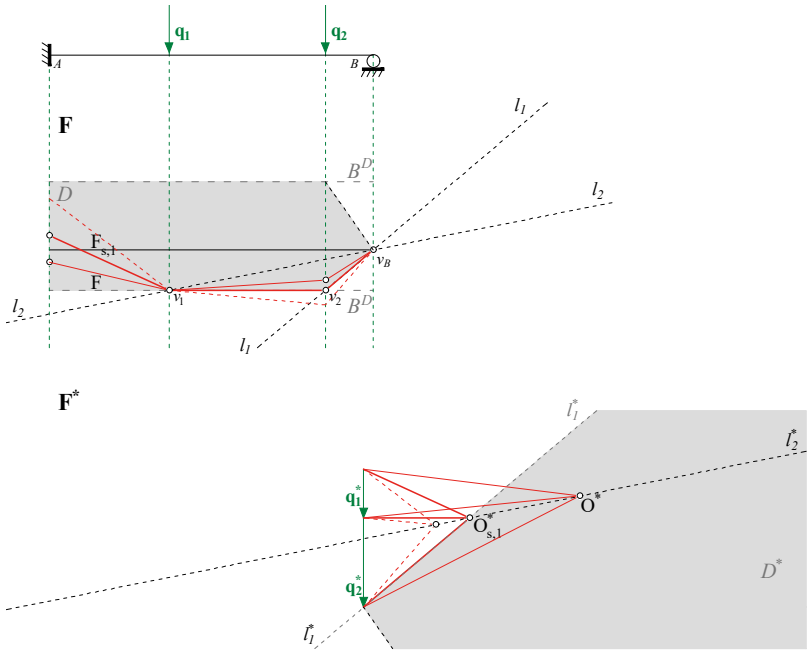

Figure 69 *Constructing D^* - Three funicular polygons sharing the same closing line l_2 joining v_B and v_1: a limit polygon* $\mathrm{F_{s,1}}$ *(red-bold lines); an admissible polygon* F *(red-continuous lines); a non-admissible funicular polygon (red-dashed lines).*

Looking to the limit polygon $\mathrm{F_{s,1}}$ and its vertices v_1 and v_B, we can actually define another closing line l_2 joining these two vertices **(Fig. 69)**. Since $O^*_{s,1}$ is the pole corresponding to this limit polygon, the line of poles l_2^* parallel to l_2 must meet l_1^* on $O^*_{s,1}$. Any funicular polygon which pole is lying on l_2^* has the same closing line l_2 passing through v_1 and v_B. Though, the geometric constraint on the direction of $\mathbf{f_3^*}$ is still valid, so that the pole must be lying on the right-hand side of l_1^*. Besides limit polygon $\mathrm{F_{s,1}}$, **Figure 69** shows one admissible polygon F which pole O^* is lying on the half line l_2^* contained inside D^*, and another one that violates the yield conditions, which pole is situated outside of D^*.

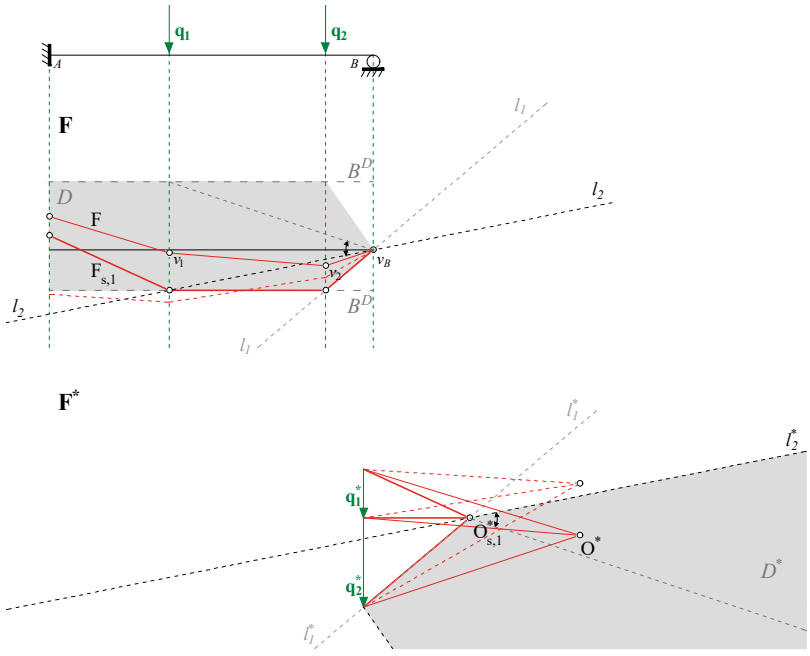

Figure 70 *Constructing D^* - In* $\mathbf{F}$*: admissible directions for l_2 in order to keep v_1 within D; in* $\mathbf{F}^*$*: corresponding force domain D^* for the pole O^*.*

Considering now that the position of vertex v_1 of the funicular polygon is defined by the direction of the closing line l_2 around v_B, this defines a new constraint on the location of the pole in $\mathbf{F}^*$. Indeed, in order to keep v_1 within the form domain D, the direction of l_2, and consequently of l_2^* its parallel in $\mathbf{F}^*$, must form a limited angle with respect to v_B. It implies that O^* may not be situated above l_2^* **(Fig. 70)**. The force domain D^* must consequently be reduced in order to correspond to this condition. A funicular polygon which pole is lying inside of D^* respects both conditions of v_1 and v_2 not being located below the lower form boundary B^D. In terms of geometric relationships as proposed by Fivet (2013), this is equivalent to use the *laterality* relationship on l_1^* and l_2^* to constraint the point O^* within the union of several half-planes.

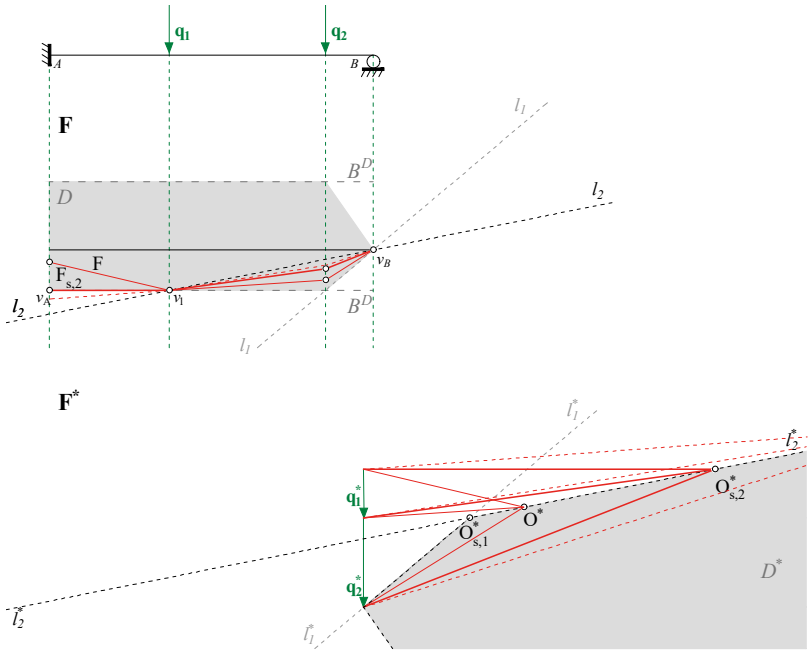

Figure 71 *Constructing D^* - In* $\mathbf{F}$*: three funicular polygons passing by both points v_2 and v_B: an admissible polygon* F *(red continuous lines), a limit polygon* $\mathrm{F}_{s,2}$ *(red bold lines) and a funicular polygon that does not respect the yield conditions (red dashed lines). The respective locations for the pole corresponding to these three polygons along the line of poles l_2^* are indicated in* $\mathbf{F}^*$.

Another specific location for the pole O^* along the line of poles l_2^* can be found, that corresponds to another limit case characterised by the limit polygon $\mathrm{F}_{s,2}$ **(Fig. 71)**. For this limit polygon, the vertices v_A and v_1 are lying on the form boundary B^D as to correspond to two plastic hinges in these sections, so that the beam is transformed into a three hinges mechanism. The corresponding limit pole $O^*_{s,2}$ lies on l_2^* in $\mathbf{F}^*$. Any pole O^* along l_2^* and located in-between $O^*_{s,1}$ and $O_{s,2}*$ is related to an admissible polygon F lying in-between $\mathrm{F}_{s,1}$ and $\mathrm{F}_{s,2}$ which vertex v_1 meets the form boundary B^D.

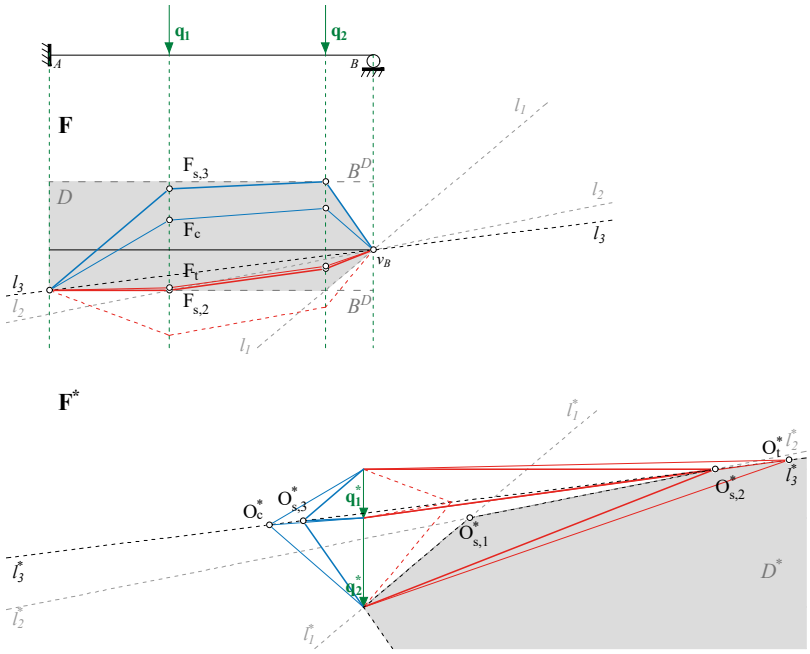

Figure 72 *Constructing D^* - In* **F***: three tensile funicular polygons sharing the same fixed positions for the vertices v_A and v_B: an admissible polygon* $\mathrm{F_t}$ *(red continuous lines), the limit polygon* $\mathrm{F_{s,2}}$ *(red bold lines) and a funicular polygon that does not respect the yield conditions (red dashed lines). The respective locations for their respective poles in* $\mathbf{F}^*$ *are lying on the line of poles l_3^* parallel to the closing line l_3 in* **F***.*

Repeating the same procedure as for l_2, we consider this time the closing line l_3 of the limit polygon $\mathrm{F_{s,2}}$, joining v_A and v_B. The line of poles l_3^* parallel to the latter and passing by the location of the limit pole $O_{s,2}^*$ corresponding to $\mathrm{F_{s,2}}$ constitutes a new limit for the force domain D^* which is related to the location of v_A: in order to keep v_A within the form domain, the pole must be lying below the line of poles l_3^*. **Figure 72** shows three tensile funicular polygons which poles lies on the same line of poles l_3^*. For corresponding to a tensile admissible polygon $\mathrm{F_t}$, the pole O^* must not go outside of the geometrical domain D^* and therefore must be situated on the right-hand side of the limit pole $O_{s,2}$. It is import-

ant to notice that, beside these tensile polygons, l_3 may be the closing line of compressive polygons which vertex v_A is located on the lower form boundary. Among these compressive polygons, it is possible to identify a limit polygon $\mathrm{F_{s,3}}$ which pole $O_{s,3}$ is lying on the line of poles l_3^* but situated on the left-hand side of the applied loads in $\mathbf{F}^*$. Any pole O_c^* of l_3^* situated on the left-hand side of the limit pole $O_{s,3}$ corresponds to an admissible polygon $\mathrm{F_c}$.

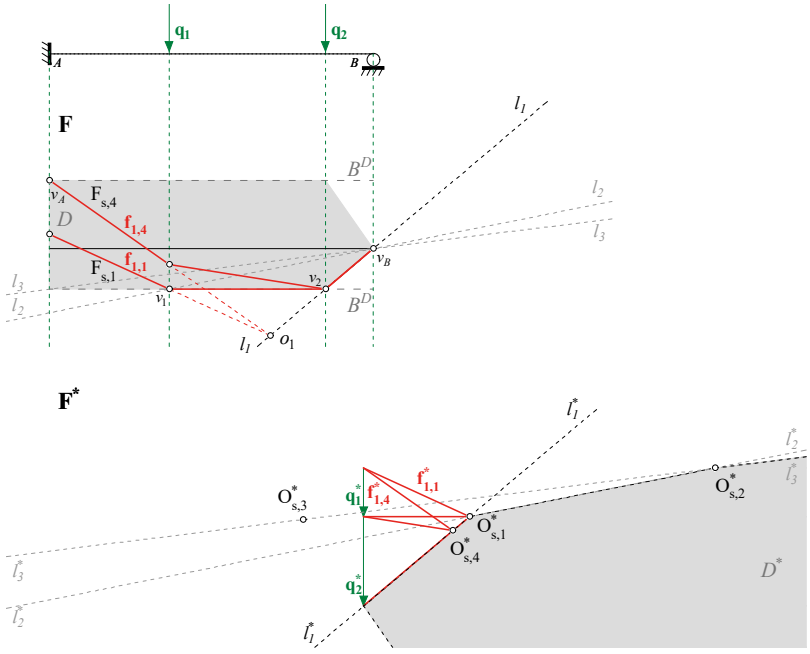

Figure 73 *Constructing D^* - Two limit polygons $\mathrm{F_{s,1}}$ and $\mathrm{F_{s,4}}$ sharing the same closing line l_1. Their corresponding limit poles $O_{s,1}$ and $O_{s,4}$ consequently lie on the lines of pole l_1^* parallel to l_1.*

Before going further into the limit analysis of the compressive reciprocal polygons, we must go back to the first limit polygon $\mathrm{F_{s,1}}$ and the correlated closing line and line of poles l_1-l_1^*. Indeed, $\mathrm{F_{s,1}}$ is not the only limit polygon which pole is lying on l_1^*. Let us call $\mathrm{F_{s,4}}$ this second limit polygon which vertices v_A and v_2 are located on the *form boundary* B^D

(Fig. 73). The corresponding limit pole $O^*_{s,4}$ lies on l^*_1, and its precise location can be determined thanks to the aforementioned theorem: being l_1 the straight line parallel to l^*_1 and joining v_B and v_2, the side $\mathrm{f}_{1,4}$ of the second limit polygon $\mathrm{F}_{s,3}$ must meet the side $\mathrm{f}_{1,1}$ of $\mathrm{F}_{s,1}$ at point o_1 on l_1. Since $\mathrm{f}_{1,4}$ must join v_A and o_1, its direction is known; so the corresponding ray $\mathrm{f}^*_{1,4}$ can be traced in $\mathbf{F}^*$ and the location of $O^*_{s,4}$ is found **(Fig. 73)**.

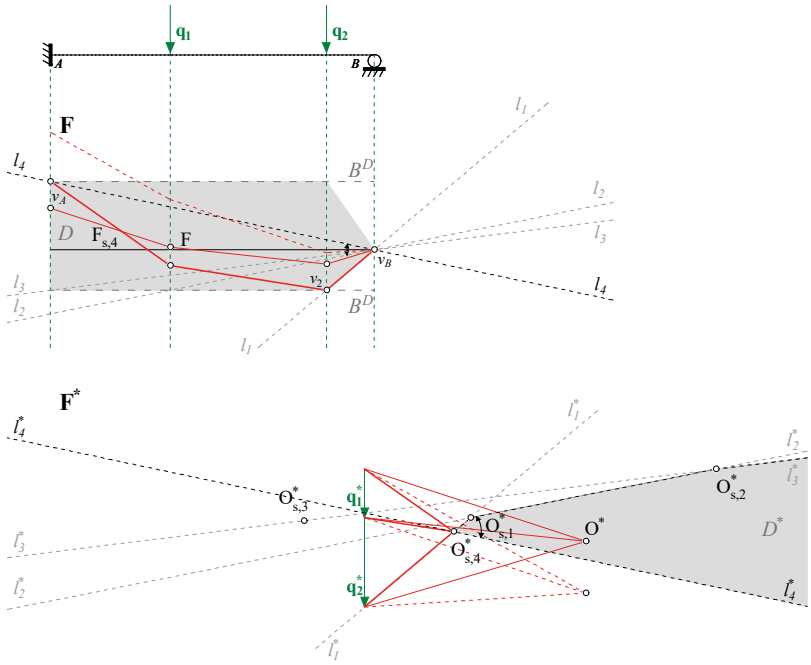

Figure 74 *Constructing D^* - In* $\mathbf{F}$*: last tensile limit polygon* $\mathrm{F}_{s,4}$ *(red bold lines) and last closing line* l_4*. In* $\mathbf{F}^*$*: last segment* l^*_4 *closing the force domain* D^**. Any pole* O^* *lying inside* D^* *corresponds to an admissible polygon* F*; any pole outside* D^* *to a non admissible polygon (red dashed lines).*

We can now draw the closing line l_4 joining v_a and v_b in $\mathbf{F}$ and the line of poles l^*_4 parallel to the latter in $\mathbf{F}^*$. Since both l_1 and l_4 are closing line for the limit polygon $\mathrm{F}_{s,4}$, l^*_1 and l^*_4 meet each other at $O^*_{s,4}$ in $\mathbf{F}^*$ **(Fig. 74)**. Since the direction of l_4 must be so that v_A lies inside of the

form domain D in order to respect the yield condition, the force domain D^* is consequently reduced once more to correspond to this condition. **Figure 74** shows an admissible polygon F which pole O^* is lying on l_4^* and a non-admissible polygon which pole lies outside of the force domain D^*.

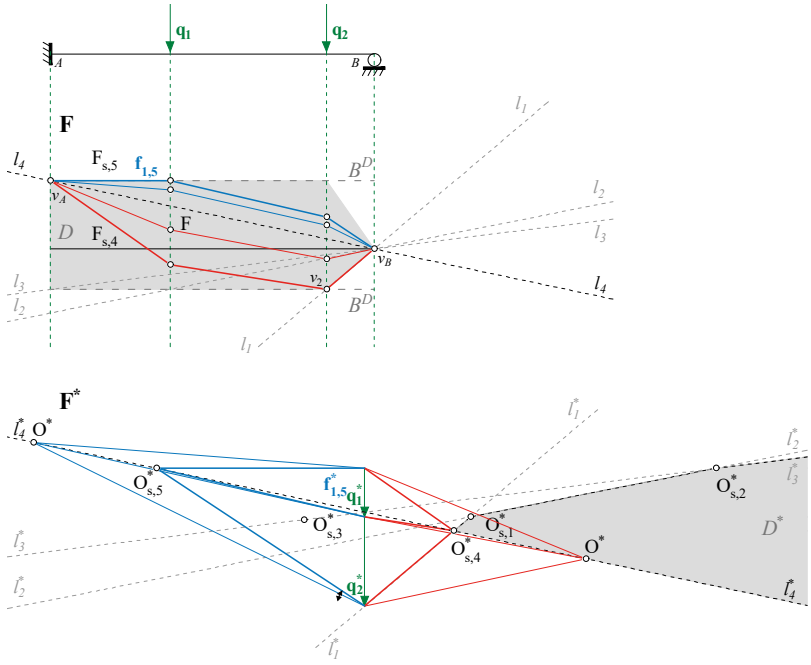

Figure 75 *Constructing D^* - Tensile (red bold) and compressive (blue bold) limit polygons* $\mathrm{F}_{s,4}$ *and* $\mathrm{F}_{s,5}$ *with shared closing line* l_4*, and tensile (red) and compressive (blue) admissible polygons for the same closing line. The corresponding poles are drawn along* l_4^* *in* $\mathbf{F}^*$*.*

As it was the case for l_3, the closing line l_4 of $\mathrm{F}_{s,4}$ is also the closing line of a compressive limit polygon $\mathrm{F}_{s,5}$ which vertices v_A and v_1 are lying on the form boundary B^D **(Fig. 75)**. The location of the corresponding limit pole $O_{s,5}^*$ is immediately found at the meeting point of l_4^* and $\mathbf{f_{1,5}^*}$. Any pole O^* lying on l_4^* on the left-hand side of $O_{s,5}^*$ or on the right-hand side of $O_{s,4}^*$ is an admissible pole which corresponding funicular polygon

is respectively a compressive or tensile admissible polygon F of **F** lying entirely inside the form domain D.

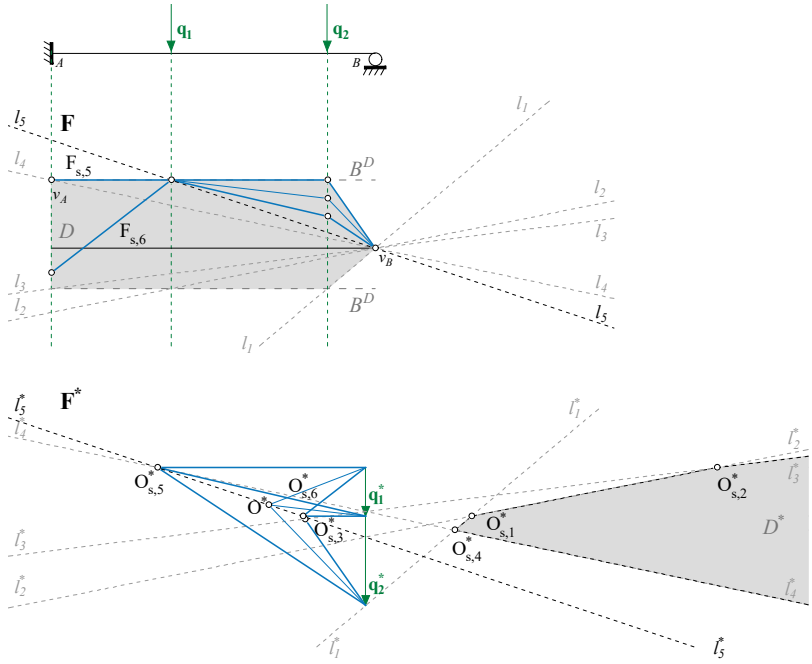

Figure 76 *Constructing D^* - Two compressive limit polygons* $\mathrm{F}_{s,5}$ *and* $\mathrm{F}_{s,6}$ *sharing the same closing line l_5 and their corresponding limit poles $O^*_{s,5}$ and $O^*_{s,6}$ in* $\mathbf{F}^*$.

In the same way, we draw l_5 , the other closing line of $\mathrm{F}_{s,5}$ which is also the closing line of another compressive limit polygon $\mathrm{F}_{s,6}$. Its corresponding limit pole $O^*_{s,6}$ lies on the line of poles l^*_5 as indicated in **Figure 76**.

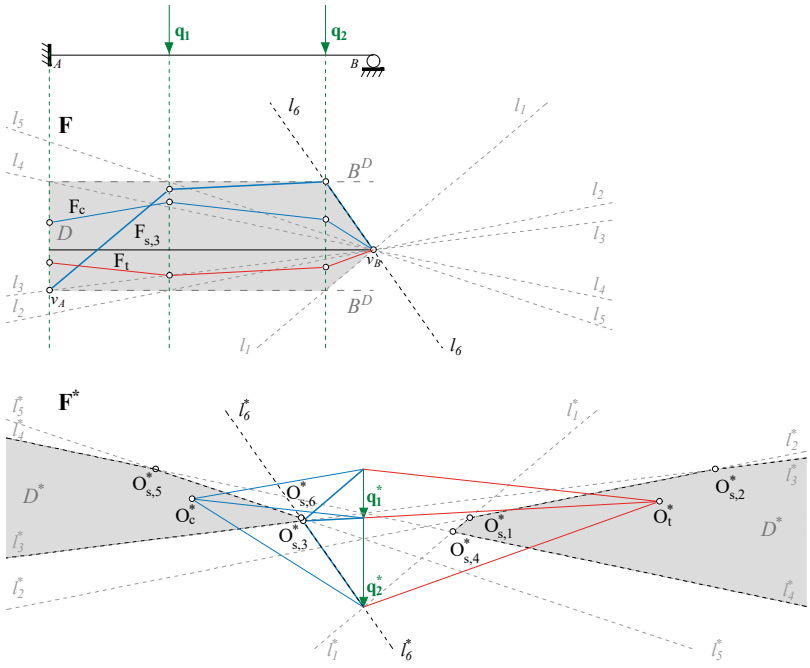

Figure 77 *Constructing D^* - The last closing line l_6 of the compressive limit polygon $\mathrm{F}_{s,6}$ and its corresponding line of poles l_6^* in closing the compressive force domain D^* in* $\mathbf{F}^*$.

Finally, the last possible closing line l_6 joining v_B and v_2 is drawn on **F**. It is the closing line of both limit polygons $\mathrm{F}_{s,6}$ and $\mathrm{F}_{s,3}$ already found previously, so that its corresponding line of poles l_6^* must joint poles $O_{s,6}$ and $O_{s,3}$. **Figure 77** shows these last limit cases and the resulting compressive force domain D for the pole in $\mathbf{F}^*$.

The methodology illustrated here presents the major advantage of being very systematic. Indeed, the force domain D* is defined as the intersection of several half planes which leading straight lines are the lines of poles corresponding to the closing lines joining two limit positions for the vertices of the funicular polygon. Since these specific locations for the vertices are determined as the meeting points of the action line of the external forces with the form boundary, all the closing lines can be generated from all the

combinations of these points by pairs. The location of the corresponding lines of poles in the force diagram is also systematically determined taking advantage of the property of reciprocal figures that ensures that all the segments that meet in a same point in one of the figures must form a closed polygon in the reciprocal one.

It is interesting to observe that every limit poles is located on one of the vertices of this convex force boundary. The visual analysis of such a domain consequently gives direct insights on the load bearing ultimate capacity of statically indeterminate beams that allow plastic redistribution of stresses. The few examples of next subsection highlight this property and show how the collapse load factor can be easily calculated using geometric observation and graphic measurements on $\mathbf{F}^*$.

5.4 Case studies: statically indeterminate beams

In order to validate our approach for the limit state analysis of statically indeterminate beams subject to bending, we have applied it to several case studies. For each of them, the results obtained by the graphic analysis of the force domain F^* are compared to the ones obtained with a kinematic approach by applying the Principle of Virtual Works on the corresponding collapse mechanism. We apply it first to the most simple case of a clamped beam, then extend this methodology to double embedded beams with various characteristics. For each of these case studies, we calculate independently the static collapse load factor $\lambda^*_{s,u}$ using our geometrical approach, and the kinematic collapse load factor$\lambda_{k,u}$ and compare the results obtained. Both formulation for $\lambda^*_{s,u}$ and $\lambda_{k,u}$ are expressed in an algebraic form in order to facilitate their comparison, although $\lambda^*_{s,u}$ could actually be obtained by simple measurements on the force diagram.

Simply supported beam

Before going to statically indeterminate cases, we apply the graphical methodology described in the previous section to a simply supported beam represented in **Figure 78**.

For determining the collapse load factor defined as the ratio between the magnitude of the force leading to collapse $\mathrm{q_u}$ and the actual magnitude of the applied force q. Since the structure is statically determinate, the closing line l is fixed as the straight line joining the two supports. There is consequently one sole limit polygon $\mathrm{F_s}$ and one sole corresponding position for the limit pole O_s lying on the line of poles l^* parallel to l, as indicated in the force diagram $\mathbf{F}^*$ of **Figure 78**. Since $\mathrm{q^*_u}$ and q^* are linearly proportional to H^*_u and H^* respectively, we can use the similar triangles relationships between the reciprocal form and force diagrams to expresses analytically the only possible value for $\lambda^*_{s,u}$ with respect to M_u, q^*, L, L_1. Equation 79 gives this value for the collapse load factor.

$$\lambda^*_{s,u} = \frac{\mathrm{q^*_u}}{\mathrm{q}^*} = \frac{H^*_u}{H^*} \cdot \frac{\mu_u s^* s}{\mu_u s^* s} = \frac{M_u}{\mathrm{r^*_B}(L - L_1)s^* s} = M_u \frac{(L/L_1)}{\mathrm{q}(L - L_1)s} \qquad (79)$$

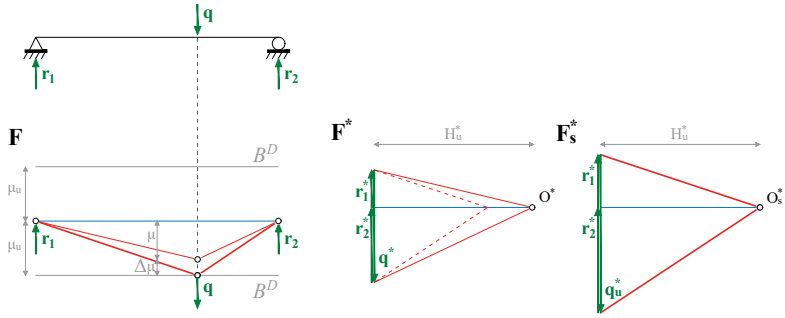

Figure 78 *Form* **F** *and force* $\mathbf{F}^*$ *diagrams at limit state for the simply supported beam AB. The limit pole* O_s *lies on line of poles* l^*

Applying now the Principle of Virtual Works to the only possible mechanism represented in **Figure 79**, Equation 80 gives the usual result for the value of the unique kinematic collapse load factor $\lambda_{k,u}$:

$$\lambda_{k,u} \cdot \mathrm{q} \cdot \theta_A L_1 = M_u \cdot (\theta_A + \theta_B) \Rightarrow \lambda_k, u = M_u \frac{(L/L_1)}{\mathrm{q}(L - L_1)} \tag{80}$$

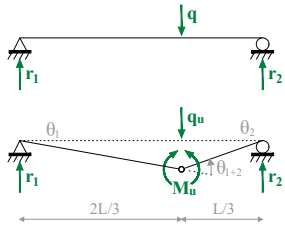

Figure 79 *Unique admissible mechanism for the simply supported beam AB*

Since these two approaches give the same value for the load factor, the uniqueness theorem ensures that $\lambda^*_{s,u}$=$\lambda_{k,u}$=λ_u.

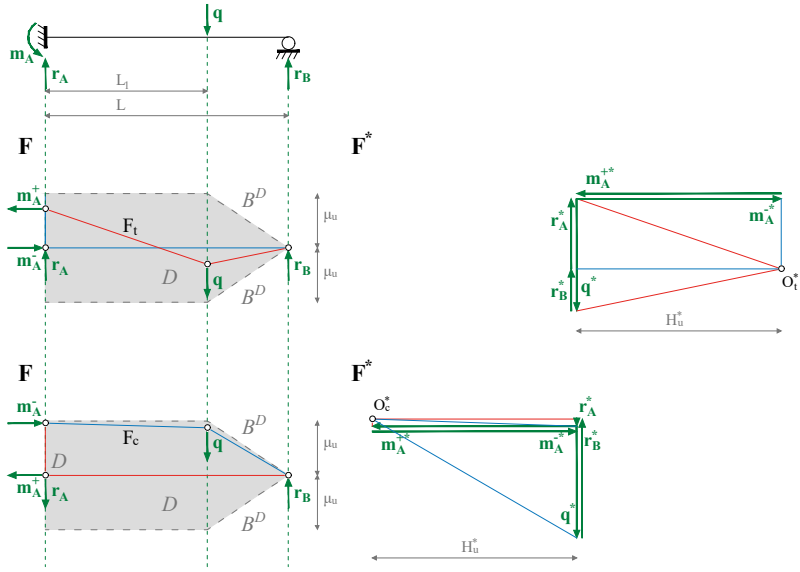

Figure 80 *Two admissible pairs of form and force diagrams. Above: tensile admissible polygon* $\mathrm{F_t}$ *in* $\mathbf{F}$ *and its related force diagram* $\mathrm{F_t^*}$ *for* H_u^* *fixed arbitrarily; below: compressive admissible polygon* $\mathrm{F_c}$ *in* $\mathbf{F}$ *and its force diagram* $\mathrm{F_c^*}$ *for the same value of* H_u^*.

Clamped-simply supported beam

Let us take into consideration the clamped-simply supported beam represented in **Figure 80**. In order to construct the reciprocal polygons corresponding to this structure, we apply simultaneously a force $\mathbf{q}$ and a couple of forces $\mathbf{m_A^-} - \mathbf{m_A^+}$ separated by a distance μ_A onto the simply supported beam **(Fig. 80)**. The forces forces $\mathbf{m_A^-}^* - \mathbf{m_A^+}^*$ are drawn on the force diagram $\mathbf{F}^*$ such to have the same magnitude H^* as the horizontal projection of the other funicular forces. The static indeterminacy makes it impossible to determine a lone value for the distance μ_A. However no indeterminacy is kept at collapse since the full plastic moment M_u must be applied to two different cross sections to produce a collapse mechanism, so that μ_A and μ_1 both must be equal to μ_u. It follows that there are only four combinations of plastic hinges that produce a possible collapse mechanism. Each of them correspond to a limit polygon characterised by

a specific location of the limit pole $O_{s,j}$, $j = 1 \rightarrow 4$. **Figure 81** represents the force domain D^* for the pole O^*, which vertices are the limit poles, and the four corresponding limit polygons $\mathrm{F_{s,j}}$, $j = 1 \rightarrow 4$. From the analysis of this domain, we can observe that, because of the symmetry between tensile and compressive limit behaviours, both poles $O^*_{s,1}$ and $O^*_{s,3}$ correspond to the minimum length of H^* so that $\frac{H^*_u}{H^*_{s,1}} = \frac{H^*_u}{H^*_{s,3}}$ is maximum. This ratio can be directly visualised in the actual force diagram $\mathbf{F}^*$ of **Figure 81**.

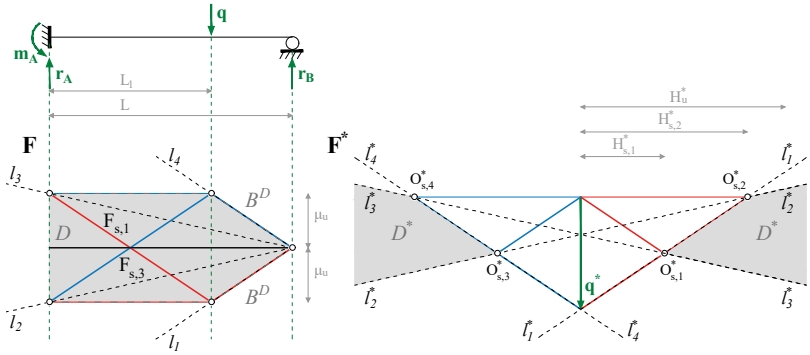

Figure 81 *Four limit polygons defined by their four closing lines $l_{1\rightarrow4}$, and their corresponding limit poles on the boundary of the force domain defined by the lines of poles $l^*_{1\rightarrow4}$.*

Taking $s = 1$ and s^*_1 so that $\mathrm{q}^* = \mathrm{q}^*_\mathrm{u}$, and taking into account that at collapse $H^*_{s,1} = H^*_u$, the relationships between the similar triangles of the reciprocal limit polygons in **Figure 81** are expressed in Equation 81, which gives therefore the value of $\lambda^*_{s,u}$:

$$\lambda^*_{s,u} = \frac{\mathrm{q}^*_\mathrm{u}}{\mathrm{q}^*} = \frac{H^*_{s,1}}{\mathrm{q}^*} \cdot \left(\frac{\mu_u + \mu_u}{L_1} + \frac{\mu_u}{L - L_1}\right) = \frac{M_u}{\mathrm{q}} \cdot \left(\frac{2}{L_1} + \frac{1}{L - L_1}\right) \quad (81)$$

Applying the PVW to the corresponding collapse mechanism **(Fig. 82)**, Equation 82 gives the same value for the load factor as the one obtained in Equation 81 by the static approach so that $\lambda^*_{s,u}{=}\lambda_{k,u}{=}\lambda_u$.

$$\lambda_{k,u}{\cdot}\mathrm{q}{\cdot}\theta_A L_1 = M_u{\cdot}\theta_A{+}M_u{\cdot}(\theta_A{+}\theta_B) \Rightarrow \lambda_{k,u} = \frac{M_u}{\mathrm{q}}{\cdot}\left(\frac{2}{L_1}{+}\frac{1}{L - L_1}\right) \quad (82)$$

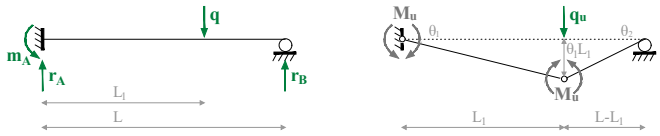

Figure 82 *Collapse mechanism corresponding to the static limit state represented by* $\mathrm{F}_{s,1}$ *and* $O^*_{s,1}$ *in* ***Figure 81****.*

Perfectly clamped beam

Considering now the same beam embedded at both ends **(Fig. 83)**, which requires three plastic hinges to be transformed into a mechanism, and considering that they may only be situated at the critical sections A, B, C and D because of the construction rules of the reciprocal diagrams, we draw the force domain D^* for the pole. In **Figure 83**, the four tensile limit polygons $\mathrm{F}_{s,1\to4}$ are drawn in $\mathbf{F}$ so that each of them has three vertices lying on the form boundaries B^D. The related positions for the pole are respectively noted $O_{s,1\to4}$ in the force diagram $\mathbf{F}^*$. Each of these positions is characterised by a specific length, noted $H^*_{s,1\to4}$ respectively. Applying the lower bound theorem of limit analysis, a lower bound value $\lambda^*_{s,u}$ for the collapse load factor is obtained by applying Equation 78. Equation 83 expresses this value obtained by measuring H^*_u and $H^*_{s,1\to4}$ on the the force diagram $\mathbf{F}^*$:

$$\lambda_{s,u} = \frac{H^*_u}{min_{j=1\to4}\left\{H^*_{s,j}\right\}} = \frac{H^*_u}{H^*_{s,3}} \tag{83}$$

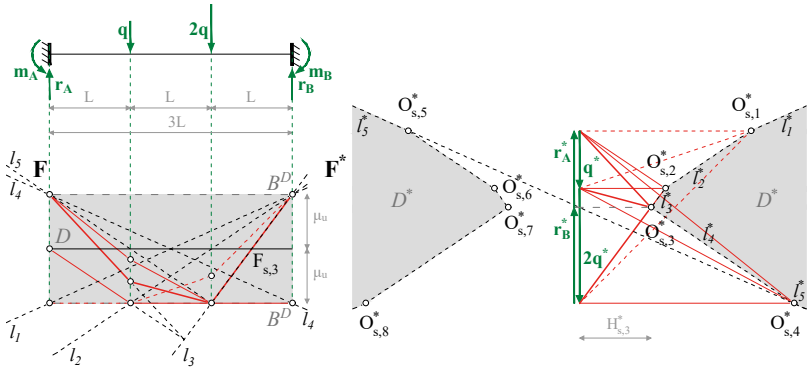

Figure 83 *Four tensile limit polygons defined by the four closing lines $l_{1\to4}$, and their corresponding limit poles on the boundary of the force domain D^* defined by the lines of poles $l^*_{1\to4}$. The collapse limit state is represented by* $\mathrm{F_{s,3}}$ *in* $\mathbf{F}$ *and* $O^*_{s,3}$ *in* $\mathbf{F}^*$

In this geometrically simple case, it is easy to express $H^*_{s,3}$ as an expression of other geometrical data coming from $\mathbf{F}$ and $\mathbf{F}^*$. Indeed, the similar triangle relationships between the two reciprocal diagrams can be written as a system of two equations:

$$\begin{cases} (\mathrm{r^*_B} - \mathrm{q^*}) \cdot \dfrac{L}{H^*_{s,3}} + \mathrm{r^*_B} \cdot \dfrac{L}{H^*_{s,3}} = 2\mu_u \\ \mathrm{r^*_A} \cdot \dfrac{L}{H^*_{s,3}} = 2\mu_u \end{cases} \tag{84}$$

Replacing $\mathrm{r^*_A}$ by $(3\mathrm{q^*} - \mathrm{r^*_B})$ and eliminating $\mathrm{r^*_B}$ from the equations gives:

$$H^*_{s,3} = \frac{5\mathrm{q^*}L}{6\mu_u} \tag{85}$$

Combining Equation 84 and Equation 85 with $s = 1$ gives the lower bound value for the load factor:

$$\lambda_{s,u} = \frac{6 \cdot \mu_u \cdot H^*_u}{5 \cdot \mathrm{q^*} \cdot L} = \frac{6}{5} \cdot \frac{M_u}{\mathrm{q}L} \tag{86}$$

The advantage of expressing this value for the load factor in an algebraic form instead of using geometrical terms is that it can be compared with

the results obtained using other approaches. In particular, it allows us to test the validity of this result by proceeding to a complete kinematic analysis in order to determine an upper-bound value for λ_u. The kinematically admissible mechanisms and their corresponding load factors $\lambda_{k,i}$ are represented in **Figure 84**. Applying the upper bound theorem of limit analysis on these values leads to the same conclusion as the one obtained by the static graphic approach:

$$\lambda_{k,u} = min_{i=1\to 4}\{\lambda_{k,i}\} = \lambda_{k,3} = \frac{6}{5} \cdot \frac{M_u}{qL} \tag{87}$$



Figure 84 *Collapse mechanism corresponding to the collapse funicular polygon* $F_{s,3}$ *in* ***Figure 83***

Therefore, the theorems of limit state analysis ensure that the correct value for the collapse load factor has been found since $\lambda_{s,u} = \lambda_{k,u} = \lambda_u$.

Case study on a perfectly clamped beam

The next case is devoted to the analysis of a S235-steal beam composed from two different profiles (IPE 240 - IPE200), perfectly continuous and perfectly clamped at each end. This beam supports a series of six applied forces as shown in **Figure 85**.

We draw the external forces vectors in the force diagram $\mathbf{F}^*$ at scale s^* and the arbitrarily chosen distance $H_u^* = 25$ *u.l.*. Being $M_{u1} = 86.245$ $[kNm]$ the full plastic moment of the IPE240 and $M_{u2} = 51.935$ $[kNm]$ the full plastic moment of the IPE 200, we can consequently draw at scale s the form boundaries at distances μ_{u1} and μ_{u2} respectively from the beam axis, so that $M_{u1} = \mu_{u1} H_u^*(ss^*)$ and $M_{u2} = \mu_{u2} H_u^*(ss^*)$. Drawing then the force domain in the force diagram $\mathbf{F}^*$ and identifying the different limit positions for the pole O^* at the vertices of the force boundaries, we can identify the closest pole from the external forces axis $O_{s,u}^*$ and measure its horizontal position $H_{s,u}^*$.

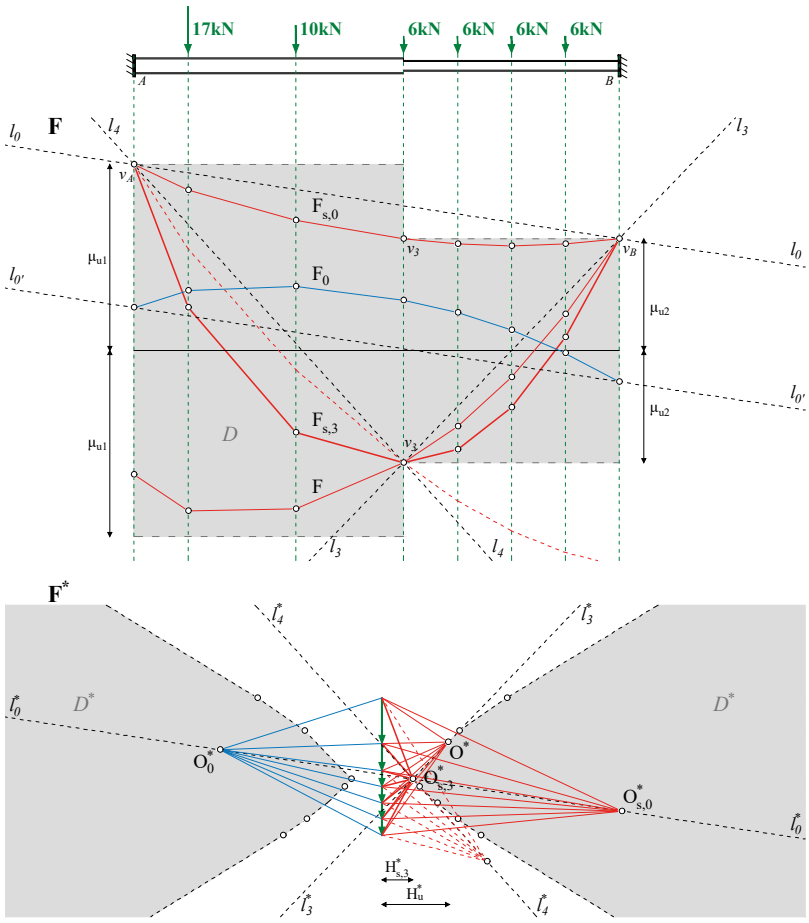

Figure 85 *Tensile collapse limit polygon* $\mathrm{F_{s,u}}$ *(red bold lines) which pole* $O^*_{s,u}$ *is the meeting point of three lines of poles* l^*_0, l^*_3 *and* l^*_4. *An admissible polygon* $\mathrm{F_3}$ *(red lines) which pole* O^*_3 *lies on* l^*_3 *within* D^* *and a non-admissible polygon (red dashed lines) which pole lies on* l^*_4 *outside of* D^*. *The admissible polygon* $\mathrm{F_{s,0}}$ *is a limit polygon with no limit pole since its closing line* l_0 *may be translated to* $l_{0'}$ *and hence, correspond to many admissible polygons;* $\mathrm{F_0}$ *is one of them in compression (blue lines).*

A lower-bound value can be found for the load factor:

$$\lambda^*_{s,u} = \frac{H^*_u}{H^*_{s,u}} = \frac{25\ u.l.}{11.383\ u.l.} = 2.196 \tag{88}$$

This result is identical to the one obtained when using the PVW on the corresponding mechanism **(Fig. 86)**. So the theorems of plastic analysis ensure that $\lambda_{s,u} = \lambda_{k,u} = \lambda_u = 2.196$.

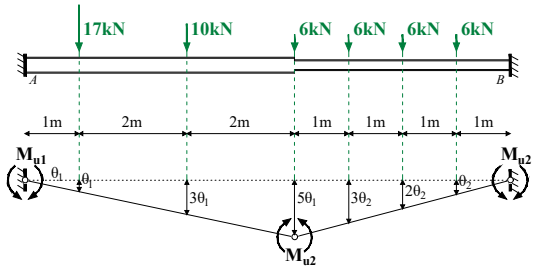

Figure 86 *Collapse mechanism for the beam AB corresponding to the collapse limit polygon* $\mathrm{F_{s,u}}$ *in* ***Figure 85****.*

Discussion. The graphical methodology proposed in this chapter is quite theoretical, and less efficient than other existing methods. Though, the concept of admissible geometrical domain introduced here could be interesting to use in different context. One application is proposed on the next chapter for evaluating the safety of masonry arches.

Chapter 6

Masonry arches

Structural analysis of ancient buildings is a sensitive matter for structural engineers. First, the non-standard properties of the building material (inhomogeneous, inelastic), then, their geometrical and static complexities, make them not easy to model. The high level of static indeterminacy of such structures – or equivalently, depending on the modelling strategy, the great amount of possible collapse mechanisms – and the lack of knowledge about the loading history may lead to a wrong estimation of the bearing capacity of such structures. This explains why classical structural analysis tools frequently fail to model efficiently the structural behaviour of heritage structures, and to give the designers information they need to assess structural performances (Shin et al., 2016). Looking for the actual stress state by elastic analyses based on original geometry and free-stress situation seems to be pointless (Huerta, 2001). Furthermore, this analysis is often useless since the principal concern of the structural engineer is to discover whether the structure is able to support the loads that are or will be applied, and to measure the safety level against collapse.

After an overview of methods developed for modeling masonry arches, the methodology used for drawing the admissible geometrical domains is adapted to those specific structures. An attempt is finally made to define a graphical safety factor.

6.1 Kinematic and static methods for structural assessment of masonry arches: a short overview

The mystery of masonry arch. In *"History of the theory of structures"*, Karl-Eugen Kurrer (2008) considers that masonry arches are *one of the mysteries of architecture"*. He says that the elaboration of masonry arch theory is the perfect example of the duality between kinematic and geometric approaches. From the first considerations on masonry arch equilibrium to most recent developments in structural analysis and numerical methods (such as distinct elements modelling), geometric and kinematic approaches have been used alternatively depending on the philosophical or scientific context of the time. The following succinct review of the main theories help to situate the approach among the existing ones and to identify its advantages and weaknesses. A deep review and very curated analysis of all these historical theories can be found in Huerta (2012).

Historical kinematic approaches. The kinematic approach of statics has prevailed until the 18th century, due to Aristotle's tradition of simple machines. Indeed, masonry arches were mainly conceived like kinematic assemblies of rigid bodies in unstable equilibrium, for which collapse could occur due to specific displacement conditions, namely at the abutments. For instance, Da Vinci proposed to consider each single stone of the arch as a wedge (Benvenuto, 1991), and consequently developed a simple measuring arrangement made of ropes and pulleys to characterise the horizontal thrust effect at the springings of the arch **(Fig. 87)**. He was one of the first engineers to propose a rule for designing arches that takes into account static considerations: *"The arch will not break if the outer arc chord does not touch the inner arc"*. This rule probably comes from the assimilation of the arch to a system of two rigid bars. This means that, assuming an arch is symmetric, its weight is transmitted from the crown down to the supports along two straight lines that intersect the extrados at the crown and at the abutments, and that lie entirely within the masonry envelope. Da Vinci's proposal can in fact be considered as a first attempt to define a thrust line lying inside the masonry envelope (Benvenuto, 1991).

Baldi (1621) was the first to propose a mechanical approach for evaluating arch stability. He therefore divided the arch into three equal rigid bodies

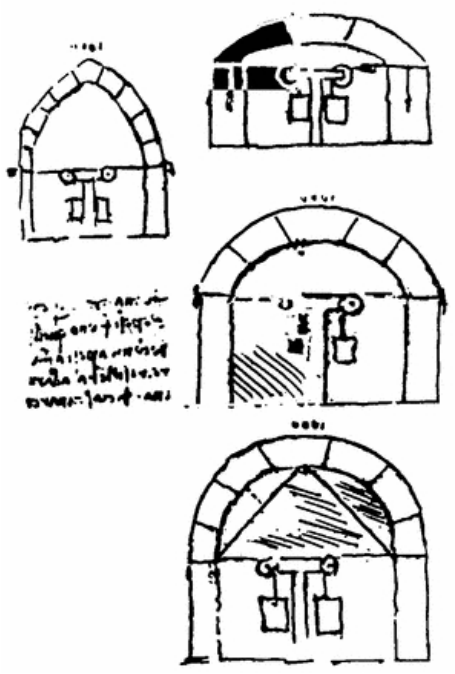

Figure 87 *Leonardo Da Vinci's arrangements for measuring the horizontal thrust in arches. Benvenuto (1991)*

and assumed that collapse would occur as soon as a displacement happens at the abutments, which would transform the central voussoir into a three-hinge mechanism **(Fig. 88)**. This kind of "kinematic approach" may be deemed archaic but is in fact still considered today as relevant. It has indeed been developed recently by authors like Smars (2002), who developed domains of kinematically admissible displacements.

After Baldi's approach, de la Hire (1729) proposed in his *Traité de mécanique* what is now referred as a kinematic ultimate load theory, in which he considered the arch and its abutments as a four-hinge mechanism in equilibrium (Kurrer, 2008). His first reasoning was based on the wedge and cranked lever mechanical principles, inherited from the five simple machines tradition. De la Hire further corrected his first theory, introducing the idea that friction in the joints is such that sliding cannot occur

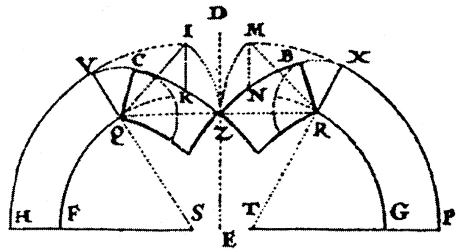

Figure 88 *Bernardino Baldi's three-hinge arch collapse mechanism. (Kurrer, 2008)*

(Heyman, 1998). The goal was to understand how to design the abutments in order to ensure the stable behaviour of the arch. Belidor (1729) reused this theory, putting forward three simplifying assumptions for practical purposes **(Fig. 89)**. First, he proposed to consider series of adjacent blocks as a sole rigid stone. He then assumed that arch's failure would occur at a 45 degrees angle, dividing the arch into four equal voussoirs. He finally supposed that the crown voussoirs are acting as wedges on the two others, which are considered as monolithically bound with the piers. Bélidor recognised that this last hypothesis puts his theory "on the safe side", since he considered no friction between voussoirs.

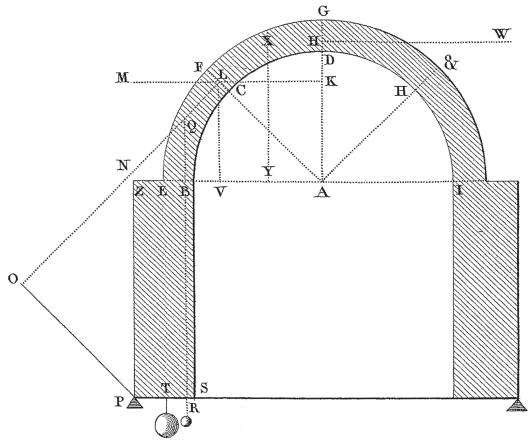

Figure 89 *Bélidor's collapse theory for masonry arches. (Belidor, 1729)*

Couplet (1731) further developed Bélidor and de la Hire's kinematic methods. He considered the same collapse mechanism, in which the arch is divided into four equal rigid bodies. But he considered instead that the failure mechanism occurs with a rotation of voussoirs around specific points of the intrados and extrados **(Fig. 90)**. He was the first to articulate explicitly the three classical assumption for masonry structures: infinite friction between voussoirs, infinite compressive strength and no tensile strength for arch material.

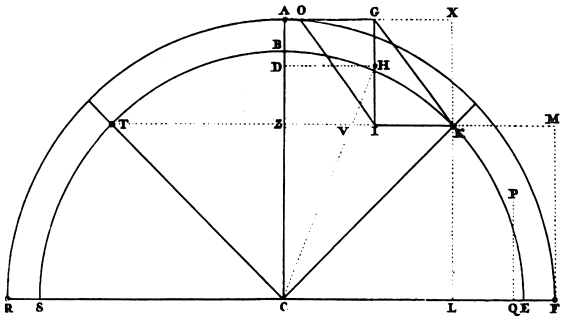

Figure 90 *Couplet (1731) theory for masonry arches' collapse.*

The thrust line theory. The kinematic approach was almost exclusively used until Perronet's observations on case studies led to a new – and more correct – theory for vaulted structures, based on a geometric approach of statics (Perronet and Chezy, 1810). This geometric point of view led to the so-called thrust line "classical approach" (Roca et al., 2010). The classical approach only deals with equilibrium considerations, the stability of vaulted structures and masonry arch bridges is ensured by the possibility of finding at least one thrust line – defined as the locus of points where the resultant force passes through the joints between the voussoirs (Ochsendorf, 2002) – lying entirely inside the masonry envelope (Huerta, 2001). The thrust line theory is attributed to Gerstner in German literature, to Méry (1840) in French literature and to Moseley (1843) in the English one. These two last authors correlate the geometry of the thrust line with collapse mechanisms: collapse indeed occurs when there is a sufficient amount of deep cracks along the arch as to transform it into a mechanism. These cracks actually react like plastic hinges occurring when the thrust line reaches the masonry envelope.

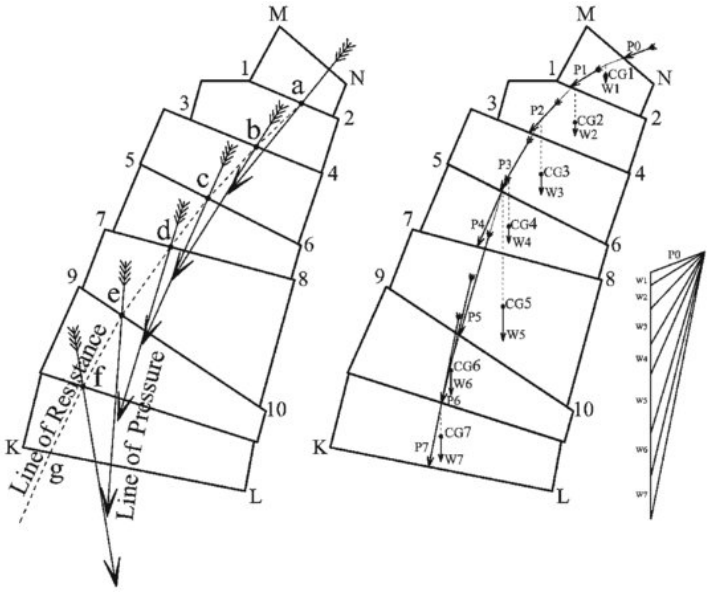

Figure 91 *The drawing presented by Moseley (1843) with a clear distinction between line of resistance (thrust line) and line of pressure (funicular polygon) (left) and its interpretation by Alexakis and Makris (2014) (right) where the successive thrust forces are consistent with the corresponding weights of the successive stone blocks. (From Alexakis and Makris (2014))*

Elasticity applied to masonry arches. The question of finding the 'true' line of thrust – intended as the one actually defining the equilibrium conditions – has led to various interpretations. Moseley (1843) used his principle of least resistance **(Fig. 91)** to choose, among the infinite number of possible lines, the one corresponding to the minimum value of the horizontal thrust (Timoshenko, 1953). Poncelet (1852) used a graphical method to determine the position of the cross section of rupture on the intrados. Culmann (1866) set up his *principle of minimum loading* in order to fix the position of the actual line of thrust as the one with the smallest deviation from the axis of the arch.

Indeed, for statically indeterminate structures, pure static considerations for constructing the thrust line are not sufficient to determine one unique solution for the load bearing system: this would require to integrate the real material behaviour into the masonry arch model. From the early 19th century, considerations on elastic compatibility prevailed thanks to Navier's elastic theory for beams and frames (Navier, 1833). Navier also developed Coulomb's voussoir rotation theory for masonry arches Navier (1826), by adding considerations on the compressive stresses acting in the joints. He assumed that a triangular distribution of compressive stresses must occur in order for the linear elastic relationship between stress and strain to be respected. He also used his theory to analyze wooden or metallic arches. The same elastic assumptions were used by Rankine (1858), for whom the stability of a masonry arch is guaranteed *"when a line of thrust due to a given loading case can be drawn through the middle third of all arch cross-section"*. In his *Méthode des aires de stabilité*, Durand-Claye (1867) attempted to integrate elastic stress distributions within a kinematic limit state analysis based on the eight possible collapse modes for a symmetric arch **(Fig. 92)**. These collapse modes may result for combinations of voussoirs rotations and slidings. A detailed analysis of his contribution can be found in Foce and Aita (2003).

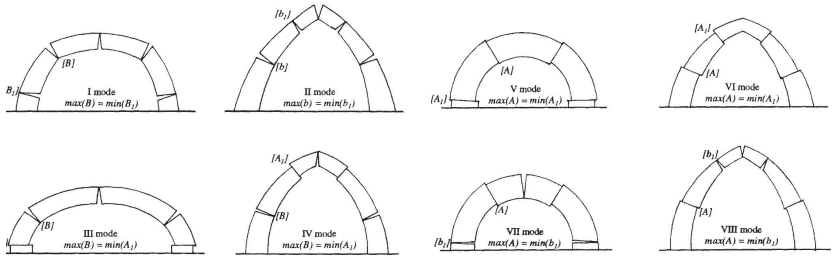

Figure 92 *Durand-Claye's eight collapse modes for a symmetric arch (Foce and Aita, 2003).*

Despite several alternative proposals, like Bandhauer (1831)'s symmetric distribution of stresses around the resulting normal force that kind of anticipated the plastic approach of Heyman (1995), elasticity almost became universal structural theory, especially after the energetic theorems of Menabrea (1875), Maxwell (1864b) or Castigliano (1873) among others.

They developed powerful tools for working with elastic stiffness. Winkler (1879) focuses in particular on the integration of theory of masonry arch within elastic theory in order to find the correct thrust line when the arch is at *normal state*, *i.e.* when the arch is not subjected to disruptions like cracks, incomplete joints, leaning supports, etc. His theorem states that *"for a constant thickness, the line of thrust close to the right one is the one for which the sum of the squares of the deviations form the centre-of-gravity axis is a minimum."* The elastic line of thrust theory was popularised by 19th century handbooks for engineers, for instance by Chaix (1890) who proposed various geometric procedures for masonry bridge design including abutments, vaults, etc. **(Fig. 93)**.

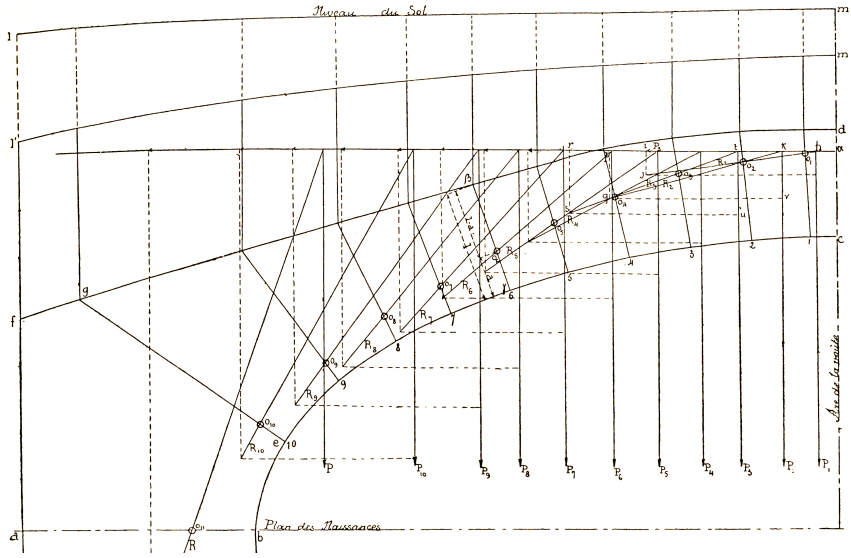

Figure 93 *Chaix (1890) methodology for dimensioning safe masonry bridges.*

The correct analytic description of the thrust line was given by Milankovitch (1907), for semi-circular arches made of radial voussoirs. Milankovitch found a ratio of 0.1075 between the minimum arch thickness and its average radius. This value was then further discussed by Makris and Alexakis (2013), while considering a different shape for the voussoirs.

Heyman's limit state of masonry structures. During the 20th century, the study of structural masonry gathered less interest as steel and iron became more popular in construction. Indeed, "it is quite difficult to find original contributions on masonry arches in specialised journals or even in engineering manuals" (Huerta, 2012, 430) until Prof. Jacques Heyman published his paper "The Stone Skeleton" (Heyman, 1966) in which he integrated the analysis of masonry load bearing structures within the theoretical framework of the Theory of Plasticity. This integration of the failure theory of the 18th and early 19th centuries is done assuming the same three fundamental hypotheses: infinite compressive strength, zero tensile strength and no failure due to voussoirs sliding. Hence, masonry can be considered as a rigid-plastic material, which ductility is due to the cracks that permit stress redistributions. Note that these hypotheses are also the ones that Méry (1840) already assumed – and discussed – in his *Mémoire*: compressive strength is usually higher than the effective stresses; neglecting tensile strength is conservative; masonry has a high coefficient of friction. Thanks to Heyman's lesson, which he later summarised and discussed rigorously for many types of masonry structures in his monograph *The stone skeleton* (Heyman, 1995), limit analysis is nowadays considered as the basis for the study of the stone skeleton (Foce and Aita, 2005).

The static approach has been followed by numerous authors who developed methods for design and analysis purposes. The work of Livesley (1978) is fundamental in this development. O'Dwyer (1999) proposed a new technique for the limit state analysis masonry vaults using a discrete network of forces in equilibrium, which is optimised to fit inside the masonry envelope. Boothby (2001) proposed other stress-strain principles distinct from Heyman's rigid plastic material law for masonry. Ochsendorf (2002) developed a general method to assess the stability of masonry buttresses against overturning or failure, taking into account the effects of leaning (Ochsendorf et al., 2004). Results were then applied to the study of buttressed arches, with a focus on the important influence of leaning buttresses on the arches stability. Block et al. (2006) further developed applications for real-time limit analysis of arches and vaults. These analytic tools allow the user to take into account the influence of increasing span for arches. Gilbert thoroughly studied the behaviour of masonry bridges (Gilbert and Melbourne, 1994; Gilbert et al., 2006; Gilbert, 2007). Smars (2002) analysed the stability of arches and vaults by describing domains of kinematically admissible displacements. Lourenço et al. (2005) did a very

important work on the modelling of dry stone masonry. Oliveira et al. (2010) evidenced the major importance of actual geometry in the bearing capacity of masonry bridges (Mauro et al., 2015). Most of these methods are explicitly or implicitly based on a combined static and kinematic limit analysis.

6.2 Conciliating lower bound theorem and thrust line theory: the equilibrium approach

The lower-bound theorem applied to masonry arches. Following Heyman's appropriate transfer of the basic methods of plastic theory from "steel" to "stone skeleton" (Sinopoli et al., 2004), the methodology developed for beams in the previous section can be adapted to the limit state analysis of masonry arches. Indeed, assuming certain hypotheses, masonry can be considered a rigid-plastic material which ductility is ensured by the possibility of cracking. Cracks play the role of plastic hinges, occurring where the resulting thrust line across a joint meets the masonry envelope. The classical hypotheses on the structural behaviour of masonry need to be assumed to achieve this: the resistance of masonry is supposed infinite in compression; masonry cannot transfer tensile forces; sliding cannot occur because of the large frictional forces acting between the blocks. Considering this, it means that the principles of Plastic Theory are applicable to masonry arches. In particular, the lower-bound theorem ensures that, if the assessment of the masonry arch is made using a static approach, the solution found is a safe estimation of the actual capacity of the arch.

Limit state analysis using thrust lines. For static analysis, the concepts of *thrust line* is used, intended as *geometrical locus of the points of application of the compressive resultant thrust that passes through the joints between voussoirs* (Ochsendorf, 2002; Alexakis and Makris, 2014). This is equivalent to Moseley's concept of line of resistance (Benvenuto, 1991). This concept is distinct from the one of line of pressure, intended as the locus of the consecutive intersections of the directions of the resultant pressures upon the joints (Benvenuto, 1991). According to Fantin and Ciblac (2016), *"(. . .) Nowadays, the line of resistance is called thrust line, and the line of pressure is called funicular polygon. (. . .) The latter is a necessary step for drawing the line of thrust in graphic statics"*. The same authors insist on the fact that the funicular polygon may exit the masonry envelope, whilst the thrust line may not. This may be of relevant importance in finding limit states for masonry arches with complex geometry. Ochsendorf et al. (2004), followed by Heyman (2009) and other numerous authors, showed that the distinction between thrust line and

line of pressure has a major relevance in the study of the stability conditions of circular arches, and on the determination of the minimum and maximum thrusts. Drosopoulos et al. (2008) and Makris and Alexakis (2013) have further discussed the influence of the stereotomy, and particularly of the inclination of the joints, on the relation between these two lines. de Arteaga and Morer (2012) have emphasised the crucial effect of geometry on the effective bearing capacity of masonry bridges.

Numerous authors such as Heyman (1995), Huerta (2001) or Ochsendorf (2002) have evidenced that it is in general impossible to know the actual thrust line acting inside the arch because its definition is highly sensitive to small geometrical perturbations due to cracking or movements at the abutments. However, it is possible to establish certain limit thrust lines depending on the magnitude of the thrust force and its application point at some critical sections.

Because of their direct parallelism with the equilibrium and yield boundaries, the set of admissible limit thrust lines constitutes a convenient geometrical representation of the domains of safety for arches. An admissible thrust line must be such as to remain within the masonry envelope (the form boundary) where it crosses the joint line. A limit thrust line is such that it correspond to the fulfilment of an instability condition. This occurs when the thrust line reaches the masonry envelope in a certain amount of sections such that the structure is transformed into a mechanism.

Advantages of equilibrium approaches. The methodology that will be followed presents several advantages. As already underlined in the previous sections for other types of structures, one of the main benefits is that it is a "safe" methodology: the thrust line determined as the collapse thrust line may only lead to an underestimation of the arch's stability. Another common benefit, inherent to graphical methods, is that the visual presentation of the results makes them easy to interpret. The last advantage, specific to masonry arches' structural assessment, is that the method is exclusively geometric. On the one hand, this makes the method easier to use for practitioners that other methods because it does not require complex computations. On the other hand, it also means that no specific numerical tool is required and that the usual CAD software can be used to achieve the analysis.

6.3 Admissible geometrical domains

In this section, we show how these limit thrust lines can be deduced from the limit reciprocal diagrams. Advantage is taken of this graphical methodology developed for beams in the previous section to construct the *force domain*, defined as *the set of statically admissible positions of the pole*.

Construction of the force domain . **Figure 94** illustrates the construction of the force domain for a four voussoirs arch under its self-weight. Since the load case is unique and fixed, we are not looking for the ultimate load that needs to be applied to provoke collapse, but rather to identify the geometrical conditions of equilibrium of this arch. These conditions are determined by the *equilibrium approach* exposed in the previous paragraph: any thrust line lying entirely within the masonry envelope represents a possible distribution of forces in equilibrium. Since each of these thrust lines is correlated to a funicular polygon characterised by the position of its pole O in the force diagram $\mathbf{F}$, the set of the statically admissible (*i.e.* for which equilibrium and yield conditions fulfilled) positions for the pole is the admissible geometrical domain of the arch D, and its boundary B^D is equivalent to the yield surface characterising the structure.

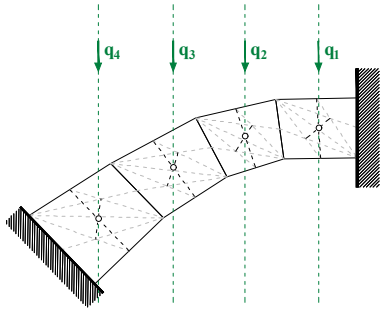

Figure 94 *A four voussoirs arch with infinite compressive strength, no tensile strength and high friction in the joints.*

Any funicular polygon in equilibrium with the loads is unequivocally defined, *i.e.* geometrically determinated, when three of its points are known. Equivalently, a masonry arch is statically determinate when three cracks (equivalent to plastic hinges) have formed (Heyman, 1995). It follows that, in case of a masonry arch, a limit polygon must reach the form boundary within three joints, producing cracks within these joints. Consequently, any of these limit polygons can easily be generated by choosing three points at the intrados or extrados of the joints through which the funicular polygon must pass. **Figure 95**, **Figure 96**, and **Figure 97** show the construction of the eight limit polygons $\mathrm{F}_{\mathrm{s},1\to 8}$ and the closing lines $l_{0\to 8}$, which parallels in $\mathbf{F}^*$, $l^*_{0\to 8}$ form the borders of the force domain D. Each limit pole $O^*_{1\to 8}$ is situated at one of the vertices of the convex force boundary B^{D*}, where two lines of poles intersect.

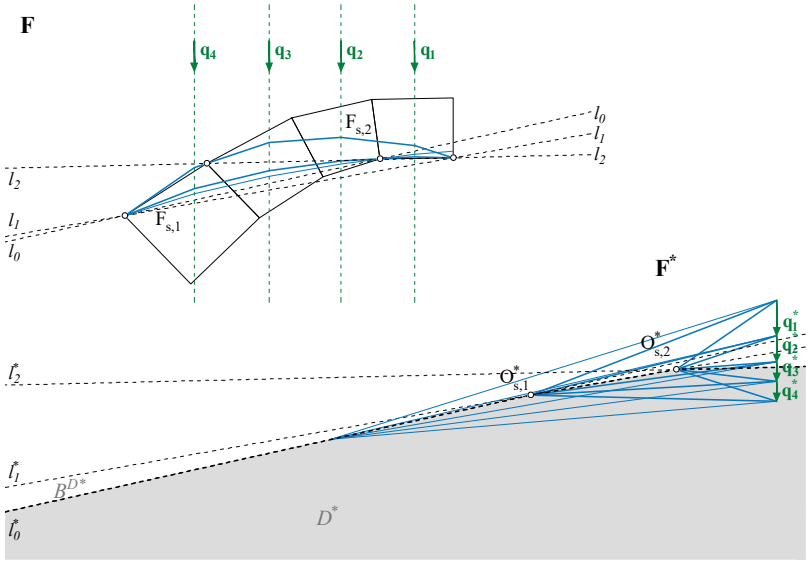

Figure 95 *In* $\mathbf{F}$*: two limit polygons,* $\mathrm{F}_{\mathrm{s},1}$ *with closing lines* l_0 *and* l_1*, and* $\mathrm{F}_{\mathrm{s},2}$ *with closing lines* l_1 *and* l_2*. In* $\mathbf{F}^*$*, their poles* O^*_1 *and* O^*_2*, where lines of poles* l^*_0*,* l^*_1 *and* l^*_2 *intersect. The black dashed bold lines are a first segment of the force boundary* B^{D*}*.*

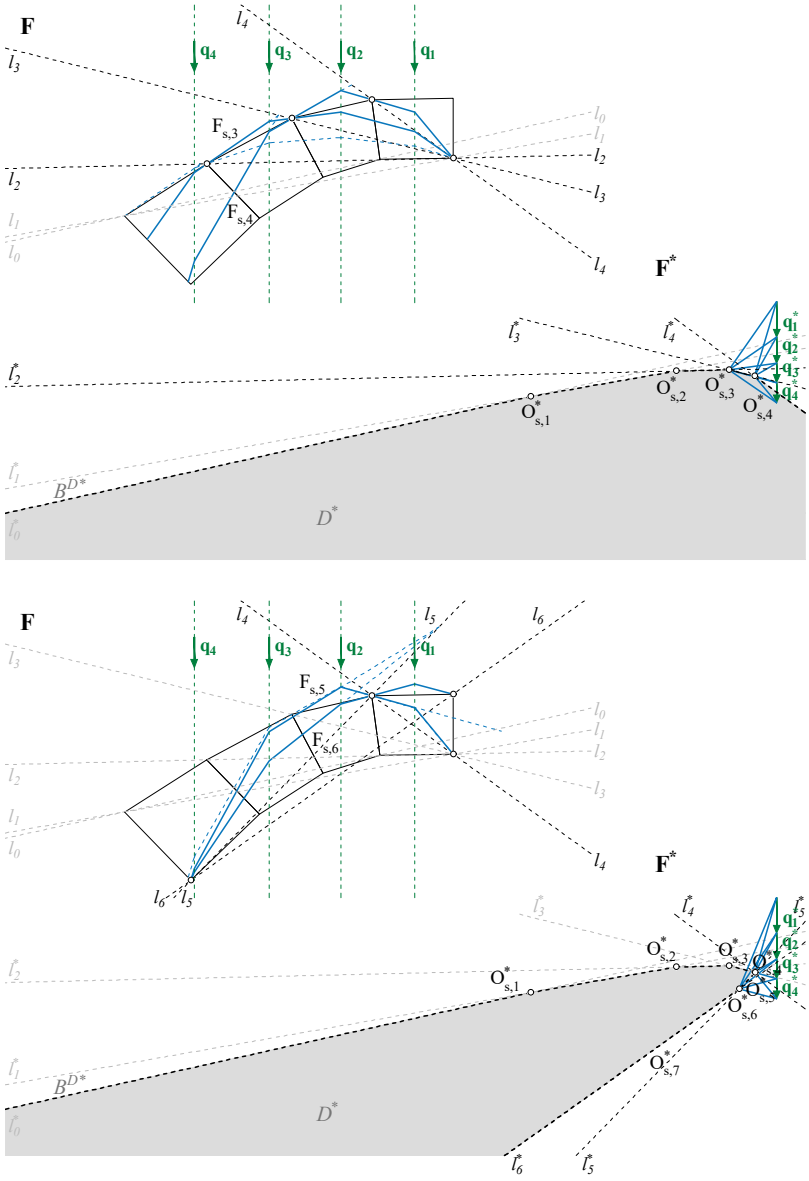

Figure 96 *Construction of the force domain D^* in $\mathbf{F}^*$ of a masonry arch, where poles O_3^*, O_4^*, O_5^* and O_6^* correspond to limit funicular polygons.*

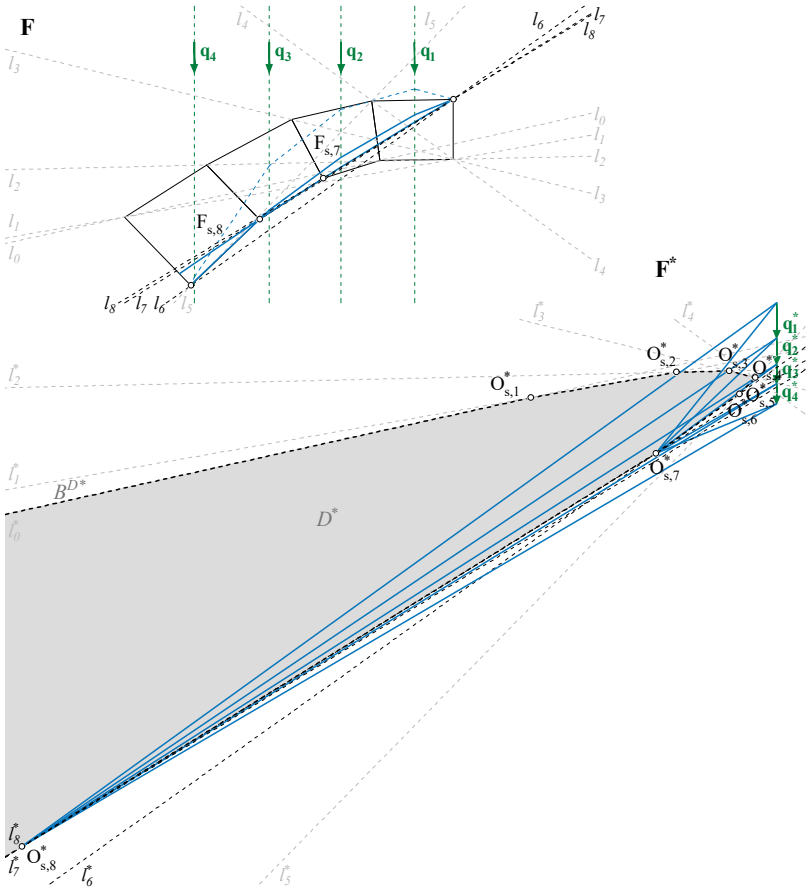

Figure 97 *In* **F***: two limit polygons,* $\mathrm{F}_{s,7}$ *with closing lines* l_6 *and* l_7*, and* $\mathrm{F}_{s,8}$ *with closing lines* l_7 *and* l_8*. In* $\mathbf{F}^*$*, their poles* O_7^* *and* O_8^**, where lines of poles* l_6^**,* l_7^* *and* l_8^* *intersect. The force boundary* B^{D*} *is now completed and does not close on the left-hand side.*

The force domain D^* has no boundary on the left-hand side, because of the infinite compressive strength hypothesis, and because closing lines l_0 and l_8 cross over the entire arch without getting out of the masonry envelope. Therefore, the pole may be translated infinitely along the two corresponding lines of poles l_0^* and l_8^*.

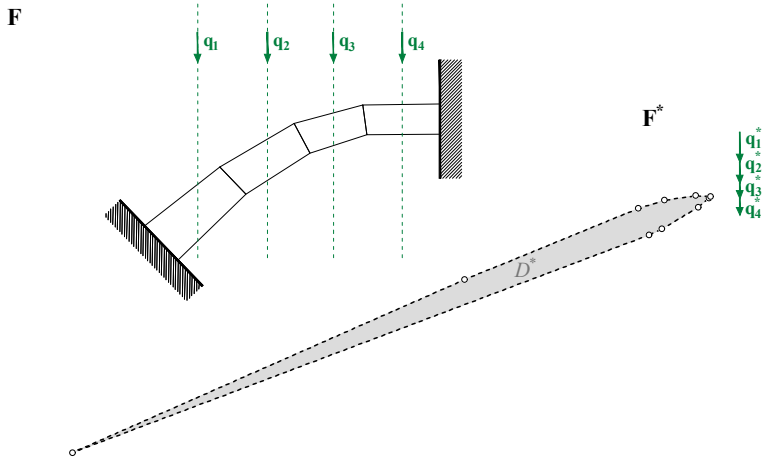

Figure 98 *Force domain D^* of an arch composed of four voussoirs, with a thickness reduced to half.*

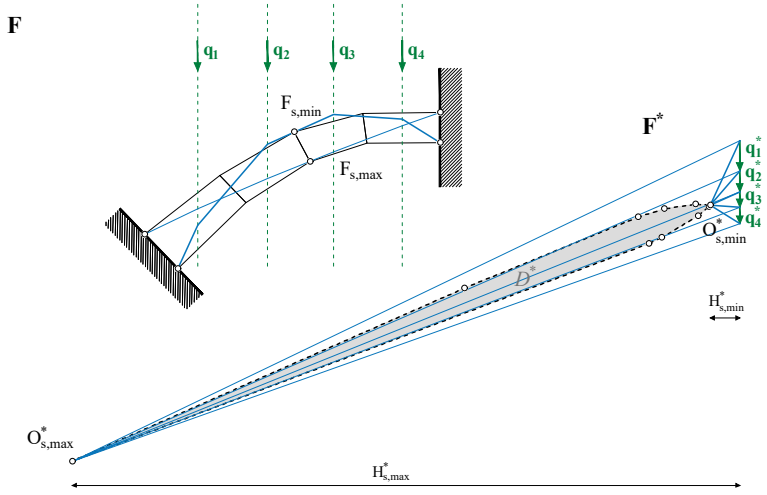

Figure 99 *In* **F***: limit funicular polygons corresponding to the maximum and minimum thrusts; in* $\mathbf{F}^*$*: magnitudes of the maximum and minimum thrusts related to the position of the pole O^*.*

Analysis of the force domain. Now a four-voussoirs arch similar to the one of **Figure 94** is considered, which thickness has been reduced to the half of the original one **(Fig. 98)**. Its force domain D^* has been generated using the same methodology as in the previous paragraph. This domain is not infinite since no straight line can be enclosed within the form boundaries.

Figure 99 shows the limit funicular polygons $\mathrm{F_{s,min}}$ and $\mathrm{F_{s,max}}$ corresponding respectively to the minimum and maximum thrust lines. The corresponding poles $O^*_{s,min}$ and $O^*_{s,max}$ are located at distances $H^*_{s,min}$ and $H^*_{s,max}$ from the line of the applied forces in the force diagram $\mathbf{F}^*$.

Any vertex of the force boundary corresponds to a limit position for the pole that is related to a limit polygon. **Figure 100** shows two of these limit polygons and the correlated position of the pole.

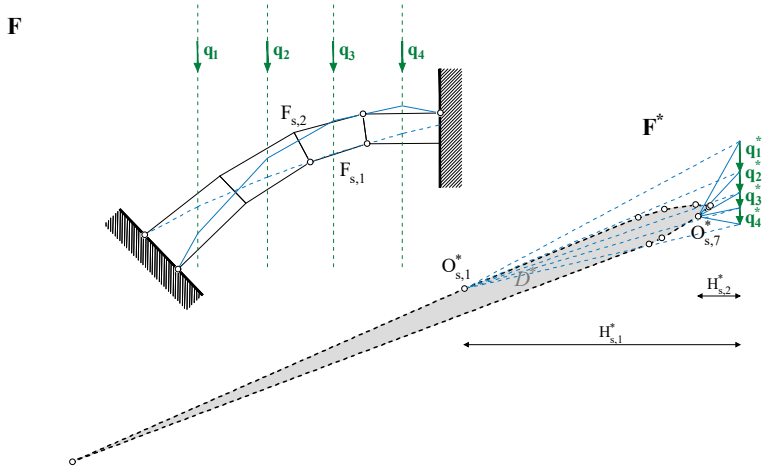

Figure 100 *In* $\mathbf{F}$*: two limit polygons* $\mathrm{F_{s,1}}$ *and* $\mathrm{F_{s,6}}$*; in* $\mathbf{F}^*$*: magnitudes of the corresponding thrusts and position of the limit poles* $O^*_{s,1}$ *and* $O^*_{s,6}$.

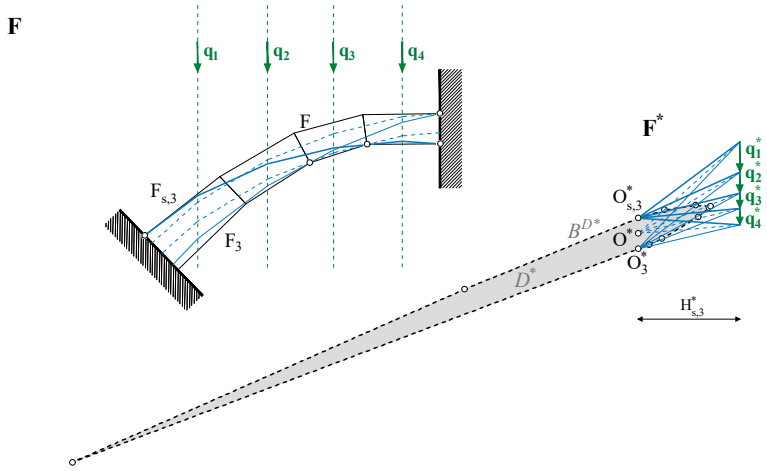

Figure 101 *Different funicular polygons corresponding to the same horizontal thrust* $H^*_{s,3}$.

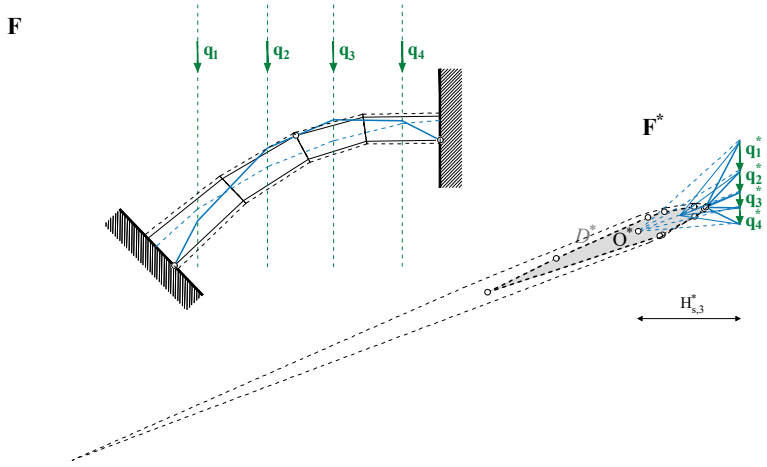

Figure 102 *Reduction of the force domain correlated to a reduction of the arch thickness to a ratio 0.8 the original thickness.*

Pole $O^*_{s,3}$ in **Figure 101** corresponds to a magnitude of the horizontal thrust force $H^*_{s,3}$ for which the vertical distance between the two sides of the force boundary B^{D*} is maximum. This means that the corresponding thrust force provides the highest amount of statically admissible thrust lines. This means that a major plastic redistribution can occur in this situation. Indeed, if positioning the pole O^* in the middle of the vertical line enclosed within D^*, the corresponding funicular polygon F can be translated vertically within the masonry envelope in a large range of positions. Consequently, the thickness of the arch may be reduced without provoking its collapse, since the translated thrust line may lie within the reduced envelope. **Figure 102** shows how the force domain D^* is reduced when decreasing the thickness to 80% of its initial one.

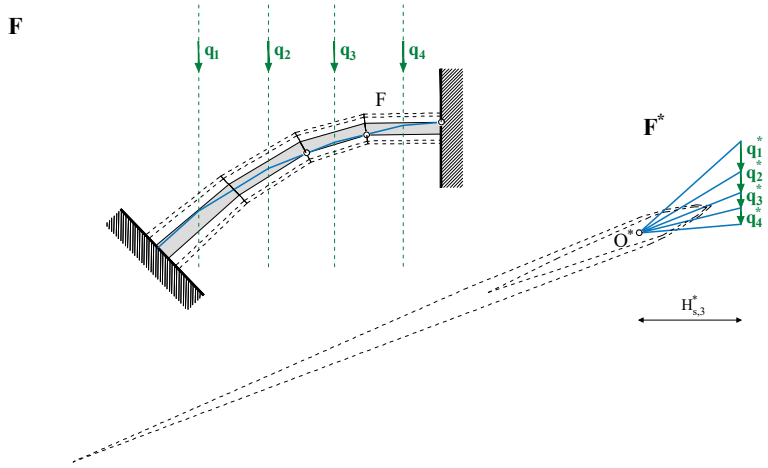

Figure 103 *Minimum thickness arch, for which the force domain reduces to a point.*

In **Figure 103**, the arch's thickness is decreased until the force domain is almost reduced to a sole point. The construction has been done by the successive reduction of the masonry envelope, thus of the force domain. Because of the arch's irregular geometry, no systematic procedure for determining the position of this unique pole has been found yet. Though, even if the position obtained by this iterative procedure may not correspond to the optimal position, *i.e.* the one corresponding to the minimum

thickness of the arch, our solution corresponds to a lower-bound estimation of this minimum thickness. This underestimation of the conditions of collapse is very tiny and would not have major consequences in a practical situation of safety assessment.

Next section shows some results obtained with an automatic procedure for generating the force domain. The results are compared with those found in litterature in terms of relative thickness of semi-circular arches.

6.4 Graphical safety of masonry arches

Stability assessment according to Eurocode 0. When assessing the structural response of an existing building, an engineer may focus on three main requirements: stability, strength, and stiffness (Heyman, 2008). The two first requirements are linked to structural safety and the third to the serviceability of the building. Concerning historical masonry structures, as the mean acting stresses are typically relatively low (strength requirement), local crushing of the material is hardly affecting the global integrity (Heyman, 1995). In the same vein, working deflections are usually not occurring (stiffness requirement) because the sections are generally large and a rigid material behaviour can be considered. For masonry arches, the focus can then be exclusively put on ultimate limit states related to equilibrium issues (stability requirement), as demonstrated by Huerta (2006). This means avoiding a loss of static equilibrium within the global structure, as well as within any part of it considered as a rigid body. As developed in the *Eurocodes* (EN90, 1990), the most common approach for evaluating structural response is to consider the structure in terms of limit states, intended as states beyond which the structure no longer fulfils the relevant design criteria. This can be formulated as:

$$E_{d,dst} = E_{dst} \cdot \gamma_{dst} \leq E_{d,stb} = \frac{E_{stb}}{\gamma_{stb}} \tag{89}$$

where E_{dst} is the characteristic value related to the effects of destabilising actions; and E_{stb} the characteristic value for stabilising actions. Design values for these actions (with d indices) are obtained by applying the corresponding safety factors γ_i. EN90 (1990) recommends the following values for the safety factors:

- dead-load - destabilising action: $\gamma_{G,dst} = 1.1$;
- dead-load - stabilising action: $\gamma_{G,stb} = 0.9$;
- variable-load - destabilising action: $\gamma_{Q,dst} = 1.5$;
- variable-load - stabilising action: $\gamma_{Q,stb} = 0$.

Heyman's geometric safety factor. For masonry arches, the question of measuring structural safety as in Equation 89 is not straightforward. The general expression of the safety factor as a ratio between stabilizing and destabilizing actions induces a difficulty for the choice of the appropriate parameter, especially for arches under self-weight only. Heyman (1995) proposed instead a geometric safety factor, defined as the ratio between the actual thickness of the voussoirs and the minimum one, *i.e.* the one for which the limit state of equilibrium is reached. This way of defining structural safety is interesting, because it only deals with the geometrical characteristics of the arch rather than with material strength. Assuming for instance a geometric safety factor of three would mean that it is possible to find a thrust line contained in the middle third of the arch. This corresponds to the classical design criteria for masonry developed in Eurocode 6, for blocky elements without specific performances (Hurez et al., 2009).

However, Heyman's approach might be hard to use in practice when it comes to irregular geometries that would require to identify the critical section to which apply the safety factor. Another limitation of this method is that it cannot easily be linked with the safety factor formulations commonly used by structural engineers, which are expressed in terms of ratios between characteristic and design stresses or related to the magnitudes of the external loads acting on the structure. This is not an issue for existing structures under self-weight only, but it becomes for instance a clear drawback when evaluating the response of an existing structure under a modified external loading. Furthermore, Heyman's approach cannot easily be linked with the safety factor formulations commonly used by structural engineers, which are expressed in terms of ratios between characteristic and design values for stresses and deformations.

Safety and force domains. Working with the force domain generated in the force diagram $\mathbf{F}^*$ for the pole O^* of the funicular polygon acting within the masonry envelope may enable to overcome these limitations. Indeed, as already highlighted several times in this dissertation, and by numerous authors like Zalewski and Allen (1998); Baker et al. (2012); Fivet and Zastavni (2013); Mazurek et al. (2016), graphic statics presents the advantage of being a very simple and visual tool to control force equilibrium. The concept of graphical region developed by Fivet (2013), transformed here in the case of limit analysis into admissible domains, are used in that

context. For masonry arches as wall as for beams, this domain is intended as the locus of statically admissible positions for the pole of the funicular polygon leading to thrust lines that lie entirely within the masonry envelope. Therefore, this force domain depicts all the statically admissible equilibrium configurations. Points on the vertices of the force domain are then related to possible limit states, as the corresponding thrust lines reach the masonry envelope in such a way that it produces a mechanism (Rondeaux and Zastavni, 2017). Based on the lower-bound theorem of plasticity, this means that failure can only occur if its admissible geometrical domain is an empty set of points. Consequently, we believe that some indicators of the structural safety of an arch can be deduced from the analysis of its force domain.

In Rondeaux et al. (2018b) and Deschuyteneer et al. (2018b), the possibility to excavate several indicators of safety and robustness of masonry arches from the force domain is outlined. The safety indicator is obtained by considering the magnitude of the thrust characterising some specific vertices of the force boundary and linked to the assessment of the overall stability. The robustness indicator takes advantage of the force domain's area and the ways it is modified in case of damage to measure the level of structural robustness.

6.4.1 Stability under self-weight

Self-weight stability indicator. The first evaluation of the arch's stability, proposed in Rondeaux et al. (2018b), is relative to the overall ability of the arch to support its self-weight. The proposal consists in measuring safety by a safety indicator λ_H^*:

$$\lambda_H^* = \frac{H_{max}^*}{H_{min}^*} \tag{90}$$

Values for H_{max}^* and H_{min}^* are measured in the force diagram $\mathbf{F}^*$, and represent the characteristic values related to the maximum and minimum admissible horizontal thrusts acting inside the arch. They are respectively linked with the leftmost and rightmost positions of the pole within the force domain **(Fig. 104)**. Safety indicator λ_H^* is obtained by measuring the lengths of H_{max}^* and H_{min}^* in $\mathbf{F}^*$:

$$\lambda_H^* = \frac{18.75 u.l.}{2.52 u.l.} = 7.44 \tag{91}$$

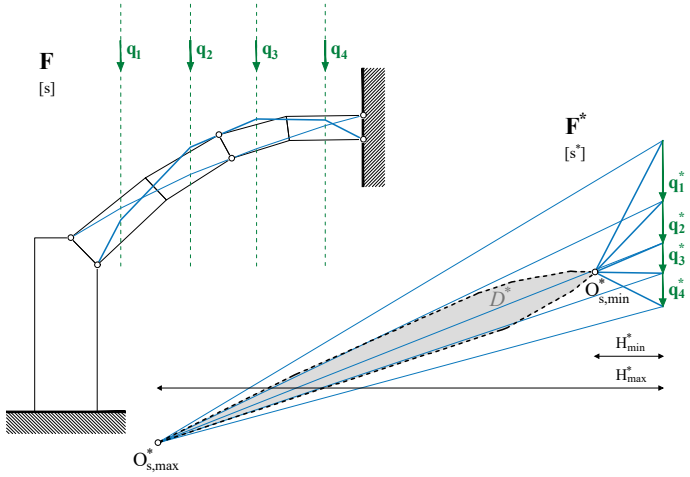

Figure 104 *Safety indicator relative to arch's stability of this arch under self-weight.*

Validation by comparison to Heyman's geometric safety factor. In order to validate the proposed safety indicator, comparison is made with proposed Heyman's geometric safety factors. For an arch with an irregular geometry as in **Figure 104**, the minimum thickness is not always easy to determine. However, there is plethora of pieces of literature concerning semi-circular arches since many authors have addressed the question of its minimum thickness. For this purpose, three historical theories for obtaining the minimum arch's thickness are chosen. The force domain corresponding to each of them is generated, considering that the arch is divided into 21 radial voussoirs. The minimum thickness according to each of these theories can be compared to the correct one obtained by Milankovitch (1907) **(Fig. 105)**.

Da Vinci's arch. First, the arch is given a minimal thickness as proposed by Da Vinci **(Fig. 106)**. According to Benvenuto (1991), Da Vinci's proposal that *"the arch will not break if the outer arc chord does not touch the inner arc"* probably comes from the assimilation of the arch to a system of two rigid bars (Section 6.1).

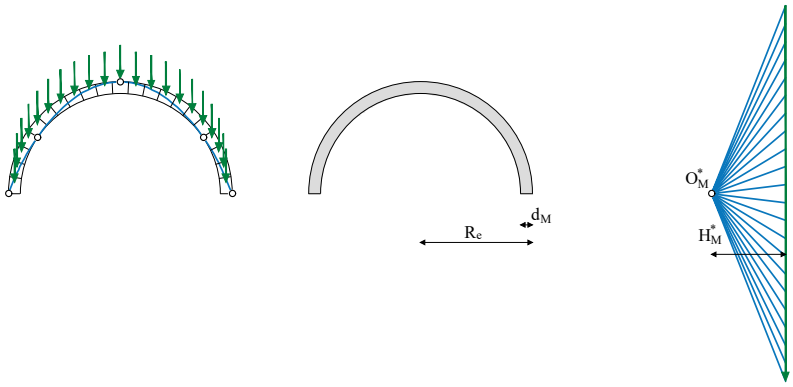

Figure 105 *Milankovich's arch with minimum thickness.*

The orientation of the chords being uniquely defined, this gives for the minimal arch thickness:

$$d_V = 0.293 R_e \tag{92}$$

with R_e the external radius.

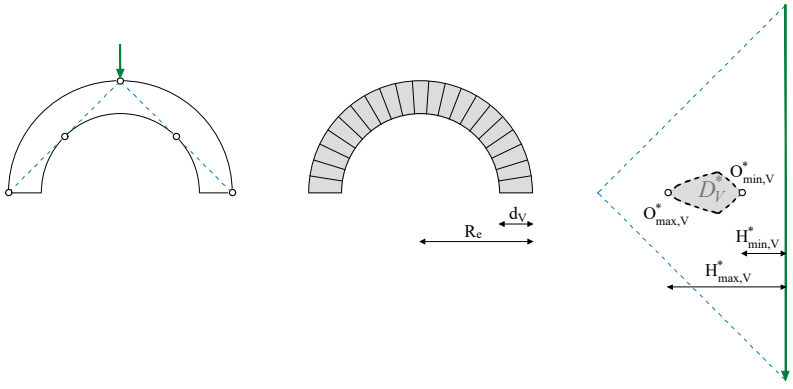

Figure 106 *Interpretation of Vinci's two rigid bars arch theory (left); minimum thickness arch suggested by Vinci (center); corresponding force domain for the pole according to thrust line theory (right).*

An arch of radius d_V is depicted in **Figure 106**, whith the corresponding force domain D_V^*, constructed assuming a 21-voussoirs subdivision of the arch.

Fabri's arch. Following Fabri's construction rule given by Benvenuto (1991) and reproduced in **Figure 107**, the arch is then given a minimal thickness:

$$d_F = 0.343 R_e \tag{93}$$

with R_e the external radius of the arch.

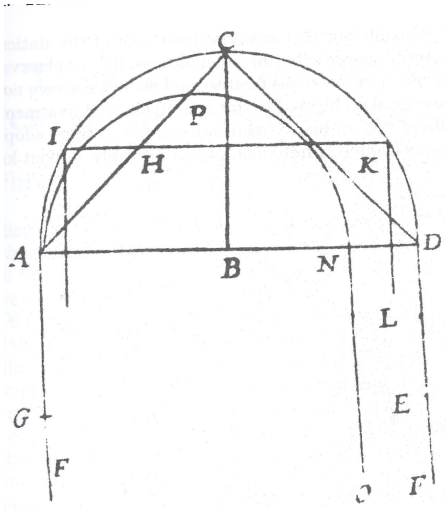

Figure 107 *Fabri's drawing for his discussion on the thrust of an arch and the introduction of chains (Benvenuto, 1991).*

In **Figure 108** we follow Fabri's procedure for tracing the arch and interpret his rule in terms of a "thrust line" reduced to two straight lines lying entirely inside the masonry envelope. The actual force domain D_F^* depicted in **(Fig. 108)** shows the admissible positions for the pole O_F^*, and in particular the ones corresponding to the actual minimum and maximum thrust lines which are depicted in **Figure 108**. This figure also depictes the "force domain" that would correspond to Fabri's (incorrect) theory.

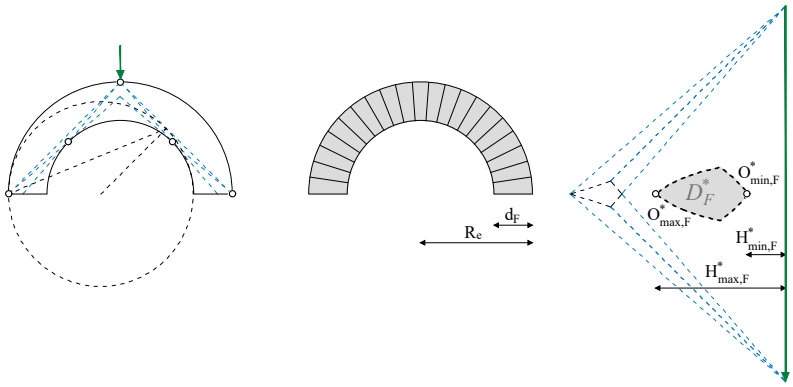

Figure 108 *Construction of the minimum thickness arch (center) according to Fabri's rule (left); force domain for the pole according to thrust line theory (right).*

Bélidor's arch. A third arch's thickness is deduced from Bélidor's four voussoirs theory, in which the internal resulting forces applied on the voussoirs are determined in terms of direction (perpendicular to the joints) and position (middle point of the 45 degrees cross sections):

$$d_B = 0.261 R_e \tag{94}$$

Figure 109 depicts the corresponding geometrical construction and the resulting arch geometry. The pole O_B^* of the funicular polygon corresponds to Bélidor's analysis for an arch subdivided into four-voussoirs. It lies within the force domain generated from the 21-voussoirs subdivision adopted.

Table 3 summarises the values obtained for minimum thickness ratios d_i/R_e as well as the maximum and minimum thrusts $H^*_{max,i}$ and $H^*_{min,i}$ for the 21-voussoirs arch geometries. It can be observed that the thicker the arch is, the larger the force diagram becomes. Safety indicators $\lambda^*_{H,i}$ have then been calculated as in Equation 90, using the results obtained via the proposed domain approach. These values are then compared to the geometrical safety factor as intended by Heyman (1995), obtained by dividing each arch's thickness d_i by the minimum thickness d_M as given by

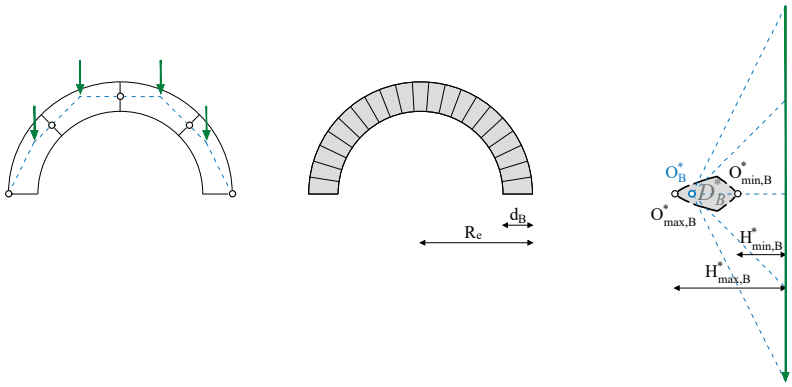

Figure 109 *Interpretation of Bélidor's four voussoirs arch theory (left) and construction of the corresponding minimum thickness arch (center); force domain for Bélidor's arch according to thrust line theory (right).*

Milankovitch (1907). Both these values are given in the last two columns of **Table 3**. It can be observed that both values are very close to each other, since only slight differences (less than 3%) can be noted. This means that, although it is computed using a discrete analysis, the proposed approach based on force domains provides a very good estimation of the structural safety of masonry arches. Moreover, the approach gives in each case a safe estimation of structural safety, as the values obtained for $\lambda^*_{H,i}$ are always smaller or equal to those of $d_M d_i$.

Authors	d_i/R_e	$Ad_{om,i}$	$H_{max,i}$	$H_{min,i}$	λ^*_H	d_i/d_M
Da Vinci	0,293	113.45	29.39	10.82	2.72	2.87
Fabri	0,343	498.17	53.81	16.04	3.36	3.36
Bélidor	0,261	38.99	19.48	8.42	2.31	2.55
Milankovitch	0,102	0	1.26	1.26	1	1

Table 3 *Results of the comparative analysis.*

6.4.2 Stability related to the abutments

For a masonry arch to be able to stand, forces generated by its self-weight (or by other applied loads) need to be balanced by thrust forces at its abutments. H^*_{min}, the horizontal distance in the force diagram between the rightmost point of the domain and the force polygon describing the external forces' equilibrium, corresponds to the minimum horizontal force at the arch's supports necessary to find a thrust line lying entirely inside the masonry envelope. In order to evaluate the arch's stability, H^*_{min} can be compared with the maximum thrust H^*_{ab} that the abutments are able to support. A second safety indicator can be consequently defined as:

$$\lambda^*_{ab} = \frac{H^*_{ab}}{H^*_{min}} \tag{95}$$

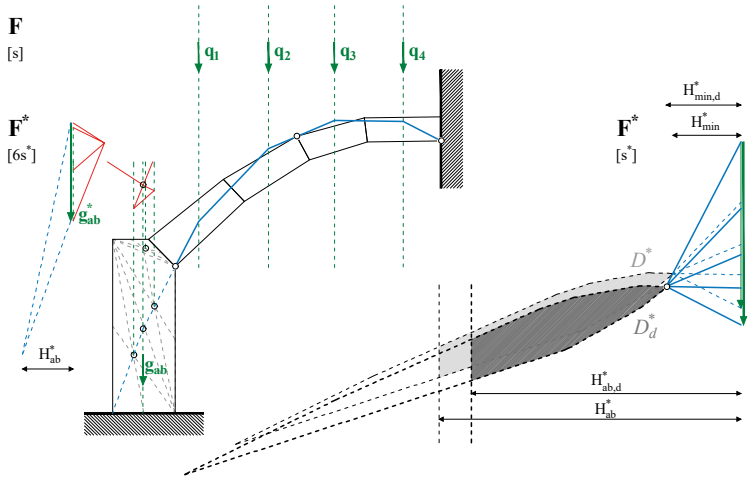

Figure 110 *Reduction of the domain when taking into account the equilibrium conditions of the abutments: characteristic (D^*) and design (D^*_d) reduced force domains.*

Figure 110 depicts an analysis done on a simplified case study. As recommended in the Eurocodes (EN90, 1990) for equilibrium verification, the partial safety factor for the active dead loads γ_{dst} is taken equal to 1.1 and the one for the resisting dead loads γ_{stb} to 0.9, so that:

$$H^*_{min,d} = \gamma_{dst} \cdot H^*_{min} = 1.1 \cdot H^*_{min} \qquad H^*_{ab,d} = \gamma_{stb} \cdot H^*_{ab} = 0.9 \cdot H^*_{ab} \tag{96}$$

6.5 Current work and perspectives

In order to refine the methodology proposed for evaluating the safety of masonry arches, we proposed in Deschuyteneer et al. (2018b) an analysis of a semi-circular planar masonry arch. The structure is subjected to a load case composed of its self-weight as well as a vertical point load **q** applied at the arch crown. Aurélie Deschuyteneer has developed a model under Rhinoceros and its parametrical algorithm editor Grasshopper that generates the corresponding force domains. In this model, the different parameters (arch dimensions and weight, voussoirs geometry, applied forces, material strength) are controlled by sliders. These parameters can thus be easily modified, the impact of their manipulation being directly visible on the size and shape of the force domain.

The main results obtained by this analysis are listed below.

- The influence of the point load at the arch's crown on the structural safety is analysed by drawing the admissible geometrical domains corresponding to different values of the applied load. It can be observed that increasing the magnitude of load leads to a decreasing area of the domain as well as to an increasing distance between the domain and the applied forces.

- Studying the influence of stereotomy, it is shown that the shape of the voussoirs has nothing but a very small influence on the maximum point load. This result is in adequacy with the conclusions of Makris and Alexakis (2013): the radial pattern for joints is not conservative nor safe, as it leads to a larger ultimate value for force the point load q. This conclusion is valid only assuming the no-sliding hypothesis and must consequently be considered with prudence.

Geometric indicators of robustness. Among the fundamental requirements recommended in the design codes, it is mentioned that a structure must be robust, which means this structure has to *"withstand events like fire, explosions, impact or consequences of human error, without being damaged to an extent disproportionate to the original cause"* (EN91, 1991). In practice, there are several types of numerical approaches aiming to assess the level of robustness of existing structures (Starossek and

Haberland, 2011). Deschuyteneer et al. (2018b) propose to use the area $A^{*(D)}$ of the admissible geometrical domain as a graphic indicator of structural robustness. As already suggested in Zastavni et al. (2016), the force domain can indeed be representative of the arch's ability for plastic stress redistribution, since it contains the set of poles related to statically admissible thrust lines lying inside the masonry envelope. In case of local failure, a larger remaining domain area $A^{*(D)}_{dam}$ damaged will then indicate a larger structural capacity for finding new equilibrium's between the applied forces and the internal thrusts.

This ongoing research on admissible force domains is very promising, not only for the limit analysis of existing structures, or the evaluation of the level of robustness, but also in terms of structural design. As already mentioned in the previous chapters, integration of force domains within design-oriented graphical environments can lead to a better informed early stage structural design as well as to a better integration of analysis and robustness considerations in the design process.

Conclusions

Purpose of the thesis. Within the theoretical framework of plasticity, the fundamental objective of this thesis is to investigate the consequences of static indeterminacy on graphic statics reciprocal diagrams. We take advantage of the lower-bound theorem of plasticity for achieving static limit state analyses on various structural types. The thesis puts forward theoretical knowledge and proposes methodologies for implementing geometrical operations on force diagrams that can be useful for limit analysis of existing structures as well as for design purposes.

Graphic statics having proven being an outstanding tool for early structural design, especially when combined with strut-and-tie modelling, we assume that the knowledge of the limit states of equilibrium of strut-and-tie networks can improve the quality of the design process. This is particularly the case if the results of the limit analysis are available within the same graphical environment used for design. Since interactive design tools have recently been developed, which propose to visualise, control and manipulate stress distributions by means of parametric form and force diagrams, we expect that the methodology proposed in the thesis can be integrated in this environment.

Summary of the results. In the first chapter we presented the founding principles of the Theory of Plasticity and the assumptions made on the ductile behaviour of the structural material. The available methods for applying this theory to limit state analysis or design of structures are exposed, especially the ones based on the lower-bound theorem. Then, we emphasised the advantages of modelling the structural behaviour with strut-and-tie networks, especially when combined with graphic statics reciprocal diagrams. They allow to manage strut-and-tie networks static equilibrium in a clear and visual way. A review of the recently developed design tools was proposed as closing section of chapter 2. The next chapter consists in a proposal to manipulate statically indeterminate structures by means of graphic statics reciprocal diagrams. Considering the force diagram as a combination of independent stress states, the graphical approach proposed allows to manipulate the structural behaviour of 2D statically indeterminate networks. In particular, the geometrical freedom of the force diagram is used to develop a methodology for the graphical limit state analysis of strut-and-tie networks, as well as to propose several approaches for plastic design. Manipulating force diagrams allows the modification of stress distribution in order to obtain force diagrams

corresponding to statically admissible limit states. Taking advantage of the lower-bound theorem of plasticity, the comparison of these limit states allows for the identification of the collapse one and of the ultimate load bearing capacity of the structure. The methodology was adapted in a direct way to pin-jointed trusses for which the geometrical and mechanical characteristics are known. The methodology was also applicable to the analysis of statically indeterminate beams subjected to bending thanks to funicular polygons. The position of the pole of these polygons within an admissible geometrical domain characterises the stress distribution: the vertices of this domain polygonal boundary correspond to statically admissible limit states, among which we can recognise the collapse one. Using similar constructions for compression funicular polygons only, the methodology is extended to the study of the load bearing capacity of masonry arches.

Further directions of research. We believe that pursuing research in the field of structural design methodologies and tools is of major importance in the today's context of lack of natural resources and necessary ecological transformations of the building processes. The important role that structural engineers play in sustainability has been emphasised by numerous authors. De Wolf et al. (2015), for instance, analysed the major ecological impact of building structures in terms of embodied carbon dioxide, which is associated with materials extraction, manufacturing, transportation, construction, maintenance and demolition. In that context, avoiding material waste and producing the least structural material are two major concerns. We conclude this thesis with two directions for further research that we estimate to be worth of interest in this context.

The first one is related to the development of efficient, interactive structural design tools that provide understandable results. In Section 2.3, we emphasised the essential role played by these tools in the structural designer's creativity and intuition, especially when managed thanks to graphic statics reciprocal diagrams. *Combinatorial Equilibrium Modelling* is one of them. Recently developed in three dimensions by Ohlbrock et al. (2018), it offers the designer the opportunity to control the range of possible equilibrium by constraining the nodes of both form and force diagrams, as already suggested by Fivet and Zastavni (2013). One of the challenges is to develop semi-automatic optimisation procedures that can support the designer's decision-making process. In this sense, it is crucial

to inform the user of the consequences of this choices in terms of structural response. Integrating information about the limit states by means of geometrical admissible domains (volumes in 3D) would help the work in this direction.

The second one relies on the use of admissible geometrical domains in evaluating the structural safety of existing structures or in managing their robustness. Static indeterminacy is not *in se* a guarantee for structural safety (Biondini et al., 2008); neither the degree of redundancy is a good indicator for robustness (De Biagi, 2016). Though, the ability of structures to find alternative load path in case of damages increase their reliability. Ongoing research on the use of admissible geometrical domains for characterising the robustness (Zastavni et al., 2015; Deschuyteneer et al., 2015) attempts to better describe and measure the structural properties relatives to this important requirement.

We are convinced that the graphical methodologies proposed within this thesis can contribute in some way in enhancing the understanding of structures. Taking advantage of the visual expressiveness of graphic statics would probably facilitate the dialogue between the different building protagonists. We will wager that it can help structural engineers in achieving their essential mission: acting on expected tangible reality in all conscience by transforming it into intelligible models.

List of Figures

1 Stress-strain curves for elastic-plastic and rigid-plastic materials 28
2 Kinematic (left) versus geometric (right) views of statics. 35
3 Kinematic vs geometric views of statics in relation to the theorems of plasticity. 36
4 Kinematic limit state analysis of a statically indeterminate pin-jointed truss. 37
5 Kinematic limit state analysis of a statically indeterminate beam. 39
6 One possible collapse mechanism for a masonry arch. . . . 40
7 Geometric view of statics: two admissible stress states within a semi-circular masonry arch. 41
8 Complete limit analysis of a statically indeterminate beam. 42
9 Structural design process. 44
10 Influence of the stiffening on the load bearing capacity. . . 45
11 Strut-and-tie network 50
12 Graphical equilibrium of a point. 52
13 Static equilibrium of a rope: funicular polygon and force polygon after Varignon (1725, Tome I, p. 210) 53
14 Polygon of forces and correlated polygonal frame in equilibrium from Rankine (1858, fig. 75 & 75*, p. 139) 55
15 Reciprocal diagrams inspired from Maxwell (1864a) 56
16 Graphical procedure for determining the stresses in a statically indeterminate truss by Lander and Cotton. 58
17 Graphical procedure for constructing the bending moment diagram and the elastic curve by double integration.(Mohr, 1868, Table XIV, fig.19-22, p.397) 59
18 Graphical procedure for constructing the bending moment diagram and the elastic curve of a statically indeterminate rigid frame. (Wolfe, 1921, p.351) 61
19 Comparison between statically determinate and corresponding continuous beam on three supports. 68
20 Stress fields within reinforced concrete beams. 69
21 Combination of stress-states and self-stress states. 71
22 Reciprocal diagrams $\mathbf{F_q} - \mathbf{F_q^*}$ representing the stress state within a reinforced concrete beam. 72
23 Self-stress state generated by pre-tensioning within a reinforced concrete beam. 73

24 Self-stress state in equilibrium with the pre-tensioning. . . 73
25 Combination of a stress state due to the applied loads and a self-stress state at two different scales. 74
26 Reciprocal diagrams $\mathbf{F} - \mathbf{F}^*$. 75
27 Kinematic mechanism within $\mathbf{F}^*$. 76
28 Two independent offsets of $\mathbf{F}^*$. 77
29 One only possible offset for $\mathbf{F}$. 78
30 Network with two independent self-stress states. 79
31 Network with three independent self-stress states. 79
32 Combination of one stress states and one self-stress state within a strut-and-tie network 82
33 Construction of the global force diagram $\mathbf{F}^*$, by combining the force diagram of the external forces $\mathbf{F}^*_{\mathbf{q}}$ with the one of the self-stress state $\mathbf{F}^*_{\mathbf{1}}$ for two different scale factors. . . . 83
34 Construction of the global force diagram $\mathbf{F}^*$ by linear combining the force diagrams of two independent stress states $\mathbf{F}^*_{\mathbf{q}}$ and $\mathbf{F}^*_{\mathbf{1}}$. 84
35 Four limit force diagrams $\mathbf{F}^*_{\mathbf{s,1\to 4}}$ corresponding to four different values for the load factor $\lambda^*_{s,1\to 4}$ 85
36 Prevention of yielding by modifying $\mathbf{F}^*_{\mathbf{0}}$ into $\mathbf{F}^*_{(\mathbf{a})}$ with two symmetric self-stress states. 88
37 Optimization of the stress distribution in the concrete rods by modifying the magnitude of the self-stress states. . . . 88
38 Increase of the load bearing capacity of the structure by increasing the magnitude of the self-stress states. 89
39 Graphical limit state analysis of a statically indeterminate pin-jointed truss. 94
40 Kinematically compatible mechanisms for the pin-jointed truss of **Figure 39**. 97
41 Pin-jointed truss with three independent stress states. The three pairs of form and force diagrams are respectively due to the external load $\mathbf{q}$ ($\mathbf{F_q} - \mathbf{F^*_q}$), to an excess reaction force ($\mathbf{F_{e1}} - \mathbf{F^*_{e1}}$) and to an internal indeterminacy ($\mathbf{F_2} - \mathbf{F^*_2}$) . 99
42 Full graphic static limit state analysis of the network, with six limit force diagrams $\mathbf{F^*_{s,1\to 6}}$. Diagrams $\mathbf{F^*_{s,5}}$ and $\mathbf{F^*_{s,6}}$ are two possible collapse diagrams since they both present the highest length for the applied load vector $\mathbf{q}^*$. 100
43 Kinematic analysis on the collapse mechanism. 101
44 Six-steps procedure for determining the load factor of a pin-jointed network under given loading $\mathbf{q}$. 106

45 Graphical limit state analysis of a truss with one degree of internal static indeterminacy. 108
46 Graphical limit state analysis of a truss with two degrees of external static indeterminacy. 109
47 Application of the graphical procedure for the limit state analysis of a network with two degrees of internal static indeterminacy. 112
48 Application of the graphical procedure for the limit state analysis of a network with three degrees of internal static indeterminacy. 113
49 Graphic limit state analysis of trussed beam with three different support conditions. 114
50 Statically admissible domain D_P^* of point P^*. 116
51 Two external forces q_0^* and q_1^* and their resultant q_R^* in $\mathbf{F}^*$ have action lines q_0, q_1 and q_R respectively in $\mathbf{F}$. The moment of q_0 and q_1 - or equivalently of q_R with respect to G in given by $M = \mathrm{q}_\mathrm{R}^* \cdot s^* \cdot \nu \cdot s$, with s^* and s the scales of $\mathbf{F}^*$ and $\mathbf{F}$ respectively. 122
52 Various projections of $\mathbf{d_G}$ and $\mathbf{q_R^*}$ leading to the same value of the moment of q_R with respect to G. 123
53 Two fictive forces $\mathbf{f}^*$ and $\mathbf{f_1^*}$ in equilibrium with $\mathbf{q_R^*}$. The moment of $\mathbf{q_R}$ with respect to G in given by $M = H^{*(R)}s^* \cdot \mu^{(R)}s$, with s^* and s the scales of $\mathbf{F}^*$ and $\mathbf{F}$ respectively. . 123
54 The funicular polygon F in $\mathbf{F}$ is in rotational equilibrium with a system of six external forces $\{\mathbf{q_{0\to 5}}\}$ in equilibrium. In $\mathbf{F}^*$, the tensile (red) and compressive (blue) funicular rays meeting in pole O^* are in translational equilibrium with the system of external forces $\{\mathbf{q_{0\to 5}}\}$. 124
55 Two funicular polygons in equilibrium with four external forces. 125
56 Graphical determination of the bending moment acting in sections G^A and G^B: $M^A = \mu^{(A)}s \cdot H^{*(A)}s^*$; $M^B = \mu^{(B)}s \cdot H^{*(B)}s^*$. 125
57 Graphical construction of the bending moment for a clamped beam. 126
58 Form domain D of a beam with variable rectangular cross section, delimited by the form boundary B^D. An admissible force polygon F and a limit force polygon $\mathrm{F_s}$. 128

59 In **F**: an admissible polygon F and a limit polygon F_s for the simply supported beam AB. Their corresponding force diagram F^* and F_s^* respectively, for a fixed value of H_u^* . 130
60 Three possible limit polygons $F_{s,1\to3}$ and their corresponding force polygons $\mathbf{F^*_{s,1\to3}}$ for the statically indeterminate beam AB. F_0 is not an admissible polygon since it does not respect the yield condition; $\mathbf{F_0^*}$ is consequently not a statically admissible distribution. 131
61 In **F**: three limit polygons $F_{s,1\to3}$ for the statically indeterminate beam AB. In $\mathbf{F}^*$: three limit poles $O^*_{s,1\to3}$ corresponding to the limit polygons. For fixed external forces, each of them is characterised by the horizontal distance $H^*_{s,1\to3}$. 134
62 Three funicular polygons $F_{1\to3}$ meeting in points v_1 and v_2 are related respectively to poles $O^*{}_1 \to 3$ lying on a straight line l_1^* in $\mathbf{F}^*$ parallel to the one l_1 joining v_1 and v_2 in **F**. 136
63 $l_{1\to3}$ close F in **F** so that $l^*_{1\to3}$ meet at O^* $\mathbf{F}^*$. 137
64 Limit polygon $\mathbf{F_s}$ with three closing lines and admissible positions for O^* along the three lines of poles. 137
65 Limit analysis of a statically determinate beam. 139
66 *Constructing* D^* - One tensile admissible polygon F (red) for a statically indeterminate beam AB and its corresponding pole O^* in $\mathbf{F}^*$. The location of v_B in **F** is fixed to respect the support condition. 140
67 *Constructing* D^* - In **F**: admissible directions for $\mathbf{f_3}$ in order to keep v_2 within D; In $\mathbf{F}^*$ corresponding force domain D^* for the pole O^* 141
68 *Constructing* D^* - Three funicular polygons passing by both points v_2 and v_B: an admissible polygon F (red continuous lines), a limit polygon F_s (red bold lines) and a funicular polygon that does not respect the yield conditions (red dashed lines). The respective locations for the pole corresponding to these three polygons along the line of poles l_1^* are indicated in $\mathbf{F}^*$. 142
69 *Constructing* D^* - Three funicular polygons sharing the same closing line: a limit polygon $F_{s,1}$; an admissible polygon F; a non-admissible funicular polygon 144
70 *Constructing* D^* - In **F**: admissible directions for l_2 in order to keep v_1 within D; in $\mathbf{F}^*$: corresponding force domain D^* for the pole O^*. 145

71 *Constructing* D^* - In $\mathbf{F}$: three funicular polygons passing by both points v_2 and v_B: an admissible polygon F (red continuous lines), a limit polygon $\mathrm{F_{s,2}}$ (red bold lines) and a funicular polygon that does not respect the yield conditions (red dashed lines). The respective locations for the pole corresponding to these three polygons along the line of poles l_2^* are indicated in $\mathbf{F}^*$. 146
72 *Constructing* D^* - In $\mathbf{F}$: three tensile funicular polygons sharing the same fixed positions for the vertices v_A and v_B: an admissible polygon $\mathrm{F_t}$ (red continuous lines), the limit polygon $\mathrm{F_{s,2}}$ (red bold lines) and a funicular polygon that does not respect the yield conditions (red dashed lines). The respective locations for their respective poles in $\mathbf{F}^*$ are lying on the line of poles l_3^* parallel to the closing line l_3 in $\mathbf{F}$. 147
73 *Constructing* D^* - Two limit polygons $\mathrm{F_{s,1}}$ and $\mathrm{F_{s,4}}$ sharing the same closing line l_1. Their corresponding limit poles $O_{s,1}$ and $O_{s,4}$ consequently lie on the lines of pole l_1^* parallel to l_1. 148
74 *Constructing* D^* - In $\mathbf{F}$: last tensile limit polygon $\mathrm{F_{s,4}}$ (red bold lines) and last closing line l_4. In $\mathbf{F}^*$: last segment l_4^* closing the force domain D^*. Any pole O^* lying inside D^* corresponds to an admissible polygon F; any pole outside D^* to a non admissible polygon (red dashed lines). 149
75 *Constructing* D^* - Tensile (red bold) and compressive (blue bold) limit polygons $\mathrm{F_{s,4}}$ and $\mathrm{F_{s,5}}$ with shared closing line l_4, and tensile (red) and compressive (blue) admissible polygons for the same closing line. The corresponding poles are drawn along l_4^* in $\mathbf{F}^*$. 150
76 *Constructing* D^* - Two compressive limit polygons $\mathrm{F_{s,5}}$ and $\mathrm{F_{s,6}}$ sharing the same closing line l_5 and their corresponding limit poles $O_{s,5}^*$ and $O_{s,6}^*$ in $\mathbf{F}^*$. 151
77 *Constructing* D^* - The last closing line l_6 of the compressive limit polygon $\mathrm{F_{s,6}}$ and its corresponding line of poles l_6^* in closing the compressive force domain D^* in $\mathbf{F}^*$. 152
78 Form $\mathbf{F}$ and force $\mathbf{F}^*$ diagrams at limit state for the simply supported beam AB. The limit pole O_s lies on line of poles l^* 155
79 Unique admissible mechanism for the simply supported beam AB 155

80 Two admissible pairs of form and force diagrams. Above: tensile admissible polygon $\mathrm{F_t}$ in **F** and its related force diagram $\mathrm{F_t^*}$ for H_u^* fixed arbitrarily; below: compressive admissible polygon $\mathrm{F_c}$ in **F** and its force diagram $\mathrm{F_c^*}$ for the same value of H_u^*. 156
81 Four limit polygons defined by their four closing lines $l_{1\to4}$, and their corresponding limit poles on the boundary of the force domain defined by the lines of poles $l_{1\to4}^*$. 157
82 Collapse mechanism corresponding to the static limit state represented by $\mathrm{F_{s,1}}$ and $O_{s,1}^*$ in **Figure 81**. 158
83 Four tensile limit polygons defined by the four closing lines $l_{1\to4}$, and their corresponding limit poles on the boundary of the force domain D^* defined by the lines of poles $l_{1\to4}^*$. The collapse limit state is represented by $\mathrm{F_{s,3}}$ in **F** and $O_{s,3}^*$ in $\mathbf{F}^*$ 159
84 Collapse mechanism corresponding to the collapse funicular polygon $\mathrm{F_{s,3}}$ in **Figure 83** 160
85 Tensile collapse limit polygon $\mathrm{F_{s,u}}$ (red bold lines) which pole $O_{s,u}^*$ is the meeting point of three lines of poles l_0^*, l_3^* and l_4^*. An admissible polygon $\mathrm{F_3}$ (red lines) which pole O_3^* lies on l_3^* within D^* and a non-admissible polygon (red dashed lines) which pole lies on l_4^* outside of D^*. The admissible polygon $\mathrm{F_{s,0}}$ is a limit polygon with no limit pole since its closing line l_0 may be translated to $l_{0'}$ and hence, correspond to many admissible polygons; $\mathrm{F_0}$ is one of them in compression (blue lines). 161
86 Collapse mechanism for the beam AB corresponding to the collapse limit polygon $\mathrm{F_{s,u}}$ in **Figure 85**. 162
87 Leonardo Da Vinci's arrangements for measuring the horizontal thrust in arches. *Benvenuto (1991)* 166
88 Bernardino Baldi's three-hinge arch collapse mechanism. *(Kurrer, 2008)* 167
89 Bélidor's collapse theory for masonry arches. 167
90 *Couplet (1731)* theory for masonry arches' collapse. 168

91 The drawing presented by Moseley (1843) with a clear distinction between line of resistance (thrust line) and line of pressure (funicular polygon) (left) and its interpretation by Alexakis and Makris (2014) (right) where the successive thrust forces are consistent with the corresponding weights of the successive stone blocks. (*From Alexakis and Makris (2014)*) 169
92 Durand-Claye's eight collapse modes for a symmetric arch (Foce and Aita, 2003). 170
93 Chaix (1890) methodology for *dimensioning* safe masonry bridges. 171
94 A four voussoirs arch with infinite compressive strength, no tensile strength and high friction in the joints. 176
95 In **F**: two limit polygons, $\mathrm{F_{s,1}}$ with closing lines l_0 and l_1, and $\mathrm{F_{s,2}}$ with closing lines l_1 and l_2. In $\mathbf{F}^*$, their poles O_1^* and O_2^*, where lines of poles l_0^*, l_1^* and l_2^* intersect. The black dashed bold lines are a first segment of the force boundary B^{D*}. 177
96 Construction of the force domain D^* in $\mathbf{F}^*$ of a masonry arch, where poles O_3^*, O_4^*, O_5^* and O_6^* correspond to limit funicular polygons. 178
97 In **F**: two limit polygons, $\mathrm{F_{s,7}}$ with closing lines l_6 and l_7, and $\mathrm{F_{s,8}}$ with closing lines l_7 and l_8. In $\mathbf{F}^*$, their poles O_7^* and O_8^*, where lines of poles l_6^*, l_7^* and l_8^* intersect. The force boundary B^{D*} is now completed and does not close on the left-hand side. 179
98 Force domain D^* of an arch composed of four voussoirs, with a thickness reduced to half. 180
99 In **F**: limit funicular polygons corresponding to the maximum and minimum thrusts; in $\mathbf{F}^*$: magnitudes of the maximum and minimum thrusts related to the position of the pole O^*. 180
100 In **F**: two limit polygons $\mathrm{F_{s,1}}$ and $\mathrm{F_{s,6}}$; in $\mathbf{F}^*$: magnitudes of the corresponding thrusts and position of the limit poles $O_{s,1}^*$ and $O_{s,6}^*$. 181
101 Different funicular polygons corresponding to the same horizontal thrust $H_{s,3}^*$. 182
102 Reduction of the force domain correlated to a reduction of the arch thickness to a ratio 0.8 the original thickness. . . 182

103 Minimum thickness arch, for which the force domain reduces to a point. 183
104 Safety indicator relative to arch's stability of this arch under self-weight. 188
105 Milankovich's arch with minimum thickness. 189
106 Interpretation of Vinci's two rigid bars arch theory (left); minimum thickness arch suggested by Vinci (center); corresponding force domain for the pole according to thrust line theory (right). 189
107 Fabri's drawing for his discussion on the thrust of an arch and the introduction of chains (Benvenuto, 1991). 190
108 Construction of the minimum thickness arch (center) according to Fabri's rule (left); force domain for the pole according to thrust line theory (right). 191
109 Interpretation of Bélidor's four voussoirs arch theory (left) and construction of the corresponding minimum thickness arch (center); force domain for Bélidor's arch according to thrust line theory (right). 192
110 Reduction of the domain when taking into account the equilibrium conditions of the abutments: characteristic (D^*) and design (D_d^*) reduced force domains. 193

References

Addis, W. (1994). *The art of the structural engineer*. Artemis, London.

Alexakis, H. and Makris, N. (2014). Limit equilibrium analysis of masonry arches. *Archive of Applied Mechanics*, 85(9):1363–1381.

Allen, E. and Zalewski, W. (2009). *Form and Forces: Designing Efficient, Expressive Structures*. Wiley and Sons.

Baker, J. F., Horne, M. R., and Heyman, J. (1956). *The Steel Skeleton, vol. 2: Plastic Behavior and Design*. Cambridge University Press, New York.

Baker, W. F., Beghini, A., and Mazurek, A. (2012). Applications of structural optimization in architectural design. *Proceedings of the ASCE structures congress*.

Baker, W. F., Beghini, L., Mazurek, A., Carrion, J., and Beghini, A. (2013). Maxwell's reciprocal diagrams and discrete michell frames. *Structural Multidisciplinary Optimization*, 48:267–277.

Baldi, B. (1621). *In mechanica Aristotelis problemata exercitationes. Adiecta succinta narration de autoris vita et scriptis*. Viduae Ioannis Albini, Moguntiae.

Bandhauer, C. (1831). *Bogenlinie des Gleichgewichts oder der Gewölbe und Kettenlilien*. Hartmann'sche Buchhandlung, Leipzig.

Bauschinger, J. (1871). *Elemente der Graphischen Statik*. R. Oldenbourg, München.

Beghini, L. L., Carrion, J., Beghini, A., Mazurek, A., and Baker, W. F. (2013). Structural optimization using graphic statics. *Structural Multidisciplinary Optimization*, 49:351–366.

Belidor, B. F. (1729). *La science des ingénieurs dans la conduite des travaux de fortification et d'architecture civile. Nouvelle édition avec des notes par M. Navier*. F. Didot, Paris.

Benvenuto, E. (1985). The parallelogram of forces. *Meccanica*, 20:99–109.

Benvenuto, E. (1991). *An introduction to the History of Structural Mechanics. Part II: Vaulted structures and Elastic Systems*. Springer, New York.

Bill, M. (1949). *Robert Maillart.* Architektur, Zürich.

Billington, D. P. (1997). *Robert Maillart, Builder, Designer, and Artist.* Cambridge University Press.

Biondini, F., Frangopol, D. M., and Restelli, S. (2008). On structural robustness, redundancy and static indeterminacy. *Proceedings of the ASCE symposium: Crossing Borders.*

Block, P. (2009). *Thrust Network Analysis: Exploring Three-Dimensional Equilibrium.* PhD thesis, Massachusetts Institute of Technology.

Block, P., Ciblac, T., and Ochsendorf, J. (2006). Real-time limit analysis of vaulted masonry buildings. *Computers and Structures*, 84:1841–1852.

Block, P. and Ochsendorf, J. (2007). Thrust network analysis: a new methodology for three-dimensional equilibrium. *Journal of the International Association for Shell and Spatial Structures*, 48(3):155.

Boothby, T. E. (2001). Analysis of masonry arches and vaults. *Progress in Structural Engineering and Materials*, 56:53–60.

Boulic, L. and Schwartz, J. (2018). Design strategies of hybrid bending-active systems based on graphic statics and a constrained force density method. *Proceedings of the IASS Symposium 2018 - Creativity in Structural Design.*

Bow, R. (1873). *Economics of Construction in Relation to Framed Structures.* ICE Publishing, London.

Bryan, J. and Sauer, R. (1973). *Structures implicit and explicit.* Falcon Press, Philadelphia.

Calladine, C. R. (1978). Buckminster fuller's tensegrity structures and clerk maxwell's rules for the construction of stiff frames. *International Journal of Solids and Structures*, 14:161–172.

Castigliano, A. (1873). *Intorno ai systemi elastici.* PhD thesis, Università di Torino.

Chaix, J. (1890). *Traité des ponts. Première partie : ponts en maçonnerie et tunnels (Tome II).* Fanchon et Artus, Paris.

Charlton, T. (2002). *A History of the Theory of Structures in the Nineteenth Century*. Cambridge University Press.

Couplet, P. (1731). De la poussée des voûtes. *Histoire de l'Académie royale des sciences*, pages 79–117.

Cremona, L. (1872). *Le figure reciproche nella statica grafica*. Giuseppe Bernardoni, Milan.

Culmann, K. (1866). *Die Graphische Statik*. Von Meyer u. Zeller, Zürich.

Culmann, K. (1875). *Die Graphische Statik*. Von Meyer u. Zeller, 2nd ed., Zürich.

Culmann, K. (1880). *Traité de statique graphique*. Dunod, Paris.

D'Acunto, P., Jasienski, J.-P., Ohlbrock, P. O., and Fivet, C. (2017). Vector-based 3d graphic statics: Transformations of force diagrams. *Proceedings of the IASS Annual Symposium 2017 - Interfaces: architecture.engineering.science*.

D'Acunto, P., Ohlbrock, P. O., Jasienski, J.-P., and Fivet, C. (2016). Vector-based 3d graphic statics (part i): Evaluation of global equilibrium. *Proceedings of the IASS Annual Symposium 2016*.

de Arteaga, I. and Morer, P. (2012). The effect of geometry on the structural capacity of masonry arch bridges. *Construction and Building Materials*, 34:97–106.

De Biagi, V. (2016). Structural behavior of a metallic truss under progressive damage. *International Journal of Solids and Structures*, 82:56–64.

de la Hire, P. (1729). *Traité de mécanique*. Compagnie des libraires, Paris.

De Wolf, C., Ochsendorf, J., Cox, D., Hattan, A., Yang, F., and Charlson, A. (2015). Survey of material quantities and embodied carbon in existing building structures. *ICE Journal of Engineering Sustainability*.

Deschuyteneer, A., Rondeaux, J.-F., Pierluigi, D., and Zastavni, D. (2018a). Application of graphic statics and parametric force diagrams for the design of reinforced concrete structures. *Proceedings of the IASS Symposium 2018 - Creativity in Structural Design*.

Deschuyteneer, A., Rondeaux, J.-F., and Zastavni, D. (2018b). Structural assessment of masonry arches using admissible geometrical domains. *Proceedings of the SAHC Annual Symposium 2018*.

Deschuyteneer, A. and Zastavni, D. (2017). Structural robustness at conceptual stage. *Proceedings of the IABSE Workshop: Ignorance, uncertainty and human errors in structural engineering*.

Deschuyteneer, A., Zastavni, D., and Fivet, C. (2015). A geometrical approach to evaluating constitutive elements of structural robustness. *Proceedings of the IABSE Workshop: Safety, Robustness and Condition Assessments of Structures*, 103:210–217.

Drosopoulos, G. A., Stavroulakis, G. E., and Massalas, C. V. (2008). Influence of the geometry and the abutments movement on the collapse of stone arch bridges. *Construction and Building Materials*, 22:200–210.

Du Bois, A. (1875). *The elements of graphical statics and their application to frame structures*. John Wiley and Son, New York.

Durand-Claye, A. (1867). Note sur la vérification de la stabilité des voûtes en maçonnerie et sur l'emploi des courbes de pression. *Annales des Ponts et Chaussées*, 13:63–93.

Eddy, H. T. (1877). *New constructions in graphical statics*. D. Van Nostrand, New York.

EN90 (1990). *Eurocode 0: Basis of structural design*. European Norms.

EN91 (1991). *Eurocode 1: Actions on structures, part 1-7: general actions – accidental actions*. European Norms.

Enrique, L. and Schwartz, J. (2018). Load path network method: An equilibrium-based approach for the design and analysis of structures. *Structural Engineering International*, 27(2):292–299.

Fantin, M. and Ciblac, T. (2016). Extension of thrust network analysis with joints considerations and new equilibrium states. *International Journal of Spatial Structures*, 31(2-4).

Fivet, C. (2013). *Constraint-Based Graphic Statics, a geometrical support for computer-aided structural equilibrium design*. PhD thesis, Université catholique de Louvain.

Fivet, C. and Zastavni, D. (2012). The salginatobel bridge design process by robert maillart (1929). *Journal of the International Association for Shell and Spacial structures*, 53:39–48.

Fivet, C. and Zastavni, D. (2013). Constraint-based graphic statics: New paradigms of computer-aided structural equilibrium design. *In Proceedings of the IASS Symposium 2013 "Beyond the limits of man"*.

Fivet, C. and Zastavni, D. (2015). A fully geometric approach for interactive constraint-based structural equilibrium design. *Computer-Aided Design*, 61:42–57.

Flöry, S., Schmiedhofer, H., and M., R. (1990). *Goat: http://www.rechenraum.com/en/goat/overview.html*.

Foce, F. and Aita, D. (2003). The masonry arch between "limit" and "elastic" analysis. a critical re-examination of durand-claye method. *Proceedings of the first international congress on construction History*, 2:895–908.

Foce, F. and Aita, D. (2005). On the safety of the masonry arch: different formulations from the history of structural mechanics. *Essays in the history of theory of structures*, pages 117–142.

Frey, F. (2000). *Traité de Génie Civil de l'Ecole polytechnique fédérale de Lausanne, Volume 2, Analyse des structures et milieux continus - Mécanique des structures*. Presses polytechniques et universitaires romandes, Lausanne.

Gilbert, M. (2007). Limit analysis applied to masonry arch bridges: state-of-the-art and recent developments. *Arch bridges '07*, pages 13–28.

Gilbert, M., Casapulla, C., and Ahmed, H. M. (2006). Limit analysis of masonry block structures with non-associative frictional joints using linear programming. *Computers and Structures*, 84:873–887.

Gilbert, M. and Melbourne, C. (1994). Rigid block analysis of masonry structures. *The structural engineer*, 72(21):356–361.

Greenwold, S. and Allen, E. (visited 2018). Active statics (http://acg.media.mit.edu/people/simong/statics/).

Heyman, J. (1966). The stone skeleton. *International Journal of Solids and Structures*, 2:249–279.

Heyman, J. (1995). *The Stone Skeleton: Structural engineering of masonry architecture*. Cambridge University Press.

Heyman, J. (1998). *Structural analysis: a historical approach*. Cambridge University Press.

Heyman, J. (2008). *Basic structural theory*. Cambridge University Press.

Heyman, J. (2009). La coupe des pierres. *Proceedings of the International Congress on Construction History*, pages 807–812.

Hodge, P. G. J. (1959). *Plastic analysis of structures*. McGraw-Hill Book Company, New York.

Horne, M. R. (1979). *Plastic theory of structures*. Pergamon, Oxford.

Huerta, S. (2001). Mechanics of masonry vaults: the equilibrium approach. *Historical Constructions*, pages 47–69.

Huerta, S. (2006). Galileo was wrong: The geometrical design of masonry arches. *Nexus Network Journal*, 8(2):25–52.

Huerta, S. (2012). Wedges and plate-bandes: mechanical theories after de la hire. *L'architrave le plancher la plate-forme. Nouvelle histoire de la construction*, pages 405–435.

Hurez, M., Juraszek, N., and Pelcé, M. (2009). *Dimensionner les ouvrages en maçonnerie : guide d'application*. Eyrolles, Paris.

Jasienski, J.-P., D'Acunto, P., Ohlbrock, P. O., and Fivet, C. (2016). Vector-based 3d graphic statics (part ii): Construction of force diagrams. *Proceedings of the IASS Annual Symposium 2016*.

Johnson, S. (1990). *The NLopt optimization package: http://ab-initio.mit.edu/nlopt*.

Kamenjarzh, Jacov, A. (1996). *Limit Analysis of Solids and Structures*. CRC Press, Boca Raton.

Konstantatou, M., D'Acunto, P., and McRobie, A. (2018). Polarities in structural analysis and design: n-dimensional graphic statics and structural transformations. *International Journal of Solids and Structures*, 000:1–22.

Kurrer, K.-E. (2008). *The history of the theory of structures*. Ernst Sohn, Berlin.

Lander, Cecil, H. and Cotton, R. (1914). An application of the graphical method of deflections to statically indeterminate frames. 197:298–314.

Latteur, P. (2016). *Calculer une structure. De la théorie à l'exemple*. Academia, Ottignies-Louvain-la-Neuve.

Livesley, J. R. (1978). Limit analysis of structures formed from rigid blocks. *International Journal for Numerical Methods in Engineering*, 12:1853–1871.

Lourenço, P. B., Oliveira, D. V., Roca, P., and Orduña, A. (2005). Dry joint strone masonry walls subjected to in-plane combined loading. *Journal of Structural Engineering*, 131(11):1665–1673.

Lévy, M. (1874a). *La statique graphique et ses applications aux constructions*. Gauthier-Villars, Paris.

Lévy, M. (1886 (1874)b). *La statique graphique et ses applications aux constructions*. Gauthier-Villars, Paris.

Makris, N. and Alexakis, H. (2013). The effect of stereotomy on the shape of the thrust-line and the minimum thickness of semicircular masonry arches. *Archive of Applied mechanics*, 83:1511–1533.

Marti, P. (2013). *Theory of Structures. Fundamentals, Framed Structures, Plates and Shells*. Ernst Sohn, Berlin.

Masson, H. (1952). *Le calcul graphique à l'usages des ingénieurs*. Eyrolles, Paris.

Massonnet, C. and Save, M. (1961). *Calcul plastique des constructions - Volume 1 : ossatures planes*. Centre belgo-luxembourgeois d'information de l'acier, Bruxelles.

Mauro, A., de Felice, G., and DeJong, M. J. (2015). The relative dynamic resilience of masonry collapse mechanisms. *Engineering Structures*, 85:182–194.

Maxwell, J. C. (1864a). On reciprocal figures, frames and diagrams of forces. *Philosophical Magazine*, 27:250–261.

Maxwell, J. C. (1864b). On the calculation of equilibrium and stiffness of frames. *Philosophical Magazine*, 27:294–299.

Maxwell, J. C. (1867). On the application of the theory of reciprocal polar figures to the construction of diagrams of forces. *The Engineer*, 24.

Mazurek, A., Beghini, A., Carrion, J., and Baker, W. (2016). Minimum weight layouts of spanning structures obtained using graphic statics. *International Journal of Space Structures*, 31(2-4):112 –120.

McRobie, A., Baker, W., Mitchell, T., and Konstantatou, M. (2016). Mechanisms and states of self-stress of planar trusses using graphic statics, part ii. *International Journal of Space Structures*, 31(2-4):102–111.

Menabrea, L. F. (1875). La determinazione delle tensioni e delle pressioni nei sistemi elastici. *Atti della reale Accademia dei Lincei*, 2a(2):201–221.

Micheletti, A. (2008). On generalized reciprocal diagrams for self-stressed frameworks. *International Journal of Space Structures*, 23(3):153–166.

Milankovitch, M. (1907). Theorie der druckkurven. *Zeitschrift für Mathematik und Physik*, 55:1–27.

Mitchell, T., Baker, W., McRobie, A., and Mazurek, A. (2016). Mechanisms and states of self-stress of planar trusses using graphic statics, part i. *International Journal of Space Structures*, 31(2-4):85–101.

Mohr, C. O. (1868). *Beiträge zur Theorie der Holz- und Eisenkonstruktionen*, volume 14. Hannover.

Monge, G. (1794/95). *Géométrie descriptive*. Baudouin, Paris.

Moseley, H. (1843). *The Mechanical Principles of Engineering and Architecture*. Longman, Brown, Green & Longman, London.

Muttoni, A. (2015). *L'art des structures*. Presses polytechniques et universitaires romandes, Lausanne.

Muttoni, A., Schwartz, J., and Thürlimann, B. (1996). *Design of concrete structures with stress fields*. Birkhäuser.

Méry, E.-H.-F. (1840). Equilibre des voûtes en berceau. *Annales des ponts et chaussées*, pages 51–70.

Mörsch, E. (1929). *Der Eisenbetonbau, seine Theorie und Anwendung.* Konrad Wittwer Verlag, Stuttgard.

Müller-Breslau, H. (1887). *Die Graphische Statik der Baukonstruktionen, Band I.* Baumgärtner's Buchhandlung, Leipzig.

Navier, H. (1826). *Résumé des Leçons données à l'Ecole Royale des Ponts et Chaussées sur l'Application de la Mécanique à l'Etablissement des Constructions et des Machines. Première partie : Leçons sur la résistance des matériaux et sur l'établissement des constructions en terre, en maçonnerie et en charpente.* Firmin Didot père et fils, Paris.

Navier, H. (1833). *Résumé des leçons données à l'Ecole des Ponts et Chaussées sur l'Application de la Mécanique à l'Etablissement des Constructions et des Machines (Vol.1).* Carilian-Goeury, Paris.

Ochsendorf, J. A. (2002). *Collapse of masonry structures.* PhD thesis, University of Cambridge.

Ochsendorf, J. A. (2005). Practice before theory: The use of the lower bound theorem in structural design from 1850-1950. *Essays in the history of the theory of structures*, pages 353–366.

Ochsendorf, J. A., Hernando, J. I., and Huerta, S. (2004). Collapse of masonry buttresses. *Journal of Architectural Engineering*, 10(3):88–97.

Ohlbrock, P. O., D'Acunto, P., and Jasienski, J.-P. (2018). Hierarchical form-finding with combinatorial equilibrium modelling. *Proceedings of the IASS Annual Symposium 2018 - Creativity in Structural Design.*

Ohlbrock, P. O., D'Acunto, P., Jasienski, J.-P., and Fivet, C. (2016). Vector-based 3d graphic statics (part iii): Designing with combinatorial equilibrium modelling. *Proceedings of the IASS Annual Symposium 2016.*

Oliveira, D. V., Lourenço, P. B., and Lemos, C. (2010). Geometric issues and ultimate load capacity of masonry arch bridges from the northwest iberian peninsula. *Engineering Structures*, 32:3955–3965.

O'Dwyer, D. (1999). Funicular analysis of masonry vaults. *Computers and Structures*, 73(1-5):187–197.

Pelsser, Y., De Groof, B., Nizet, F., and Rondeaux, J.-F. (2017). Approche de la matérialité par l'analyse d'exemples - partage d'une expérience pédagogique développée dans le cadre du cours d'analyse des structures 2 à loci-bruxelles. *Lieux-dits*, pages 1–23.

Perronet, J. R. and Chezy (1810). De la poussée des voûtes. *Recueil de divers mémoires extraits de la Bibliothèque impériale des ponts et chaussées, à l'usage de MM. les ingénieurs*, pages 243–274.

Pirard, A. (1950). *La statique graphique : science introductive à l'art de construire*. Vaillant-Carmanne, Liège.

Pirard, A. (1960). *Traité d'hyperstatique analytique et graphique*. Vaillant-Carmanne, Liège.

Poncelet, J.-V. (1822). *Traité des propriétés projectives des figures*. Paris.

Poncelet, J.-V. (1852). Examen critique et historique des principales théories ou solutions concernant l'équilibre des voûtes. *Comptes-rendus de l'Académie des Sciences*, 35(17):494–502, 532–540, 577–587.

Rankine, William, J. M. (1858). *A Manual of Applied Mechanics*. C. Griffin Co., London.

Rankine, William, J. M. (1864). Principle of the equilibrium of polyhedral frames. *Philosophical Magazine*, 27(4):92.

Rinke, M. and Schwartz, J., editors (2010). *Before Steel. The introduction of structural iron and its consequences*. Verlag Niggli AG, Zürich.

Ritter, W. (1888). *Anwendungen der Graphischen Statik*. Meyer Zeller, Zürich.

Rjanitsyn, A. (1959). *Calcul à la rupture et plasticité des constructions*. Eyrolles.

Roca, P., Cervera, M., Gariup, G., and Pela, L. (2010). Structural analysis of masonry historical constructions. classical and advanced approaches. *Archives of Computational Methods in Engineering*, 17:299–325.

Rondeaux, J.-F., D'Acunto, P., Deschuyteneer, A., and Zastavni, D. (2018a). Limit state analysis of 2d externally statically indeterminate networks using graphic statics. *Proceedings of the IASS Annual Symposium 2018 - Creativity in Structural Design*.

Rondeaux, J.-F., D'Acunto, P., Schwartz, J., and Zastavni, D. (2017). Limit state analysis of 2d statically indeterminate networks using graphic statics. *Proceedings of the IASS Annual Symposium 2017*.

Rondeaux, J.-F., Deschuyteneer, A., and Zastavni, D. (2018b). Assessing geometrically the structural safety of masonry arches. *Building Knowledge, Constructing Histories. Proceedings of the sixth international congress on construction history*, 2:1129–1136.

Rondeaux, J.-F. and Zastavni, D. (2017). A fully graphical approach for limit state analysis of existing structures: application to plane elastic-plastic bended structures and to plane masonry arches. *International Journal of Architectural Heritage: conservation, analysis, and restoration*, pages 1–23.

Schwartz, J. (2010). *Bending and confusion. The long development of bending theory and its impact on the design and construction of beams*, pages 193–209. In Rinke and Schwartz (2010).

Schwartz, J. (2012). *Structural Theory and Structural Design*, pages 243–247. Birkhauser GmbH, Basel.

Schwartz, J. (2016). The art of structure. *Proceedings of the International Conference on Structures and Architecture ICSA*.

Shin, H., Porst, C. F., Vouga, E., Ochsendorf, J., and Durand, F. (2016). Reconciling elastic and equilibrium methods for static analysis. *ACM Transactions on Graphics*, 35(2):1–16.

Sinopoli, A., Rapallini, M., and Smars, P. (2004). Plasticity, coulomb friction and sliding in the limit analysis of masonry arches. *Arch bridges IV – Advances in assessment, structural design and construction*.

Smars, P. (2002). *Etude sur la stabilité des arcs et voûtes, confrontation des méthodes de l'analyse limite aux voûtes gothiques en Brabant*. PhD thesis, Katolieke Universiteit Leuven.

Spofford, C. M. (1928). *The Theory of Structures*. McGraw-Hill Book Company, New York.

Starossek, U. and Haberland, M. (2011). Approaches to measures of structural robustness. *Structure and Infrastructure Engineering*, 7 (7-8):625–631.

Stevin, S. (1586). *De Beghinselen der Weeghconst*. Raphelinghen, Leiden.

Thompson, F. and Haywood, G. (1986). *Structural Analysis using Virtual Work*. Chapman and Hall Ltd, London.

Timoshenko, S. (1953). *History of strength of materials*. McGraw-Hill Book Company, New York.

Timoshenko, S. and Young, D. (1945). *Theory of structures*. McGraw-Hill Book Company, New York.

Trautz, M. and Koj, C. (2009). Self-tapping screws as reinforcement for timber structures. *Proceedings of the International Association for Shell and Spatial Structures. Evolution and Trends in Design, Analysis and Construction of Shell and Spatial Structures*.

Ungewitter, G. and Mohrmann, K. (1901). *Lehrbuch der Gotischen Konstruktionen*. Chr. Herm. Tauchnitz, address = Leipzig.

Van Mele, T., Lachauer, L., Rippmann, M., and Block, P. (2012). Geometry-based understanding of structures. *Journal of the International Association for Shell and Spatial Structures*, 53(4):285–295.

Varignon, P. (1725). *Nouvelle Mécanique ou Statique*, volume 2 vols. C. Jombert, Paris.

Winkler, E. (1879). Die lage der stützlinie im gewölbe. *Deutsche Bauzeitung*, 13:117–119/127–130.

Wolfe, W. S. (1921). *Graphical analysis: a text book on graphic statics*. McGraw-Hill, New York.

Zalewski, W. and Allen, E. (1998). *Shaping structures: Statics*. John Wiley and Sons, New York.

Zastavni, D. (2008). *La conception chez Robert Maillart : morphogenèse des structures architecturales*. PhD thesis, Université catholique de Louvain.

Zastavni, D., Cap, J.-F., Jasienski, J.-P., and Fivet, C. (2014). Load path and prestressing in conceptual design related to maillart's vessy bridge. *Proceedings of the IASS-SLTE 2014 Symposium "Shells, Membranes and Spatial Structures: Footprints"*.

Zastavni, D., Deschuyteneer, A., and Fivet, C. (2015). Admissible geometrical domains within the context of graphic statics for evaluating constitutive elements of structural robustness. *Proceedings of the IASS2015 Annual International Symposium on Future Visions*.

Zastavni, D., Deschuyteneer, A., and Fivet, C. (2016). Admissible geometrical domains and graphic statics to evaluate constitutive elements of structural robustness. *International Journal of Space Structures*, 31(2-4):165–176.

"I was looking at the ceiling...

... And then I saw the sky."

John Adams & June Jordan, 1995, Berkeley